R.P.Noorlandt

A seismic vibrator driven by linear synchronous motors

Developing a prototype vibrator, investigating the vibrator-ground contact and exploring robust signal design

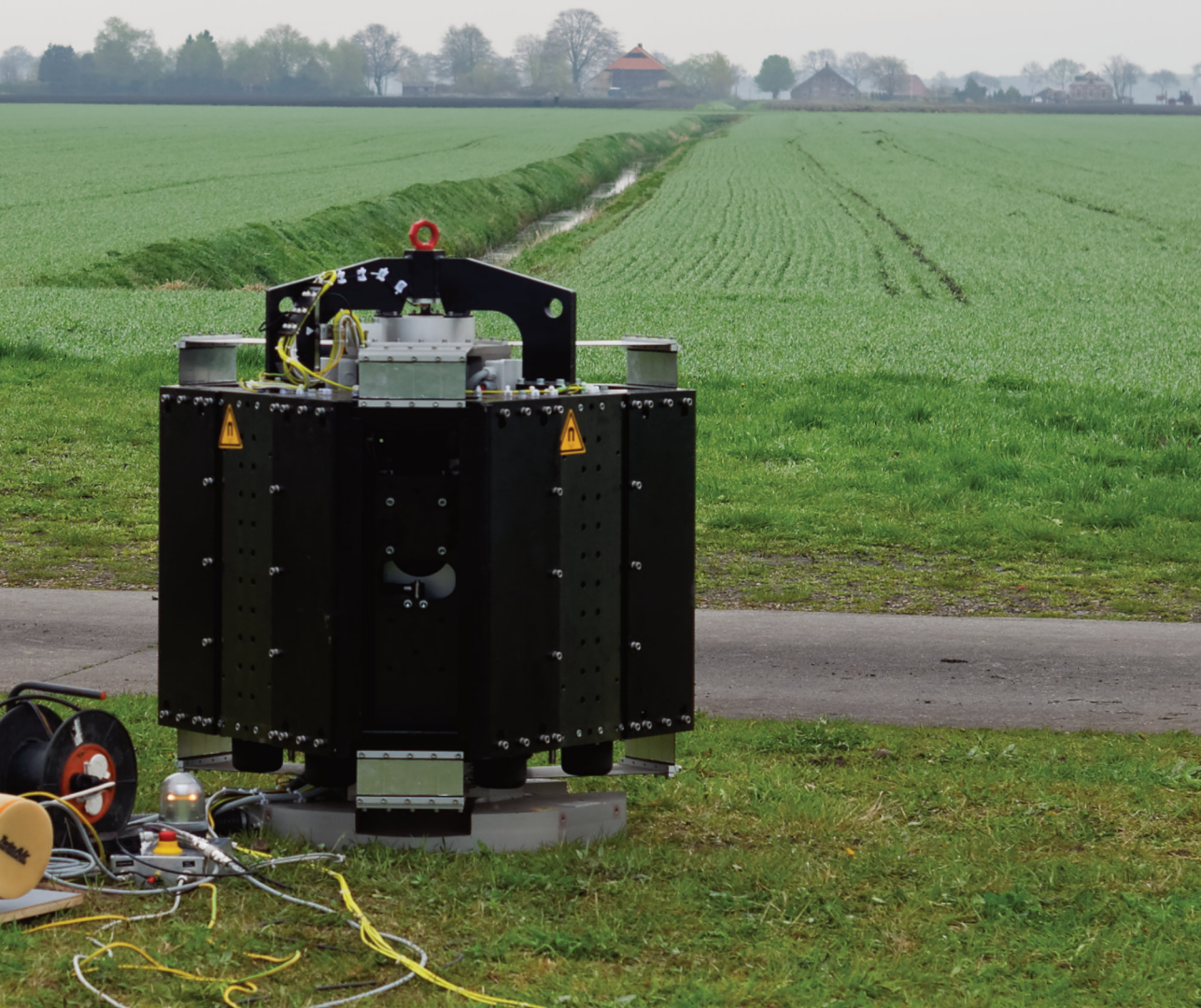

Propositions

accompanying the dissertation

A SEISMIC VIBRATOR DRIVEN BY LINEAR SYNCHRONOUS MOTORS

DEVELOPING A PROTOTYPE VIBRATOR, INVESTIGATING THE VIBRATOR-GROUND CONTACT AND EXPLORING ROBUST SIGNAL DESIGN

by

Richard Pim NOORLANDT

1. The advantages of seismic vibrators driven by linear synchronous motors justify replacing hydraulic vibrators (chapter 2 of this thesis).
2. Because the contact between the vibrator and ground is important (chapter 4 of this thesis), seismic vibrators should be designed to optimize this.
3. Instead of trying to optimize sources for an ideal signal, it is better to design signals for a less ideal source (chapter 5 of this thesis).
4. Damaged ground absorbs signal; therefore a seismic source should cause as little damage as possible.
5. The principle of Wikipedia is scientifically more productive than that of scientific journals.
6. The increasing use of internet automatically causes a decrease of privacy.
7. The importance of prime numbers for signal analysis cannot be overestimated.
8. To assess whether development is truly sustainable, a complete inventory of all effects is necessary.
9. The way the patent system is exploited for commercial benefits is not in the interest of general development.
10. Communication is vital in a complex society as ours; therefore it is frightening that languages develop slower than communication technologies.

These propositions are regarded as opposable and defendable, and have been approved as such by the promotor Prof. dr. ir. C.P.A. Wapenaar.

A SEISMIC VIBRATOR DRIVEN BY LINEAR SYNCHRONOUS MOTORS

DEVELOPING A PROTOTYPE VIBRATOR, INVESTIGATING THE VIBRATOR-GROUND CONTACT AND EXPLORING ROBUST SIGNAL DESIGN

A SEISMIC VIBRATOR DRIVEN BY LINEAR SYNCHRONOUS MOTORS

DEVELOPING A PROTOTYPE VIBRATOR, INVESTIGATING THE VIBRATOR-GROUND CONTACT AND EXPLORING ROBUST SIGNAL DESIGN

Proefschrift

ter verkrijging van de graad van doctor
aan de Technische Universiteit Delft,
op gezag van de Rector Magnificus prof. ir. K. C. A. M. Luyben,
voorzitter van het College voor Promoties,
in het openbaar te verdedigen op
woensdag 7 december 2016 om 10:00 uur

door

Richard Pim NOORLANDT

Master of Earth Science
geboren te Rhenen, Nederland.

Dit proefschrift is goedgekeurd door de:

promotor:	Prof. dr. ir. C.P.A. Wapenaar
copromotor:	Dr. ir. G.G. Drijkoningen

Samenstelling promotiecommissie:

Rector Magnificus,	voorzitter
Prof. dr. ir. C.P.A. Wapenaar,	Technische Universiteit Delft, promotor
Dr. ir. G.G. Drijkoningen,	Technische Universiteit Delft, copromotor

Onafhankelijke leden:

Prof. dr. ir. J.T. Fokkema,	Technische Universiteit Delft
Prof. dr. A.V. Metrikine,	Technische Universiteit Delft
Prof. dr. ir. P.P.J. van den Bosch,	Technische Universiteit Eindhoven
Dr. A.P.E. Ten Kroode,	Shell Global Solutions International BV
Dr. J.H. Brouwer,	TNO

ISBN 978-94-92516-23-7

Keywords: vibrator, seismic source, linear synchronous motors, LSM, vibrator-ground contact, contact mechanics, sweep, chirp, optimal signals.

This research was funded by the Netherlands Research Centre For Integrated Solid Earth Science (ISES) and was also supported by the Nederlandsche Aardolie Maatschappij (NAM) and Deltares.

Contact: rik.noorlandt@gmail.com

Printed by: Gildeprint

An electronic version of this dissertation is available at
http://repository.tudelft.nl/

CONTENTS

Summary vii

Zusammenfassung ix

Samenvatting xi

1 Introduction 1
- 1.1 Background . . . 1
- 1.2 Being loud or being smart . . . 1
  - 1.2.1 Sweep signals . . . 3
- 1.3 Practical difficulties . . . 5
  - 1.3.1 Harmonics . . . 6
- 1.4 Motivation and outline of this thesis . . . 7

References . . . 8

2 Linear synchronous motor vibrator 9
- 2.1 Introduction . . . 10
- 2.2 Design and principle of a linear-motor vibrator . . . 11
  - 2.2.1 Mechanical modeling . . . 11
  - 2.2.2 Principle of a linear synchronous motor . . . 14
  - 2.2.3 Coil-magnet track synchronization . . . 16
  - 2.2.4 Multiple motor synchronization . . . 16
  - 2.2.5 Air spring support . . . 17
  - 2.2.6 Suppressing support spring resonance and temperature effects . . . 19
- 2.3 Field case . . . 22
  - 2.3.1 Regular linear sweep . . . 22
  - 2.3.2 Harmonics . . . 22
  - 2.3.3 Other driving signals . . . 24
- 2.4 Discussion . . . 27
- 2.5 Conclusion . . . 31

References . . . 31

3 Experiments on the behavior of vibrators 33
- 3.1 Introduction . . . 33
- 3.2 Influencing ground-vibrator coupling by Mats . . . 34
- 3.3 Increasing power . . . 37
  - 3.3.1 With drive level . . . 38
  - 3.3.2 With sweep duration . . . 41
- 3.4 Drive-level and repeatability experiment . . . 41
  - 3.4.1 Field layout and experiment setup . . . 41
  - 3.4.2 Experiment results . . . 44

3.5 Conclusion . . . 50
References . . . 50

4 Vibrator-earth contact **51**
4.1 Introduction . . . 51
4.2 Contact mechanics . . . 54
4.2.1 Simple contact geometry . . . 54
4.2.2 Rough surface contact . . . 55
4.2.3 Contact dynamics; single nonlinear spring . . . 58
4.2.4 Contact dynamics; Winkler foundation . . . 60
4.3 Field observations . . . 61
4.4 Discussion . . . 65
4.4.1 Implications for field measurements . . . 66
4.5 Conclusion . . . 67
References . . . 67

5 Optimizing vibrator signals **71**
5.1 Introduction . . . 71
5.2 Linear Sweeps . . . 72
5.2.1 Role of tapers . . . 72
5.2.2 Phase offset to control low frequencies . . . 73
5.2.3 Phase offset to separate sources . . . 74
5.2.4 Shortcomings and harmonics . . . 76
5.3 Nonlinear Sweeps: control on harmonic correlation noise . . . 79
5.4 Nonlinear Sweeps: power spectrum shaping by sweep rate variation . . . 81
5.5 Conclusion . . . 84
References . . . 85

6 General discussion and outlook **87**
6.1 General discussion . . . 87
6.2 Outlook . . . 89

Acknowledgments **91**

Curriculum Vitæ **93**

SUMMARY

The seismic method is an important indirect method to investigate the subsurface of the earth. By analyzing how the earth affects the propagation of mechanical waves, the structure of the earth and its seismic properties can be inferred. The seismic vibrator is the most commonly used land source in active-source exploration and monitoring to generate these waves and is the subject of this thesis. The goal of a seismic vibrator is to produce seismic waves with a known signal signature. Commonly sinusoidal signals whose frequency varies over time, called sweeps, are used for this purpose. These signals are typically quite lengthy to compensate for the fact that the instantaneous amplitudes of the vibrator are relatively weak compared to the ones from impulsive sources and the target depths faced. Via the processing step of correlation, the lengthy source signature is collapsed and virtual records are generated as if the vibrator would have released all energy at once. The quality of these virtual records depends on the ability of the vibrator engines to generate the force signature wanted and the ability of the vibrator mechanics and the vibrator-ground interaction to successfully transform the driving force to a seismic wave. In this thesis we investigate the feasibility of driving a vibrator with linear synchronous motors, the influence of drive level on the signals a vibrator generates, the effect of the vibrator-ground coupling, and the possibilities to design more robust source signals.

A linear synchronous motor (LSM) is an electric motor that can produce large controllable forces and is therefore suitable as a driving engine for a seismic vibrator. This motor consists of two independent elements, a magnet track and a coil track, allowing practically unlimited motor displacements. This makes the LSM very suitable for expanding the source frequency band to the lower frequencies in which larger strokes are needed. We successfully designed and built a multi-LSM prototype vibrator of some 1200 kg. In this thesis we describe its design and how we addressed the LSM control and the suppression of its mechanical resonances of this vibrator. The seismic data acquired in field tests proved that the prototype LSM vibrator acted very well as a seismic source. It has no trouble generating pseudorandom sweeps, and even given its limited size, it generated signals within the low-frequency regime, down to 2 Hz, rather easily.

In a number of field experiments described in this thesis, we show the influence of the coupling between a vibrator and the ground, the sweep rate, and drive level on the behavior of a vibrator and the spectra it generates. Just after the prototype LSM vibrator was built, several field tests near Schoonebeek were performed. These tests, among others, consisted of placing different mats between the vibrator and the ground, performing the same sweep at different drive levels and with different sweep rates. These experiments showed that coupling mats and drive level change the shape of the vibrator's spectral amplitude, while the sweep rate scales the spectrum uniformly. The change with drive level was investigated in more detail in another experiment using a hydraulic driven exploration vibrator, able to generate forces up to 266 kN. So a much wider range

of drive levels could be studied. From this second dataset we conclude that: the vibrator signal is very repeatable for a given drive level and fixed position; the repeatability of smaller drive levels is reduced when higher drive levels are performed in between; the interaction of the base plate and the ground depends on the drive level in a nonlinear way. If these effects are not taken into account, they produce arrival-time and amplitude errors in the seismic records.

The influence of the contact between a vibrator and the earth on their dynamics was further investigated. Although a vibrator might appear to be well-coupled with the earth on a macro scale, perfect coupling certainly does not occur on the micro scale. With the aid of contact mechanical modeling and concepts, it is shown in this thesis that this lack of contact at the micro scale, or rather the change thereof during a sweep, can have a significant effect on the dynamics of the vibrator-earth system. Modeling of such changing contact, predicts that the dynamic behavior varies considerably with the vibrator drive level. The most significant effect predicted by the model is a decrease in the base-plate resonance frequency with an increasing drive level. Similar changes of resonance behavior with drive level were also found in the drive-level field tests.

Linear sweeps are the mostly used signals to drive seismic vibrators. Their constant amplitude over time and flat frequency spectra are desired properties. However, the transfer from the signal used to drive the vibrator to the seismic wave can affect these properties considerably. In this thesis we show that the design of the phase offset of the sweep can help to reduce the low-frequency energy of a sweep or can be used to assist in separating simultaneous-source records. The nonlinear behavior of the vibrator, the ground and their contact will distort the sweep and produce harmonics, which, after processing, show up as noise and ghost events in the records. As we show in this thesis, nonlinear sweeps, with both sweep rate and amplitude carefully designed, can be used to anticipate on these transfer functions and help to remove harmonic noise from the seismic records efficiently.

This thesis shows that the vibroseis method is complicated. Some parts of the setup are more or less static and can be controlled, such as the design of the vibrator and the signature it should produce. Other parts of the setup are more dynamic, spatially and temporally, such as ground properties and vibrator-ground contact. If one aims to improve the vibroseis method per se, all these aspects should be considered together as they are inextricably intertwined.

ZUSAMMENFASSUNG

Das seismische Verfahren ist eine wichtige indirekte Methode um das Innere der Erde zu untersuchen. Durch Analyse des Einflusses der Erde auf die Ausbreitung mechanischer Wellen kann die Struktur der Erde und seine seismischen Eigenschaften abgeleitet werden. Der seismische Vibrator ist die gängigste Quelle in der aktiven Exploration und dem Monitoring um diese Art Wellen zu erzeugen und ist das Thema dieser Arbeit. Das Ziel eines seismischen Vibrators ist es seismische Wellen mit einem vorher bekannten Signal zu erzeugen. üblicherweise werden für diesen Zweck Signale verwendet die auch Sweeps genannt werden. Sweeps sind sinusförmige Signale bei denen die Frequenz mit der Zeit variiert. Diese Signale sind in der Regel recht lang, um die Tatsache zu kompensieren, dass die momentanen Amplituden des Vibrators im Vergleich zu den Impulsquellen und zu erreichenden Tiefen relativ schwach sind. Durch den Bearbeitungsschritt der Korrelation wird die lange Signalquelle verkürzt und dadurch werden virtuelle Datensätze erzeugt die aussehen als würde der Vibrator die gesamte Energie auf einmal freigegeben. Die Qualität dieser virtuellen Aufzeichnungen ist abhängig von der Fähigkeit des Vibratormotors das gewünschte Kraftprofil herzustellen sowie die Möglichkeit der Mechanik des Vibrators und des Vibrator-Boden-Kontaktes die erzeugte Kraft erfolgreich in eine seismische Welle umzusetzen. In dieser Arbeit untersuchen wir die Möglichkeit der Konstruktion eines Vibrator mit Linearmotoren, den Einfluss des Kraftaufwandes auf die Signale die der Vibrator erzeugt, den Effekt des Kontaktes zwischen Vibrator und Boden und die Möglichkeiten robustere Quellensignale zu entwerfen.

Ein Linearmotor (LSM) ist ein Elektromotor der große steuerbare Kräfte erzeugen kann und daher als Antriebsmotor für einen seismischen Vibrator geeignet ist. Dieser Motor besteht aus zwei unabhängigen Elementen, einer Magnetreihe und einer Spulenreihe, wodurch nahezu unbegrenzte Motorbewegungen möglich sind. Dies sorgt dafür, dass der LSM sehr geeignet ist für die Erweiterung des Frequenzbereiches einer Quelle auf niedrige Frequenzen, bei denen große Bewegungen erforderlich sind. Wir haben erfolgreich ein Multi-LSM Vibrator Prototyp von ca. 1200 kg entworfen und gebaut. In dieser Arbeit beschreiben wir den Entwurf, die LSM-Steuerung und eine Methode um die mechanische Resonanz des Vibrators zu unterdrücken. Die seismischen Daten die wir in Feldversuchen erhalten haben, zeigen dass der LSM Vibrator eine gute seismische Quelle ist. Der Vibrator kann ohne Probleme pseudorandom Sweeps erzeugen und trotz seiner begrenzten Größe kann er relativ einfach Signale mit niedriger Frequenz, bis 2 Hz, erzeugen.

In Feldexperimenten die wir in dieser Arbeit beschreiben, wird die Wirkung des Kontaktes zwischen Vibrator und Boden, sowie die Laufgeschwindigkeit und Leistung des Sweeps auf das Verhalten des Vibrators und den Spektren die er erzeugt beschrieben. Nach dem Bau des LSM Vibrators wurden mehrere Feldexperimente in der Nähe von Schoonebeek durchgeführt. Diese Tests bestanden unter anderem darin verschiedene Gummimatten zwischen den Vibrator und dem Boden zu legen, die gleichen Sweeps bei

unterschiedlicher Leistung und mit unterschiedlicher Durchlaufgeschwindigkeit durchzuführen. Diese Experimente zeigten, dass der Kontakt und der Leistungspegel die Form der spektralen Amplitude des Vibrators verändern, während die Laufgeschwindigkeit nur das Niveau des Spektrums beeinflusst. Die Wirkung des Leistungspegels wurde in einem anderen Experiment mit Hilfe eines hydraulisch angetriebenen Explorationsvibrators weiter untersucht. Dieser Vibrator kann Kräfte bis zu 266 kN erzeugen und ermöglicht, dass ein breiteres Spektrum an Kräften untersucht werden kann. Aus diesem zweiten Datensatz schließen wir, dass das Vibratorsignal auch bei Wiederholung unverändert ist, solange der Vibrator nicht bewegt wird und das Kraftniveau gleich gehalten wird. Die Wiederholbarkeit von kleineren Kraftniveaus wird schlechter wenn zwischen den Durchläufen Sweeps mit größerer Kraft durchgeführt werden. Auch das Zusammenwirken der Bodenplatte mit dem Boden ist auf nicht-lineare Art und Weise vom Kraftniveau abhängig. Wenn diese Effekte nicht berücksichtigt werden, treten im seismischen Datensatz Fehler in Ankunftszeit und Amplitude auf.

Der Einfluss des Kontaktes zwischen dem Vibrator und der Erde auf ihre Dynamik wird detailliert untersucht. Obwohl es scheint, der Vibrator habe im Makromaßstab einen guten Kontakt, ist dieser Kontakt im Mikromaßstab bei weitem nicht perfekt. In dieser Arbeit wird gezeigt, dass durch die Verwendung von mechanischen Kontaktmodellen und -konzepten dieser Mangel an Kontakten im Mikromaßstab oder vielmehr dessen Veränderung während eines Sweeps, einen erheblichen Einfluss auf die Dynamik des Vibrators-Erde-Systems haben kann. Die Modellierung von Kontakten die sich umformen, sagt das dynamische Verhalten vorher, das stark mit dem Leistungspegel des Vibrators variiert. Die Hauptwirkung, die durch das Modell vorhergesagt wird, ist eine Abnahme in der Resonanzfrequenz der Grundplatte mit zunehmendem Leistungspegel. ähnliche änderungen im Resonanzverhalten wurden auch in den Feldexperimenten gefunden.

Linear-Sweeps sind Signale die am häufigsten verwendet werden um seismische Vibratoren zu steuern. Ihre konstante Amplitude in der Zeit und ihre flachen Frequenzspektren haben sich als gewünschte Eigenschaften erwiesen. Diese Eigenschaften können sich jedoch wesentlich verändern, wenn der Vibrator die Ansteuersignale in seismische Wellen umwandelt. In dieser Arbeit wird gezeigt, dass die Startphase eines Sweeps verwendet werden kann, um die Niederfrequenzenergie eines Sweeps zu reduzieren oder um gleichzeitig agierende Quellen von einander zu unterscheiden. Das nicht-lineare Verhalten des Vibrators, des Bodens, und ihres Kontaktes zueinander führt zur Verzerrung des Sweepsignals und erzeugt Obertöne, die nach der Verarbeitung als Rauschen und Scheinankünfte im seismischen Datensatz erscheinen. In dieser Arbeit zeigen wir, dass ein nicht-lineares Sweep, bei dem die Laufgeschwindigkeit und die Amplitude sorgfältig entworfen wird, diese Verzerrungen antizipieren kann und dabei hilft dieses Rauschen aus dem seismischen Datensatz zu entfernen.

Diese Arbeit zeigt, dass das Vibroseis Verfahren kompliziert ist. Einige Komponenten der Methode sind relativ statisch und können beeinflusst werden, wie zum Beispiel die Gestaltung des Vibrators, und das Signal dass sie produziert. Andere Komponenten sind dynamischer in Raum und Zeit, wie zum Beispiel die Bodeneigenschaften und der Vibrator-Boden Kontakt. Um das Vibroseis Verfahren zu verbessern, müssen alle diese Aspekte die untrennbar miteinander verflochten sind, zusammen betrachtet werden.

SAMENVATTING

De seismische methode is een belangrijke indirecte methode om de ondergrond van de aarde te onderzoeken. Door te analyseren hoe de aarde de propagatie van mechanische golven beïnvloedt, kan de structuur van de aarde en haar seismische eigenschappen worden afgeleid. De seismische vibrator is een veel gebruikte bron in de actieve exploratie en monitoring om deze golven op te wekken en is het onderwerp van dit proefschrift. Het doel van een seismische vibrator is om seismische golven te produceren met bekend signaal. Vaak gebruikte signalen voor dit doel zijn sweeps. Dit zijn sinusvormige signalen waarbij de frequentie in de tijd varieert. Deze signalen zijn meestal vrij lang ter compensatie voor het feit dat de instantane amplituden van de vibrator relatief zwak zijn vergeleken met die van impuls bronnen en de te bereiken dieptes. Via de verwerkingsstap van correlatie, wordt het lange bronsignaal ingekort en virtuele opnamen gegenereerd alsof de vibrator alle energie in één keer heeft vrijgegeven. De kwaliteit van deze virtuele opnamen is afhankelijk van de mogelijkheid van de vibratormotor om het gewenste krachtprofiel te creëren en de mogelijkheid van de vibratormechanica en de vibrator-grond interactie om die kracht succesvol om te zetten naar een seismische golf. In dit proefschrift onderzoeken we de haalbaarheid van het aansturen van een vibrator met lineaire motoren, de invloed van het krachtniveau op de signalen die een vibrator genereert, het effect van de vibrator-grond-koppeling, en de mogelijkheden om robuustere bronsignalen te ontwerpen.

Een lineaire motor (LSM) is een elektromotor die grote beheersbare krachten kan produceren en is daarom geschikt als aandrijfmotor voor een seismische vibrator. Deze motor bestaat uit twee onafhankelijke elementen, een magneetspoor en een spoelspoor, waardoor vrijwel onbeperkt motorverplaatsingen mogelijk zijn. Dit maakt de LSM zeer geschikt voor het uitbreiden van de frequentieband van de bron naar lagere frequenties waar grotere bewegingen nodig zijn. Wij hebben met succes een multi-LSM prototype vibrator van ongeveer 1200 kg ontworpen en gebouwd. In dit proefschrift beschrijven we het ontwerp, de LSM aansturing en hoe we de mechanische resonanties van deze vibrator onderdrukken. De seismische data verkregen in veldproeven tonen aan dat de LSM vibrator een goede seismische bron is. De vibrator heeft geen problemen met het genereren van pseudorandom sweeps, en kan, zelfs gezien zijn beperkte omvang, vrij gemakkelijk signalen in het laagfrequente regime, tot 2 Hz, produceren.

In een aantal, in dit proefschrift beschreven, veldexperimenten laten we de invloed van de koppeling tussen de vibrator en ondergrond, de sweepsnelheid en van het krachtniveau op het gedrag van een vibrator en de spectra die deze genereert zien. Nadat de LSM vibrator gebouwd is, zijn verschillende veldproeven in de buurt van Schoonebeek uitgevoerd. Deze tests bestonden onder meer uit, het plaatsen van verschillende matten tussen de vibrator en de grond, het uitvoeren van dezelfde sweep op verschillende krachtniveaus en het uitvoeren van sweeps met verschillende sweepsnelheden. Deze experimenten toonden aan dat de koppeling en het krachtniveau de vorm van de spectrale

amplitude van de vibrator veranderen, terwijl de sweepsnelheid het spectrum enkel uniform beïnvloedt. Het effect van het krachtniveau is verder onderzocht in een ander experiment met behulp van een hydraulisch aangedreven exploratie vibrator die krachten kan genereren tot 266 kN. Hierdoor kon een breder spectrum aan krachten bestudeerd worden. Uit deze tweede dataset concluderen wij dat: het vibratorsignaal herhaalbaar is zolang de vibrator niet verplaatst en het krachtniveau gelijk gehouden wordt; de herhaalbaarheid van kleinere krachtniveaus verminderd wordt wanneer er tussendoor sweeps met groter krachtniveaus worden uitgevoerd en dat de interactie van de grondplaat en de grond op niet-lineaire wijze afhankelijk is van het krachtniveau. Indien er geen rekening gehouden wordt met deze effecten kunnen aankomsttijd- en amplitudefouten optreden in de seismische opname. Verder is de invloed van het contact tussen een vibrator en de aarde op hun dynamica nader onderzocht. Hoewel een vibrator op een macroschaal in goed contact met de aarde lijkt te zijn, is het contact op microschaal verre van perfect. In dit proefschrift wordt met behulp van contact mechanische modellen en concepten aangetoond dat dit gebrek aan contact op microschaal, of liever de verandering ervan gedurende een sweep, een significante invloed kan hebben op de dynamiek van het vibrator-aarde systeem. Modellering van zulke wisselende contacten, voorspelt dat het dynamisch gedrag sterk varieert met het krachtniveau van de vibrator. Het belangrijkste effect dat door het model voorspeld wordt, is een afname van de resonantiefrequentie van de grondplaat bij toenemende krachtniveaus. Soortgelijke veranderingen in resonantie gedrag werden ook gevonden in de veldproeven.

Lineaire sweeps zijn de meest gebruikte signalen om seismische vibratoren aan te sturen. Hun constante amplitude in tijd en hun vlakke frequentiespectra zijn gewenste eigenschappen. Echter kunnen deze eigenschappen aanzienlijk veranderen op het moment dat de vibrator de aansturingssignalen omzet naar seismische golven. In dit proefschrift wordt aangetoond dat de startfase van een sweep gebruikt kan worden om de laagfrequente energie van een sweep te verminderen of om te helpen bij het scheiden van simultaan opererende bronnen. Het niet-lineaire gedrag van de vibrator, de grond en hun contact leidt tot de vervorming van het sweepsignaal en genereert boventonen, die na verwerking verschijnen als ruis en schijnaankomsten in de seismische opname. In dit proefschrift laten we zien dat een niet-lineaire sweep, waarvan zowel de sweep snelheid als de amplitude zorgvuldig ontworpen is, gebruikt kan worden om te anticiperen op deze vervormingen en kan helpen om deze ruis efficiënt te verwijderen uit de seismische opname.

Dit proefschrift laat zien dat de vibroseis methode ingewikkeld is. Sommige onderdelen van deze methode zijn min of meer statisch en kunnen worden beïnvloed, zoals het ontwerp van de vibrator en het signaal dat ze moet produceren. Andere onderdelen zijn dynamischer in ruimte en tijd, zoals de grondeigenschappen en het vibrator-grond contact. Om de vibroseis methode te verbeteren, moeten deze aspecten die onlosmakelijk met elkaar zijn verweven gemeenschappelijk beschouwd worden.

1

INTRODUCTION

1.1. BACKGROUND

There are many reasons to investigate the subsurface. The quest for resources, like oil, gas, metals, minerals, water, heat, etcetera, led to the development of many different techniques to study the earth below our feet. Besides the direct techniques like digging and drilling, there are indirect methods available to gain insight. Geophysical methods characterize the subsurface by assessing the physical properties of the earth and the spatial and temporal changes thereof.

One class of these indirect investigation techniques is the seismic method. Seismic methods rely on the propagation of mechanical waves through the earth. By analyzing how the earth affects the propagation of the wave, properties of the composition of the earth can be inferred. Many different seismic techniques are possible, and they are typically named by the "wave type" they use, like surface and body waves or by the propagation "effect" they use to analyze, like wave dispersion, reflection, refraction and scattering. Irrespective of the wave type and effect used, the seismic method can be passive or active. In passive seismic methods the "source" of the waves is not specifically controlled and the seismic signal might be generated by wind, ocean motion, traffic, earth quakes, etcetera. In active seismic methods a dedicated source is used to produce the seismic signal. The seismic vibrator is one type of active source and is the subject of this thesis. To put things in perspective, this introduction chapter presents an overview of the signals generated by vibrators, how the vibrator operates and the difficulties involved. With this in mind the motivation for the work carried out and described in subsequent chapters is given.

1.2. BEING LOUD OR BEING SMART

In the simplest model of the seismic experiment the output (recorded signal at the geophone) is a linear reaction to the input (source signal). In an ideal, noise and distortion-free case the signal received at a geophone, $y(t)$, is the convolution of the source signal

1

$s(t)$ with the impulse response of the earth $h(t)$,

$$y(t) = s(t) * h(t). \tag{1.1}$$

In this system $h(t)$ contains all information obtainable for a certain source-receiver pair. If $s(t)$ would be a Dirac delta distribution $\delta(t)$, the recorded signal would, by definition, be equal to the earth's impulse response,

$$y(t) = \delta(t) * h(t) = \int_{-\infty}^{\infty} \delta(t-\tau)h(\tau)\mathrm{d}\tau = h(t). \tag{1.2}$$

Seismic sources can be divided in two groups, based on the method they use to approximate the delta distribution.

Impulsive sources, like explosives, weight drops, hammer blow and air guns, use a direct approach, approximating a band-limited Dirac delta distribution by producing a signal that is as short and as strong as possible. The difficulty with this approach is that a perfect delta pulse can not physically be generated and typically the duration and strength of the pulse are not independent. Furthermore, the stronger the pulse, the more likely the linear assumption is to fail. Also the repeatability of an impulsive source can be very low.

The other group of sources, like seismic vibrators, try to circumvent these problems by focusing on the frequency-domain characteristics of the delta distribution. Realizing that the delta distribution has an infinitely wide, flat power spectrum, vibrator signals are designed to send out frequencies over the widest range possible. However, instead of releasing all energy at once, the energy is distributed over time, reducing the need for large instantaneous amplitudes like the delta distribution. In the processing of vibratory data the distribution is collapsed to construct a virtual record as if the source would have released all its energy at once.

The compression of the source wavelet is normally done by correlation or deconvolution. Instead of applying these operations directly in the time domain, the data is typically transformed to the frequency domain, where these operations become simple multiplications. The frequency-domain equivalent of equation 1.1 is,

$$Y(\omega) = S(\omega)H(\omega), \tag{1.3}$$

where $S(\omega)$ is the source spectrum and $H(\omega)$ is transfer function of the earth. By multiplying equation 1.3 with the conjugate of the source signal, $\overline{S(\omega)}$, the phase of the source signal is removed and the spectrum of the correlated signal,

$$C(\omega) = Y(\omega)\overline{S(\omega)} = |S(\omega)|^2 H(\omega), \tag{1.4}$$

is found to be equal to the transfer of the earth scaled by the power spectrum of the source, $|S(\omega)|^2$. As expected, the more frequencies present in the power spectrum of the source that carry significant amplitude, the more frequencies of the earth's transfer function H are captured in C. The impact of the power spectrum imprint in C can be reduced in two ways. Firstly by making sure that the source produces a flat spectrum, which makes $|S(\omega)|^2$ effectively a constant and secondly by deconvolving the data for the source signal, i.e. dividing C by $|S(\omega)|^2$ in a stabilized way.

Another informative way to describe the process of distributing a band-limited signal over time at acquisition and enable its compression during processing, is by considering statistical moments of a signal. It can be shown, see the book of Cohen Cohen (1995), that the moments of the energy signal in the time domain can be determined in the frequency domain,

$$\begin{aligned} < t^n > &\equiv \int_{-\infty}^{\infty} t^n |f(t)|^2 \mathrm{d}t \\ &= \frac{1}{2\pi} \int_{-\infty}^{\infty} F(\omega) \frac{d^n}{j^n d\omega^n} \overline{F(\omega)} \mathrm{d}\omega, \end{aligned} \tag{1.5}$$

where $f(t)$ is the time signal and $F(\omega)$ is its equivalent in the frequency domain.

The zeroth moment, $n = 0$, represents the energy of the signal and equation 1.5 becomes Parseval's relation. The first moment is a measure of the location of the center of the signal and the second moment is a measure of the spread of the signal. If the signal considered is centered around zero, having a zero first moment, the variance, a measure of duration in the time domain, is given by,

$$\sigma^2 = \frac{< t^2 >}{< t^0 >} = \frac{\int_{-\infty}^{\infty} \left(\left[\frac{dR(\omega)}{d\omega} \right]^2 + \left[R(\omega) \frac{d\psi(\omega)}{d\omega} \right]^2 \mathrm{d}\omega \right)}{\int_{-\infty}^{\infty} \left[R(\omega) \right]^2 \mathrm{d}\omega} \tag{1.6}$$

where we make use of the fact that the frequency spectra of the signal can be written in terms of its amplitude and phase components, $F(\omega) = R(\omega) e^{j\psi(\omega)}$, where $R(\omega)$ and $\psi(\omega)$ are real functions.

To maximize resolution, the ability to distinguish different arrivals, σ should be minimized. The optimal value equals 0 for a delta distribution, because in that case $\frac{d\psi(\omega)}{d\omega}$ and $\frac{dR(\omega)}{d\omega}$ are zero, while $R = 1$. For a band-limited impulse, as many frequencies as possible should be present, maximizing the denominator but at the same time having small values of $\frac{dR(\omega)}{d\omega}$ over the domain. Optimally R would be constant except for two smooth edges at the lower and higher end of its spectrum. The signal in the field has a phase such that its energy is distributed well over time (larger σ), but in processing the phase should be removed to make $\frac{d\psi(\omega)}{d\omega}$ zero and reduce σ to its minimal value given the source amplitude spectra $R(\omega)$.

1.2.1. SWEEP SIGNALS

One signal that is very well suited to probe a transfer function, and is commonly used to drive seismic vibrators, is the linear sweep. The linear sweep has a relatively flat amplitude spectrum as well as an excellent time distribution. The linear sweep signal can be calculated through

$$s(t) = A(t) \sin(\phi_0 + 2\pi f_0 t + \pi \alpha t^2), \tag{1.7}$$

where $A(t)$ is an amplitude term, ϕ_0 is a phase offset in radians, f_0 is the starting frequency in Hz and α is the sweep rate in Hz/s. The amplitude term typically is constant for most of the sweep except at the start and end of the sweep where a taper is applied.

1

For $\alpha > 0$ the frequency increases over time and the sweep is called an upsweep. For $\alpha < 0$ the frequency decreases over time and we have a downsweep. For $\alpha = 0$, the signal is just a monotonic sinusoidal with a frequency f_0.

An example of a sweep and some of its properties are shown in Figure 1.1. The used upsweep has a duration of 15 s, starts at $f_0 = 10$ Hz and increases with $\alpha = 6$ Hz/s such that the end frequency is 100 Hz. At the start and end of the sweep a 200 ms cosine taper has been applied, clearly visible in Figure 1.1a. The amplitude spectrum of the sweep (Figure 1.1b) is relatively flat at the interior, but oscillates and overshoots around the starting frequency of 10 Hz and final frequency of 100 Hz. Also energy leaks to frequencies outside the 10-to-100 Hz range. The trade-off between leakage and overshoot is controlled by the type and length of taper used. Because the amplitude spectrum only approximates that of a Dirac delta, the autocorrelation of the sweep contains side lobes (Figure 1.1c).

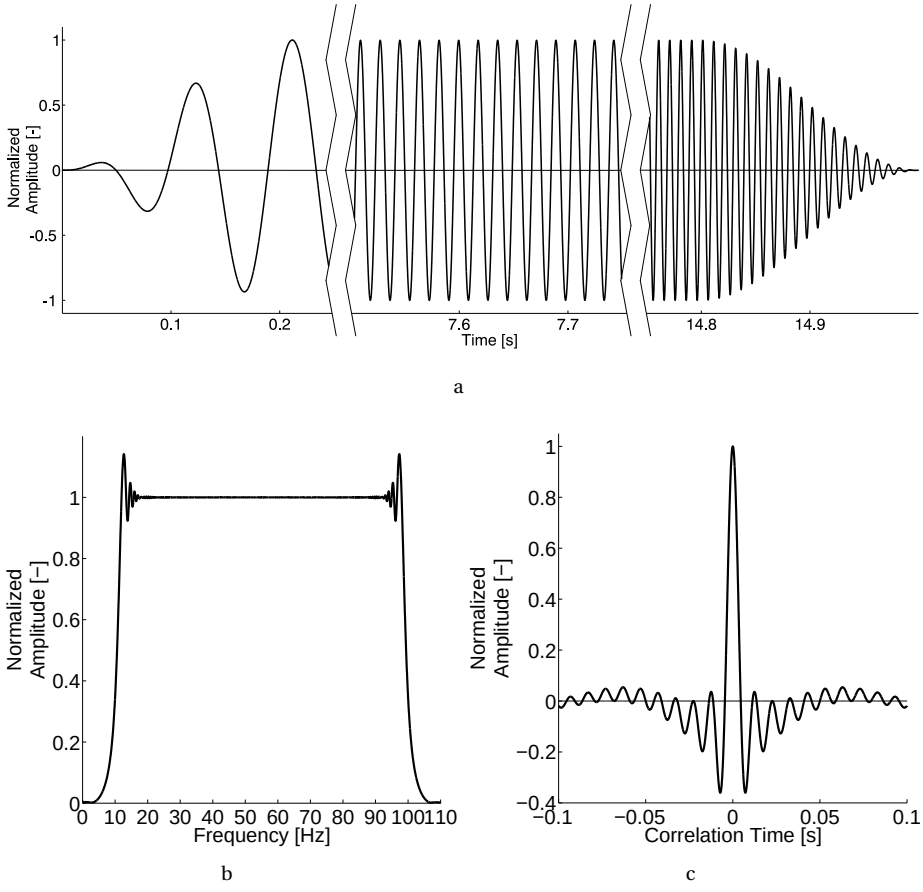

Figure 1.1: Example of a 15 s linear 10-to-100 Hz sweep with 200 ms cosine tapers (a) Segments of the time amplitude of the sweep, (b) amplitude spectrum and (c) the autocorrelation result of the sweep.

1.3. PRACTICAL DIFFICULTIES

Knowing what the seismic signal should look like, the next question is how to generate it. Mechanical seismic vibrators can be used for this purpose and consist of three main components: A driving engine, a contact body and a mass the engine can react against. For a surface vibrator the contact with the ground is made by a so-called base plate and the engine is placed between the base plate and the reaction mass. Depending on the maximal driving force and masses involved, an extra mass resting on the base plate, called a hold-down mass, might be added to prevent the plate from decoupling from the ground. A model of the main components of a vibrator is shown in Figure 1.2.

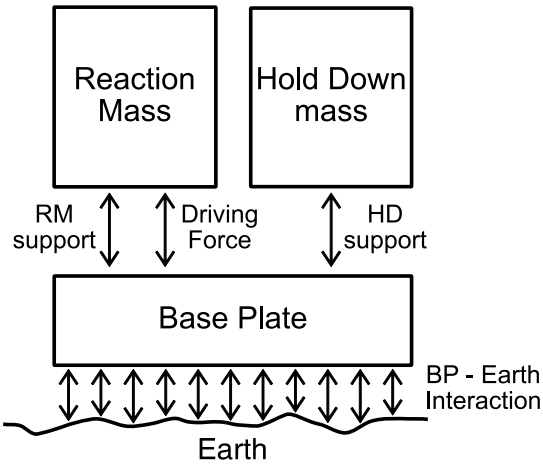

Figure 1.2: Model of main components of a seismic-exploration vibrator. The driving engine is placed between the reaction mass and base plate (driving force). Parallel to this there might be a support structure to hold the reaction mass (RM support). To prevent the base plate (BP) from decoupling from the earth a hold-down system might be present (HD support). The translation of the forces between the elements of the vibrator to a seismic wave occurs at the contact between the base plate and the earth (BP-earth interaction). From (From Noorlandt and Drijkoningen, 2016).

The masses and supporting elements of the vibrator are fixed by design and their behavior would be only marginally adjustable in the field. The plate-ground interaction changes with every ground type, condition and contact geometry. The only controllable element is the driving force, but that is also typically affected by a number of constraints. An overview of constraints applicable to hydraulic drive vibrators was given by Sallas (2010), while van der Veen *et al.* (1999) describes some of the constraints belonging to electric-driven vibrators.

One constraint all mechanical vibrators have in common, is their finite stroke, the maximum amount the reaction mass can move. Because the stroke needed for a certain force increases with decreasing frequency, the available stroke becomes a limiting factor in producing low frequencies. Below a certain frequency the vibrator simply is unable to produce a significant force. The supporting structures typically contain (air) springs and therefore resonate at certain frequencies. The ground itself acts as a low-pass filter, but

also introduces resonances and determines if and how the movement at the vibrator-ground contact gets transformed into a propagating wave.

Needless to say, because of all these constraints and interactions, it is rather difficult to generate a predefined seismic wavelet accurately under all conditions. The far-field seismic wavelet will always be a distorted copy of the designed sweep. The challenge is to make a vibrator that produces signals with a minimum amount of distortion and to estimate the true source signal, including all distortions, as accurately as possible so that the resolution can be optimized during the processing of the records. Part of the vibrator's behavior might be predictable and can be compensated with the help of feed-forward and feed-back loops. Although this works relatively well for linear interactions, the nonlinear interactions are much harder to predict and thus to control. The unknown and varying ground-plate interaction complicates matters further. In practice the source wavelet estimate $E(\omega)$ will be different from the true source wavelet $S(\omega)$ and the correlation equation 1.4 will be replaced with

$$C(\omega) = Y(\omega)\overline{E(\omega)} = S(\omega)\overline{E(\omega)}H(\omega) \tag{1.8}$$

and the deconvolution will commonly be replaced by

$$D(\omega) = \frac{S(\omega)\overline{E(\omega)}}{E(\omega)\overline{E(\omega)} + \epsilon} H(\omega), \tag{1.9}$$

where ϵ is a real-valued stabilization constant typically set to a small fraction of the maximum value of $|E(\omega)|^2$. The stabilization constant has to be chosen with care to prevent boosting the noise in the data.

1.3.1. HARMONICS

Nonlinearities of the vibrator, the ground and/or their contact cause the extra generation of other frequencies than the intended fundamental frequency. Typically, these harmonics are observed as positive integer multiples of the fundamental frequency (the higher harmonics), but different ratios, like subharmonics, can be observed in some cases as well Stiller *et al.* (2012). The effect of higher harmonics on vibrator data was described in detail by Seriff and Kim (1970). The main problem with harmonics is that they make the seismic wavelet self-similar.

This self-similarity reduces the ability to compress the wavelet in processing and produces ghost event/arrivals. To illustrate this, Figure 1.3 shows three compression situations of a linear upsweep with and without harmonics. In the top-most example I the autocorrelation of the sweep is plotted. In that case the compression is perfect and produces a central peak (Figure 1.3a I) without signal being present at larger correlation lags (Figure 1.3b I). When the sweep is contaminated with harmonics, example II, the cross correlation of the sweep-without-harmonics with the sweep-with-harmonics results in the same central peak (Figure 1.3a II), but also noise is introduced at earlier times (Figure 1.3b II). If the source signal is measured accurately enough the correlation approach can be replaced with a deconvolution approach to compress the wavelet. Example III presents the "autodeconvolution" of a sweep-with-harmonics. Two observations can be made. First, the presence of frequencies beyond the original spectrum of the sweep itself

help to reduce the width of the central peak (Figure 1.3a III). Second, the self-similarity of the signal causes harmonic noise to occur at negative as well as positive correlation times (Figure 1.3b III), albeit at lower amplitudes when compared with the cross correlation result (example II).

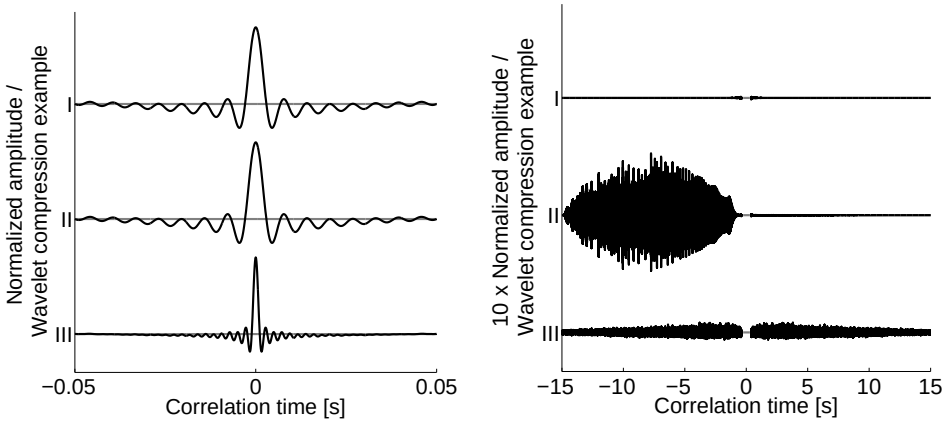

Figure 1.3: Effect of harmonics on a linear 15-s 10-to-160 Hz sweep. Different correlation and deconvolution examples at small (a) and large (b) time lags. In plot b the main peak has been muted ($|t| < 0.4$ s). See text for an explanation of the examples.

1.4. MOTIVATION AND OUTLINE OF THIS THESIS

Although the vibroseis method has successfully been applied for decades, it can still be improved. As elucidated in this chapter the vibrator source should act linearly and be able to produce waves with a known wavelet containing a wide range of frequencies.

In this thesis the possible use of a linear synchronous motor (LSM) to drive a vibrator is studied. This type of electric motor has several advantages over the commonplace hydraulic design. Most importantly the design of an LSM does not put any fundamental restrains on the vibrator's stroke, but may also behave more linear compared with other motors. Using an LSM to drive a vibrator might therefore increase the frequency range as well as reduce the distortion produced by the vibrator. Chapter 2 describes the design and functioning of the LSM prototype vibrator we built.

Some first experiments carried out with this new vibrator are described in Chapter 3. During these experiments it was observed that the coupling of the vibrator with the ground has a large impact on the behavior of the vibrator. Another observation was the nonlinear change of the spectra of the acceleration of the base-plate with changing drive level settings. This nonlinearity with drive level was studied in more detail using a hydraulic vibrator.

The interaction between the vibrator and the ground is one of the causes for the nonlinearity observed in the field. Chapter 4 focuses on the geometry of the contact and shows that even if the base plate and the ground consist of linear-elastic materials, the

geometry of the contact can react in a nonlinear way. This is seen as one reason why the behavior of the vibrator changes with drive level.

Although linear sweeps are commonly used to drive vibrators, they are not the only possible choice. Optimizing vibrator sweeps is the subject of Chapter 5. In that chapter the properties of the sweep signal are described and several means to optimize for certain situations are discussed.

In the last chapter of this thesis, Chapter 6, the topics covered in the other chapters are discussed and an outlook is given.

REFERENCES

L. Cohen, *Time-frequency analysis* (Prentice Hall, 1995).

R. Noorlandt and G. Drijkoningen, *On the mechanical vibrator-earth contact geometry and its dynamics,* Geophysics **81**, P37 (2016).

J. Sallas, *How do hydraulic vibrators work? A look inside the black box,* Geophysical Prospecting **58**, 3 (2010).

A. Seriff and W. Kim, *The effect of harmonic distortion in the use of vibratory surface sources,* Geophysics **35**, 234 (1970).

M. Stiller, K.-H. Jaeckel, and M. Weber, *Effective elimination of subharmonic ghost events from vibroseis data,* Geophysical Prospecting **60**, 1095 (2012).

M. van der Veen, J. Brouwer, and K. Helbig, *Weighted sum method for calculating ground force: an evaluation by using a portable vibrator system,* Geophysical prospecting **47**, 251 (1999).

2

A SEISMIC VERTICAL VIBRATOR DRIVEN BY LINEAR SYNCHRONOUS MOTORS

Rik Noorlandt, Guy Drijkoningen, Johan Dams and Rob Jenneskens

A linear synchronous motor (LSM) is an electric motor that can produce large controllable forces and is therefore suitable as a driving engine for a seismic vibrator. This motor consists of two independent elements, a magnet track and a coil track, allowing practically unlimited motor displacements. This makes the LSM very suitable for expanding the source frequency band to the lower frequencies in which larger strokes are needed. In contrast to hydraulic engines, the LSM performs equally well over the whole frequency range, making possible a smaller amount of signal distortion, especially at the low frequencies. To find the feasibility of an LSM-driven vibrator, we successfully designed and built a multi-LSM prototype vibrator of some 1200 kg. We addressed the synchronization between the individual motor tracks and the different motors. To lower the energy consumption, a spring mechanism was implemented that delivered the force needed to lift the vibrator mass to its neutral position. The resonance belonging to this spring mechanism was successfully suppressed with the help of a position feedback control that also suppressed the temperature effects. The seismic data acquired in the field tests proved that

This chapter has been published as a journal paper in Geophysics, 80(2), EN57–EN67 (Noorlandt *et al.*, 2015) and has received the award for Best Paper in Geophysics 2015. Note that minor changes have been introduced to make the text consistent with the other chapters of this thesis.

the prototype LSM vibrator acted very well as a seismic source. It has no trouble generating pseudorandom sweeps, and even given its limited size, it generated signals within the low-frequency regime, down to 2 Hz, rather easily.

2

2.1. INTRODUCTION

The goal of a seismic vibrator is to exert a controlled time-varying force on the ground. In a basic vibrator, this force is provided by a driving engine that moves some (reaction) mass with respect to a base plate, which is in contact with the ground. To prevent the base plate from decoupling from the ground, a hold-down system might be present to add a static force on the base plate. A more detailed description of seismic vibrators can be found in Baeten and Ziolkowski (1990) and Meunier (2011). Seismic exploration vibrators are typically driven by a hydraulic engine. Although these engines can produce very large forces, the hydraulics put unwanted limitations on the vibrator. The intrinsic nonlinearity of the hydraulic system is one of the causes of the harmonics typically observed with vibrators (Sallas, 2010). Depending on the design, the hydraulic flow rate might (Sallas, 2010) or might not (Wei and Phillips, 2013) limit the output power of the vibrator at low frequencies. At the high end of the spectrum, the output is limited as well, due to the compressibility of the hydraulic fluid (Sallas, 2010). Furthermore, the stroke, the maximal movement of the reaction mass possible, needed for the generation of low frequencies, and the volume and pressure within the hydraulic engine are directly related. Therefore, designing a vibrator with a larger stroke for more output at the low frequencies is not a trivial task.

Another possibility to drive a vibrator, which does not have the intrinsic limitations of a hydraulic system, is using a linear synchronous motor (LSM). An LSM is an electric motor able to generate linear forces and can be found in numerous applications. They are used in factories to move objects in a fast and precise way, but they can also be found in the propulsion system of some magnetic-levitation trains and roller coasters (Veltman *et al.*, 2002). Use of a linear synchronous motor to drive a seismic vibrator is proposed by Unger (2002) and Drijkoningen *et al.* (2006). The work of Drijkoningen *et al.* (2006) led to the development of the prototype LSM vibrator, which is presented in this chapter. The main goal of this LSM vibrator is to show its feasibility as a seismic source. To keep the vibrator practical for research applications, it was kept relatively small, with a weight of about 1 ton and a driving force of about 7 kN. Still, it can well be used for shallow (< 1 km) seismic exploration and is able to generate low frequencies down to 2 Hz at full force. Noorlandt *et al.* (2012) present some of the very first results obtained with this new vibrator.

In this chapter, we describe the design of the prototype LSM vibrator and the issues associated with building it. The operation of a single LSM and the synchronization of the six LSMs in the prototype vibrator is explained in some detail. The supporting structure of the prototype vibrator generates a few resonances, and we clarify their origin and a method to suppress them. Having explained the basic operation of the prototype LSM vibrator, some field data are presented. These data give insight to the harmonic behavior of the vibrator, the type of signals it can produce, and its ability to send out low-frequency signals. In the "discussion" section, we describe the lessons learned and steps to be taken to build an LSM production vibrator.

2.2. DESIGN AND PRINCIPLE OF A LINEAR-MOTOR VIBRATOR

To show the feasibility of an LSM vibrator, a compact design was chosen that does not include a hold-down mass. In this way, the design is simpler and the number of possible elements that distort the signal is reduced. The disadvantage is that the vibrator force is limited to the weight of the reaction mass. Figure 2.1 shows a drawing of the vibrator and its components. Table 2.1 shows the basic properties of the vibrator. In addition to the base plate, reaction mass, and LSMs, it also contains an air spring and a few leaf springs. The air spring supports the reaction mass, thereby greatly reducing the total driving force needed. The leaf springs guide the reaction mass in the vertical direction, constraining the movement of the reaction mass to 1 degree of freedom. The leaf springs provide a cost-effective way to guide the mass without adding any friction. Figure 2.2 shows the prototype vibrator deployed in the field.

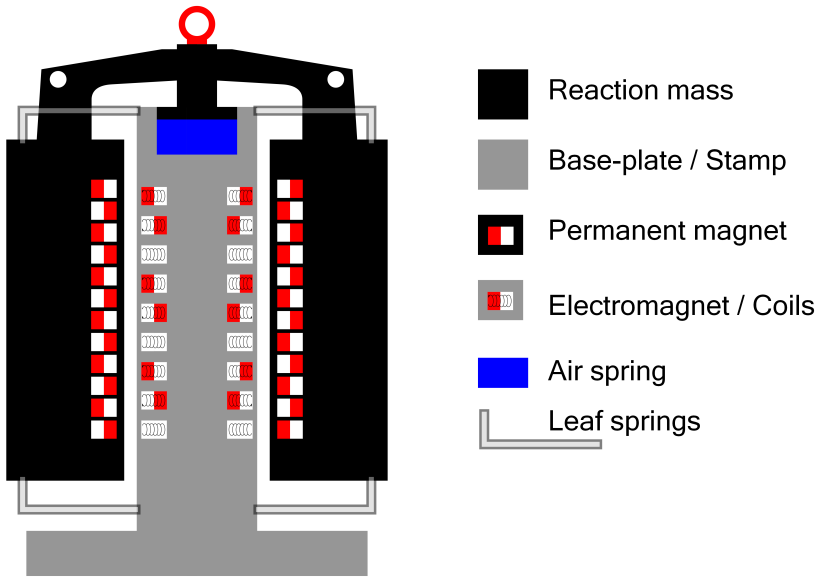

Figure 2.1: A 2D sketch showing the different components of the prototype LSM vibrator.

2.2.1. MECHANICAL MODELING

One of the most important design specifications of the vibrator is its frequency response. The amplitude response should be flat within a certain bandwidth, 2 to 200 Hz for our vibrator. To accomplish this, the dynamic behavior of the vibrator was predicted using finite-element modal analyses. The outcome of the finite-element simulation is used to create a continuous-time state-space model as described by Gawronski (2004), and this model is then used to analyze the frequency response for the (combination of) sensors and actuators. This procedure led to a few changes in the original design, removing some resonances within the frequency band of interest and making other resonances still in

Figure 2.2: Prototype vibrator, based on LSMs, deployed in the field.

Reaction mass	1027 kg
Base plate mass	230 kg
Base plate area	0.5 m^2
Number of LSMs	6
Maximal driving force	6.7 kN
Active stroke	± 42 mm
Lowest frequency at 100% drive level	2 Hz

Table 2.1: Basic properties of the prototype LSM vibrator

that band easier to control. As an example, Figure 2.3 shows the 25-Hz rocking mode of the reaction mass that was clearly visible in one of the early designs. With the help of three, instead of one, vertical accelerometers on the reaction mass, this mode can be measured. This measurement is then used to balance the forces of the actuators, such that this mode is not excited, as will be shown later on.

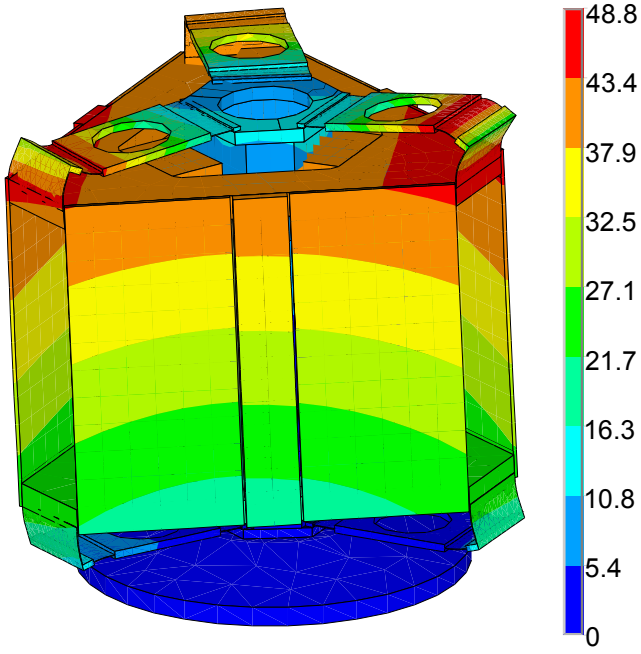

Figure 2.3: Finite-element prediction of the relative displacement of the vibrator at its 25 Hz mode. Displacements are shown at their largest values, and the colors indicate the value of the mass normalized eigenvector (Gawronski, 2004).

Another very important aspect of a vibrator is its stroke, the amount of distance the reaction mass can move up and down. Given the weight of the reaction mass and the maximum force that the driving engine can produce, the stroke fixes the lowest frequency that the vibrator can produce at full force. If the reaction mass would only experience a driving force equal to $F = MA\sin(\omega t)$, where M is the amount of mass, its displacement would follow $U = -\frac{A}{\omega^2}\sin(\omega t)$. In such a case, the displacement is related to the driving force by

$$U = -\frac{F}{\omega^2 M}. \tag{2.1}$$

So, for a fixed driving force and reaction mass, the displacement increases with decreasing frequency. To increase the maximum driving force at a fixed frequency, one has to

increase the stroke, reaction mass, or both. For our prototype vibrator with its stroke, reaction mass, and maximum driving force, as given in Table 2.1, the lowest frequency at full force is approximately 2 Hz, equal to the design specification.

2.2.2. PRINCIPLE OF A LINEAR SYNCHRONOUS MOTOR

An LSM is an electric motor that can be seen as an unrolled permanent magnet synchronous motor. The LSM used in the prototype vibrator consists of a U-shaped permanent-magnet track and a coil track sliding in between, as shown in Figure 2.4. The intercoil and intermagnet distances are chosen such that the same force can be made for any position of the tracks by controlling the current distribution over the different coils. The need for the synchronization of the track positions and the current, together with the fact that the resulting force acts along a line, i.e., is linear, gives these types of motors their name. With this geometry, the motor can drive over any distance needed. Therefore, an LSM-driven vibrator will be able to equally generate low frequencies with a large stroke as high frequencies with a relative small stroke. This is in contrast to hydraulic engines in which fluid flow and dynamics limit and distort the output at low and high frequencies (Sallas, 2010), or single-coil-magnet designs in which the linearity is lost for larger amplitudes (van der Veen *et al.*, 1999).

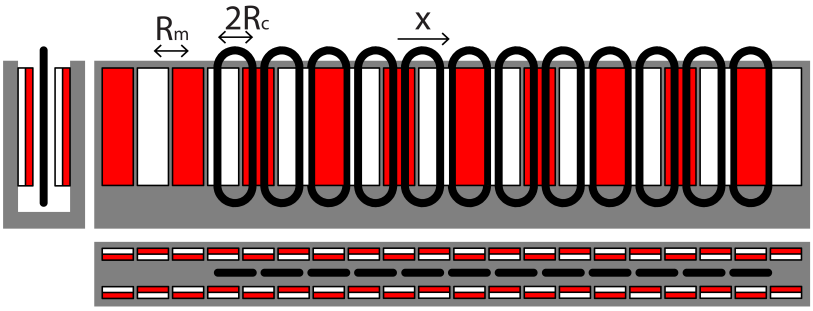

Figure 2.4: Sketch of the geometry inside the LSM motor. The two sides of the permanent magnets are colored in white and red, and the coils are black.

For a Lorentz-type motor, the force produced can be determined with the help of the Lorentz force law,

$$\vec{F} = \int \vec{I} \times \vec{B}\,\mathrm{d}l, \tag{2.2}$$

where $\vec{F}$ is the force produced by the interaction of the current, $\vec{I}$, flowing through the coil, $\int \mathrm{d}l$, inside the magnetic field, $\vec{B}$. In an ideal Lorentz motor, the magnetic field from the permanent magnets is perpendicular to the coil plane as seen in Figure 2.4. In equation 2.2, it is clear that the resulting force will, therefore, be in the plane of the coil. The distances between the straight parts of the coil $2R_C$ in Figure 2.4 and between the magnets R_m in Figure 2.4 are chosen to be the same. With such geometry, the force on both straight parts of the coil will be in the same direction. The alternating pattern of

the permanent magnets causes the magnetic field strength to vary sinusoidally in the driving direction. It is relatively easy to show that with this setup, the total force on a single coil acts only in the driving direction $\hat{x}$ equal to

$$\vec{F}(I,x) = GI\cos\left(\frac{\pi x}{R_m}\right)\sin\left(\pi\frac{R_c}{R_m}\right)\hat{x}, \tag{2.3}$$

where x is the position of the center of the coil, I is the current flowing through the coil, G is a constant that depends on the magnetic field strength and the shape of the coil, and R_m and $2R_c$ are the distances between the magnets and straight part of the coil, as shown in Figure 2.4. Because $R_m = 2R_c$, the sine term in equation 2.3 is equal to one.

To deal with the dependency on the coil position, multiple coils are used that are shifted by multiples of $\frac{2}{3}R_m$, as shown in Figure 2.4. Together, these coils form three groups for which the total force is

$$\vec{F}(i_1,i_2,i_3,x) = nG\left[i_1\cos\left(\frac{\pi x}{R_m}\right) + i_2\cos\left(\frac{\pi x}{R_m}+\frac{2\pi}{3}\right) + i_3\cos\left(\frac{\pi x}{R_m}+\frac{4\pi}{3}\right)\right]\hat{x}, \tag{2.4}$$

where n is the number of coils per group and i_1, i_2, and i_3 are the currents applied to the different coil groups. To obtain a constant force, the currents applied to these groups need to be commuted with the same phase:

$$\begin{aligned} i_1 &= I\cos\left(\frac{\pi x}{R_m}\right), \\ i_2 &= I\cos\left(\frac{\pi x}{R_m}+\frac{2\pi}{3}\right), \\ i_3 &= I\cos\left(\frac{\pi x}{R_m}+\frac{4\pi}{3}\right), \end{aligned} \tag{2.5}$$

where I is the magnitude of the current. Substituting the currents given by equation 2.5 in equation 2.4 gives

$$\begin{aligned} \vec{F}(I) &= \frac{3}{2}nGI\hat{x} \\ &= KI\hat{x} \end{aligned} \tag{2.6}$$

where K is the so-called motor constant. The total force produced by the motor is thus linearly related to the applied current I. To make the force change over time, like a sweep, one simply divides the desired force-time signal by the motor constant and uses the output as the current input of the motor $I(t) = \frac{F(t)}{K}$.

Of course, there is a limit to the force that a single LSM can produce. Heat generation, proportional to coil resistance times the square of the current, was ignored in the above derivation. The generation of heat and the transport thereof sets the maximum current that the motor can endure before damage occurs and, therefore, sets the maximum force possible. During the design phase of our vibrator, the LSMs were carefully selected, balancing the maximum force, maximum stroke, efficiency, linearity, heat dissipation, and amplifier specifications. With the current motors and cooling design, the vibrator can be used continuously.

2.2.3. COIL-MAGNET TRACK SYNCHRONIZATION

For the LSM to work efficiently, the currents as expressed in equation 2.5 need to be in-phase with the cosine terms in equation 2.4. Therefore, the displacement of the coils with respect to the magnetic field x needs to be known, but the only displacement measurement available is between the reaction mass and base plate u. This measured displacement has an unknown offset Δ relative to x that needs to be determined to be able to generate the currents of equation 2.5.

To find Δ, two currents, or forces if one multiplies with the motor constant K, are applied to the motor coils at the same time. The first set of currents applied to the coils is equal to the currents in equation 2.5, except that they are commuted with respect to the known u instead of the unknown x. The second set of currents applied to the coils are used to distort the motor behavior. They have a similar shape but a different amplitude and an extra phase offset α:

$$\begin{aligned} i_1 &= I_A \cos\left(\frac{\pi}{R_m}u\right) + I_B \cos\left(\frac{\pi}{R_m}u + \alpha\right), \\ i_2 &= I_A \cos\left(\frac{\pi}{R_m}u + \frac{2\pi}{3}\right) + I_B \cos\left(\frac{\pi}{R_m}u + \frac{2\pi}{3} + \alpha\right), \\ i_3 &= I_A \cos\left(\frac{\pi}{R_m}u + \frac{4\pi}{3}\right) + I_B \cos\left(\frac{\pi}{R_m}u + \frac{4\pi}{3} + \alpha\right), \end{aligned} \tag{2.7}$$

Substituting the currents given by equation 2.7 in equation 2.4 and making use of the fact that $u = x + \Delta$ gives

$$\overrightarrow{F}(I_A, I_B, \alpha) = K I_A \cos\left(\frac{\pi\Delta}{R_m}\right)\hat{x} + K I_B \cos\left(\frac{\pi\Delta}{R_m} + \alpha\right)\hat{x}. \tag{2.8}$$

The first term is the force of equation 2.6, but the motor efficiency to convert electric current to force is reduced depending on the value of Δ. Although the conversion efficiency of I_A is fixed, the efficiency of converting the distortion current I_B to force can be controlled with the phase offset α. This can be used in a few ways to find Δ. For our vibrator, we keep I_B constant and vary α while a position controller is used to keep the reaction mass at the same position by changing I_A. Assuming that the motor force is constant at that fixed position, a change of α is completely compensated for by the controller current I_A. Therefore, by fitting multiple realizations of I_A for different α, as shown in Figure 2.5, it is possible to determine the unknown $\frac{\pi\Delta}{R_m}$ up to a multiple of 2π. With this, we can calculate x and apply the currents given in equation 2.5, maximizing the output of the LSM.

2.2.4. MULTIPLE MOTOR SYNCHRONIZATION

Depending on the desired driving force, multiple LSMs need to work in parallel. The motors cannot all be placed at the center of the vibrator and will, therefore, produce a moment with respect to the center of gravity. In our prototype vibrator, the motors are placed symmetrically, so that if they produce an equal force, all the moments cancel and only a net vertical force is left over. The motors and amplifiers are, however, not equally strong by default.

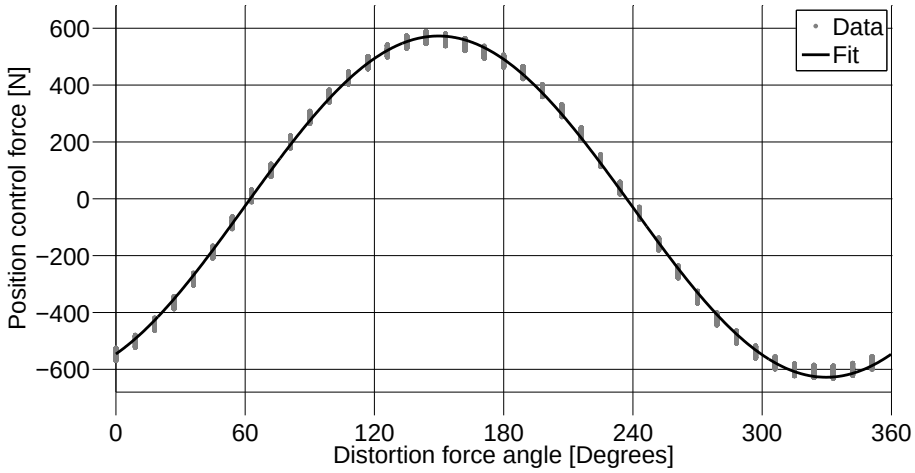

Figure 2.5: Position control force KI_A versus distortion angle α. The dots are measured data, and the line is the fit through these dots.

To find the correct gain for each amplifier-motor pair, use is made of three accelerometers located at the three edges of the reaction mass together with the rocking mode at 25 Hz as predicted by finite-element analysis (Figure 2.3). The rocking mode is clearly visible on the reaction-mass accelerometers, as shown in Figure 2.6, when the forces produced by the different LSMs are not balanced.

A grid search was performed varying the three motor gains between 90% and 100% to find gain values for which minimal rocking occurs and the forces from the linear motors are thus balanced. The results of the grid search are presented in Figure 2.7. It is clear that the minimum amount of rocking occurs if the gains of amplifier-motor pair 2 and 3 are reduced (Figure 2.7a). This means that for equal input, the force produced by the first amplifier-motor combination is less than that of the other two amplifier-motor combinations. Balancing the motor forces reduces the maximum average difference between the accelerometers' amplitude spectra by a factor of five and the different accelerometer signals are much more alike, as shown in Figure 2.8.

2.2.5. AIR SPRING SUPPORT

To avoid lifting the reaction mass to its neutral position with the LSMs and waste energy, a choice has been made to use an air spring between the reaction mass and base plate. The use of an air spring to bias the reaction mass to the center of its displacement range is also commonly found in hydraulic vibrators. If a hold-down mass is present, it is typically isolated from the base plate with an air spring as well. In both cases, the purpose of the air spring is to transfer the force at DC, without affecting the frequencies in the seismic band.

The force produced by the air spring can be predicted from the ideal gas law. The air spring can be approximated by a closed cylinder with a volume V, for which the ideal

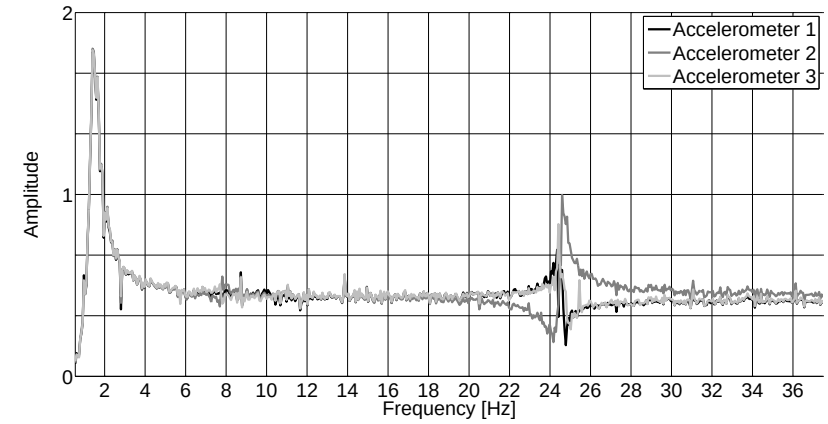

a

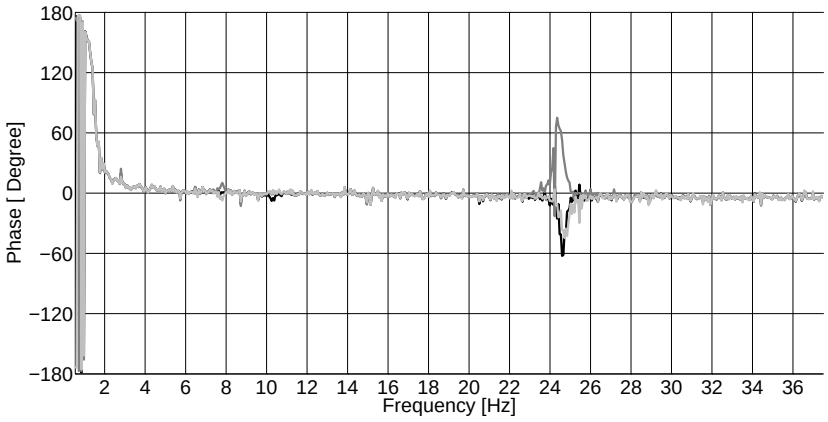

b

Figure 2.6: Example of the (a) amplitude and (b) phase response measured by the three reaction-mass accelerometers, when the three motor forces are unbalanced.

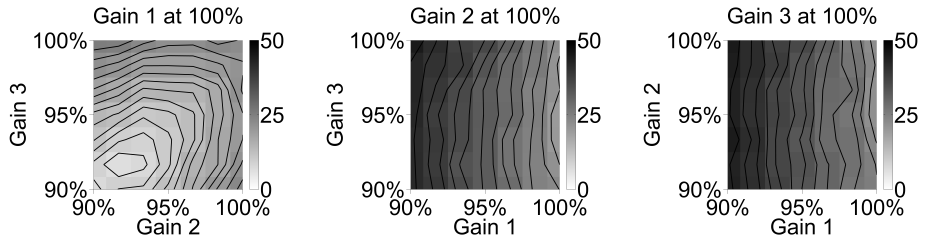

a b c

Figure 2.7: Influence of the amplifier-motor gain distribution on the difference among the reaction-mass accelerometers' responses. Colors indicate the sum of the absolute difference between amplitude spectra of each pair of reaction-mass-accelerometer signals between 20 and 30 Hz. Each panel shows the result of scanning two gains, and the third one was kept at 100%.

gas law states that

$$\frac{pV}{T} = k, \tag{2.9}$$

where p is the pressure, T is the absolute temperature inside the cylinder, and k is a constant determined by the gas properties. The force the air spring exerts on the reaction mass is then given by

$$F = k\frac{T}{h}, \tag{2.10}$$

where h is the height of the cylinder. Equation 2.10 is only valid as long as the cylinder can be compressed without changing its diameter or contact area with the reaction mass. A Taylor expansion around the neutral cylinder height h_0 gives

$$F = \frac{kT}{h_0} - \frac{kT}{h_0^2}(h-h_0) + \frac{kT}{h_0^3}(h-h_0)^2 + \mathcal{O}((h-h_0)^3) \qquad |h-h_0| < 1, \tag{2.11}$$

where use was made of the fact that the reaction-mass displacement is related to the cylinder height, through $(h-h_0)$. From equations 2.10 and 2.11, it is clear that the air spring behaves nonlinearly as a function of h and is temperature dependent.

The air spring for the prototype vibrator was selected such that the first Taylor term compensates for the gravity force, the resonance frequency of the spring is below 2 Hz, it has low damping, and it meets certain safety regulations. Although the resonance itself is outside the designed bandwidth, at approximately 1.5 Hz, it still has a significant influence to the response up to some 6 Hz, as can been seen in Figure 2.8.

2.2.6. SUPPRESSING SUPPORT SPRING RESONANCE AND TEMPERATURE EFFECTS

Because the spring resonance frequency is low, the driving force at this frequency must be limited to prevent exceeding the available stroke. To suppress the resonance behavior, two different control methods were implemented.

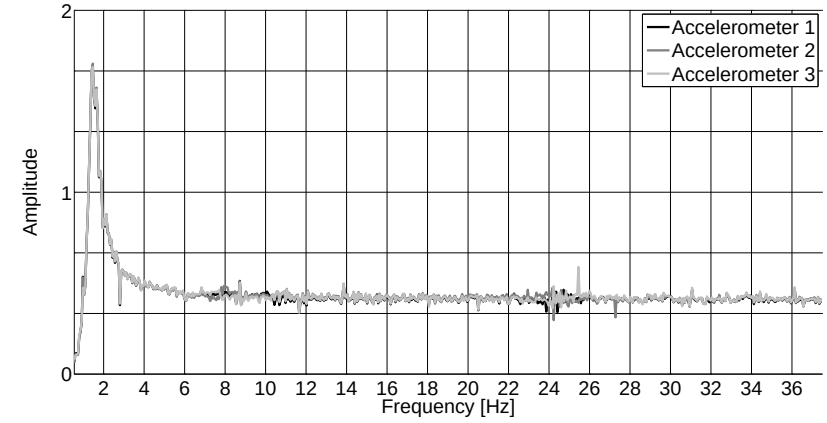

a

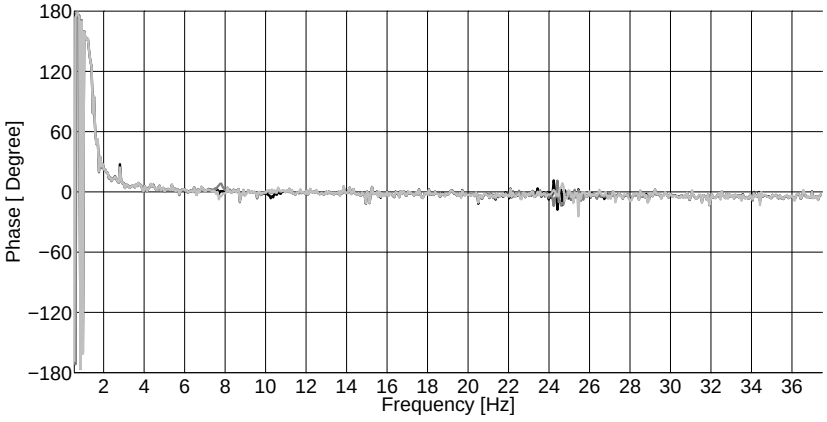

b

Figure 2.8: (a) Amplitude and (b) phase response measured by the three reaction-mass accelerometers, when the three motor forces are balanced. Note that, comparing these results with that of Figure 2.6, the air spring resonance at approximately 1.5 Hz is not affected by motor balancing, whereas the rocking mode at approximately 25 Hz is.

First, a feed-forward control was tried, changing the driving force in advance to anticipate the spring response. Although this method is theoretically more stable than the feedback method described below, it was not successful in suppressing the resonance. This mainly had to do with the hysteresis of the air spring, most probably caused by the deformation of the rubber air container, making a prediction of the exact spring force very difficult.

Therefore, use is made of a position feedback control. The position controller changes the driving force in real time such that the reaction-mass displacement follows the prescribed position curve as closely as possible. The position curve is calculated beforehand based on the pilot and desired dynamics. To prevent base-plate resonance signals from getting into the control loop, the position control is only active for low frequencies. With this setup, the LSMs try to remove any low-frequency influence the springs have on the system. A nice side effect of using a position feedback is that any temperature effect of the air spring, as described previously, is also suppressed by this controller.

As an example, the position feedback controller was used to make the reaction mass move as if gravity and the spring forces were absent, and the only force acting was the force from the LSMs. In that case, the position controller suppresses the behavior of the springs. The reaction-mass displacement belonging to the driving force only can be found by dividing the sweep force by the reaction mass and integrating it twice. We simply used the trapezoidal method on the heavily oversampled time signal for this. Figure 2.9 shows reaction-mass displacement without and with the position controller active. It is clear that, for this example, the displacement amplitude caused by the support system is larger than that of the LSMs. When the position controller is active, as shown in Figure 2.9b, the LSMs suppress the spring behavior very well. The reaction-mass displacement follows the prescribed position curve closely, and the average absolute difference between the two curves is reduced by a factor of approximately 160.

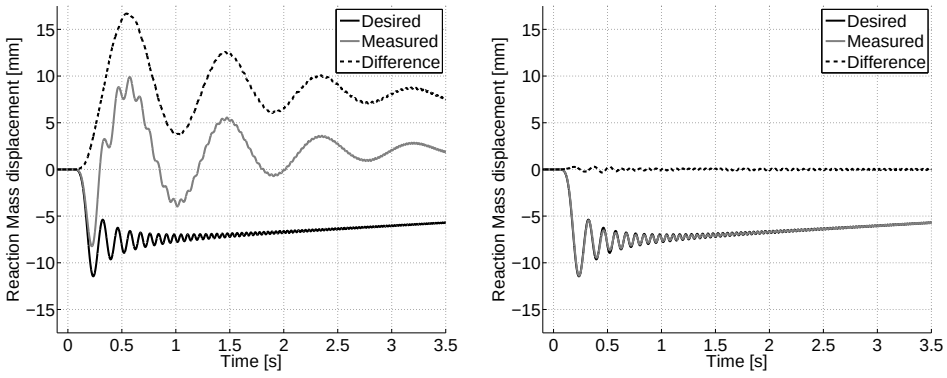

Figure 2.9: The first 3.5 s reaction-mass displacement for a 12-s linear sweep from 2 to 160 Hz. (a) Without position feedback control and (b) with position feedback control.

2.3. FIELD CASE

To show the seismic performance of the vibrator, we carried out some field tests at a seismic-monitoring site in the northeast of the Netherlands. At this site, 4C sensors, each equipped with a 3C geophone and one hydrophone, are buried at a fixed level with respect to the geoid at approximately 50 m below the surface. In this chapter, only the data from the hydrophones and vertical component of the geophones are presented. During the field tests, we also temporarily installed a few surface geophones. All the recorded data were correlated with the pilot signal. This was done to keep all distortion caused by the vibrator visible in the seismic records. It also prevented any noise from the accelerometers to propagate into the records. The accelerometer's measurements, however, are used to show the harmonic and low-frequency behavior of the vibrator.

2.3.1. REGULAR LINEAR SWEEP

The most common signal to drive a seismic surface vibrator is the linear upsweep, in which the frequency of the driving sinusoid is increased linearly with time. The signal is tapered or faded at both ends to avoid step behavior. Figure 2.10 shows the seismic record obtained with a 10-s linear sweep from 5 to 200 Hz, after being correlated with the pilot channel.The buried geophones and hydrophones show the direct arrival and a few reflections. Even though the geophones are at an approximately 50-m depth, they still pick up Rayleigh-wave energy. The hydrophones have a different sensitivity and, therefore, their record is less noisy and does not show the Rayleigh-wave arrival that strongly. Both records have some ringing, which indicated that the correlation with the pilot signal is not fully compressing the source wavelet in the seismic data.

2.3.2. HARMONICS

Signal distortion is an important issue with seismic vibrators. Especially the generation of harmonics is a common and difficult problem (Seriff and Kim, 1970). For a linear upsweep, the energy of the harmonics is mapped to earlier arrival times, possibly masking earlier events. To investigate the distortion and harmonics of the prototype vibrator, the acceleration of the reaction mass (average of the three sensors), the acceleration of the base plate, and the weighted-sum ground force are used. The weighted-sum ground force (Castanet and Lavergne, 1965; Sallas, 1984) estimates the force that the vibrator exerts on the ground by summing the acceleration of the reaction mass and base plate, weighted with their masses. In a rigid 1D approximation, the reaction mass only experiences the force from the driving engine, whereas the base plate experiences the force from the driving engine (with opposite sign) as well as the force from the ground. By summing, one thus removes the influence of the engine and is left with the force on the ground only.

It is expected that LSMs produce less harmonics compared with hydraulic engines because they act more linearly. The mechanics and ground coupling, however, also generate harmonics. Therefore, the influence of the driving engine alone on the total signal distortion cannot be determined.

Figure 2.11 shows the time-frequency analysis for the pilot signal, the measured accelerations, and the weighted-sum ground force. Next to the designed signal, these plots also show energy at other times and frequencies. The harmonics of the weighted-sum

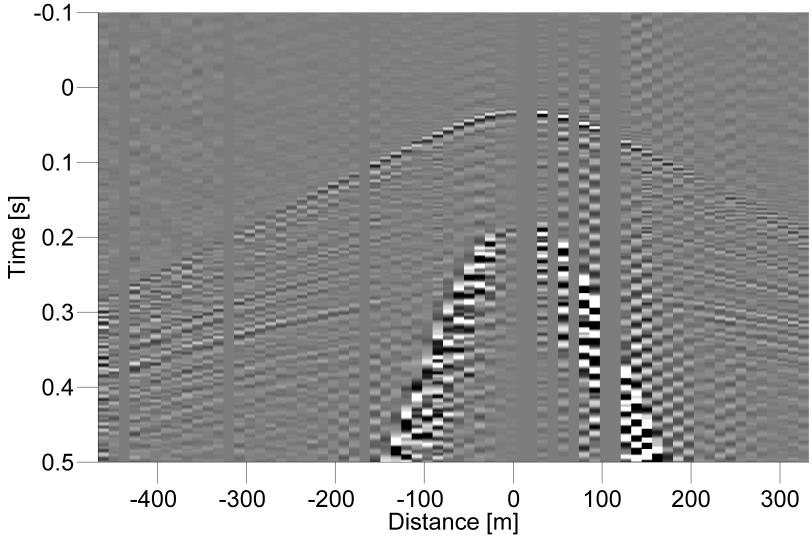

a

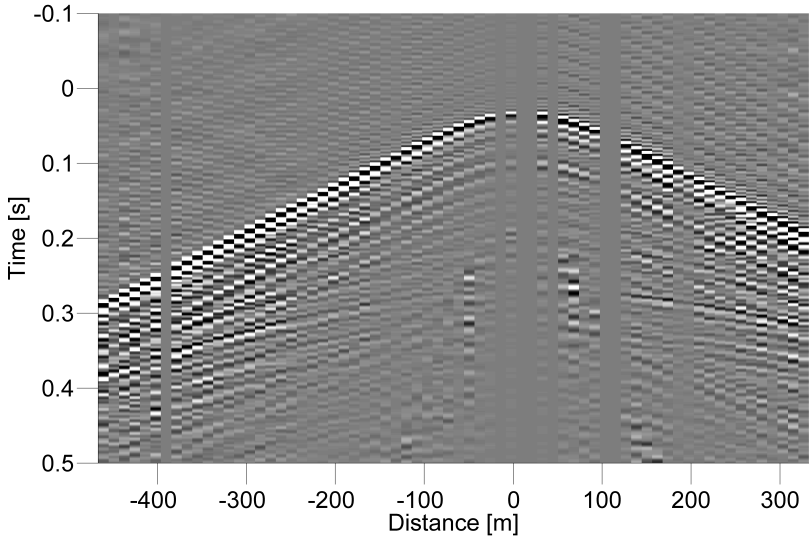

b

Figure 2.10: Seismic records obtained at 50-m depth with a 10-s linear sweep from 5 to 200 Hz. Vertical-geophone data shown in panel (a), Hydrophone data shown in panel (b). (Dead traces are blanked.)

ground force, Figure 2.11b, are on the order of 20 dB lower than the fundamental signal at all frequencies, including the lower. If we look at the signals that make up the weighted-sum ground force, the reaction-mass acceleration, shown in Figure 2.11c, and base-plate acceleration, shown in Figure 2.11d, we see that most of the weighted-sum ground-force harmonics originate from the base-plate acceleration signal. The reaction-mass harmonics are at approximately -30 dB, whereas the base-plate harmonics are already visible at -20 dB. This shows that the LSMs have a limited contribution to the harmonics found in the weighted-sum ground force. Most of the harmonics are coming from the base plate, which might be caused by the ground coupling. It is striking that the recorded pilot signal, shown in Figure 2.11a, shows harmonics as well, although these are not in the designed pilot signal. These harmonics are probably caused by the electromagnetic (EM) interference between the amplifiers and our recording equipment. If this is the case, part of the harmonic energy observed with the accelerometers actually does not originate from the movement of the masses.

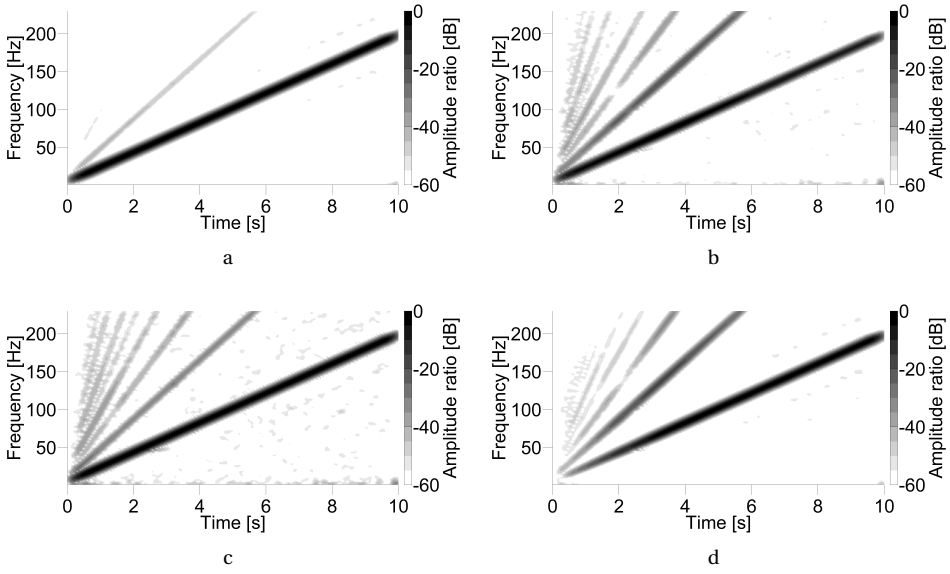

Figure 2.11: (a) Time-frequency plot of the pilot signal, (b) weighted-sum ground force, (c) reaction-mass acceleration (after time averaging the three sensors), and (d) base-plate acceleration.

2.3.3. OTHER DRIVING SIGNALS

The first step in processing the seismic records obtained with a vibrator is removing the phase of the source signal from the seismic response, thus compressing the record as if the vibrator had sent out a zero-phase wavelet. The phase of the source wavelet, therefore, can be changed at will, without affecting the seismic record. This opens up the possibility to design signals with specific properties. One of these properties might be designing multiple signals that are orthogonal to each other, i.e., have low crosscorrela-

tion. With such signals, multiple seismic vibrators could work simultaneously, reducing the acquisition time tremendously. Pseudorandom signals (for an overview, see Dean, 2014) can be designed to have such properties. One of the reasons why pseudorandom signals are not used that frequently is the difficulty to transmit them by (hydraulic) vibrators (Dean, 2014).

To show that the LSM vibrator has no problem with producing this kind of signal, we randomized the phase of a linear upsweep and compared the seismic records obtained with the original sweep and randomized one. The signals are shown in Figure 2.12. Because the amplitude spectra are the same, both signals have the same autocorrelation. However, the time and time-frequency behaviors are quite different. In the time domain, the envelopes of both signals are quite different, and the randomized sweep shows peaks that are approximately three times larger than the amplitude of the linear sweep. Although there is a simple one-to-one mapping from time to frequency for the linear sweep, there is no such relation for the randomized signal as is visible in the time-frequency plot. Figure 2.13 shows the obtained buried-geophone records. Because we maximized the force to approximately 6 kN, while keeping the amplitude spectra the same, the time-domain peaks of the randomized signal cause the seismic signal-to-noise ratio to be lower than the records as shown in Figure 2.10. The reflections are, however, still visible in Figure 2.13a and 2.13b. The difference between the records is minimal and was most likely caused by the difference in noise and the ability to fully compress the source wavelet by correlation with the pilot signal.

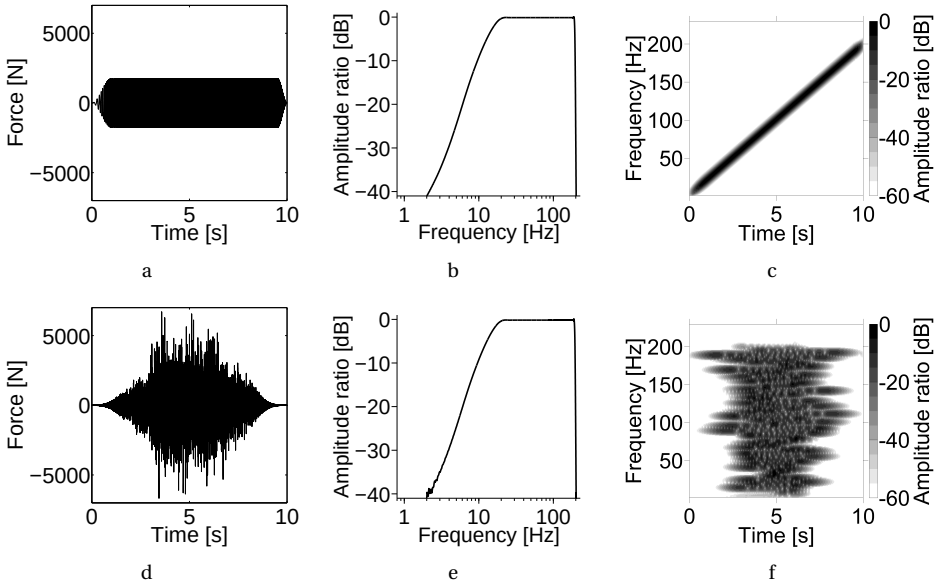

Figure 2.12: Regular linear upsweep (top) and a power-spectrum equivalent pseudorandom signal (bottom). (a and d) Time-domain Signal, (b and e) Amplitude spectra, and (c and f) time-frequency plot. Seismic records belonging to these signals are shown in Figure 2.13.

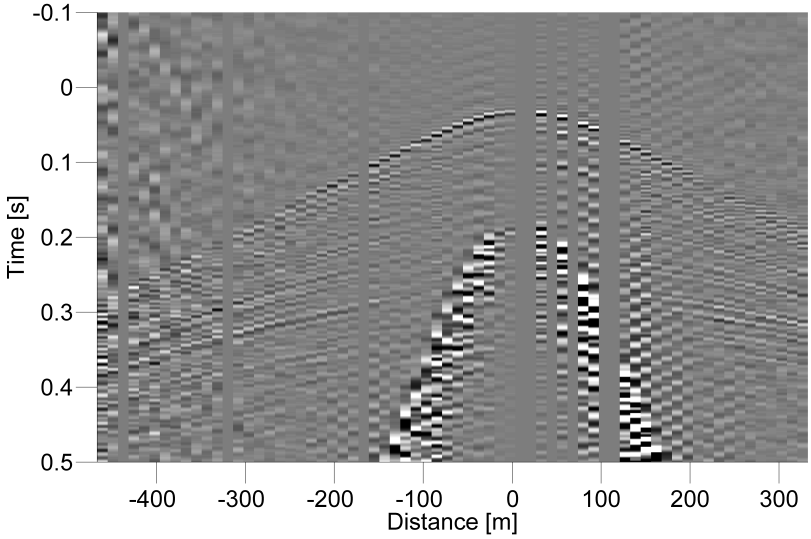

a

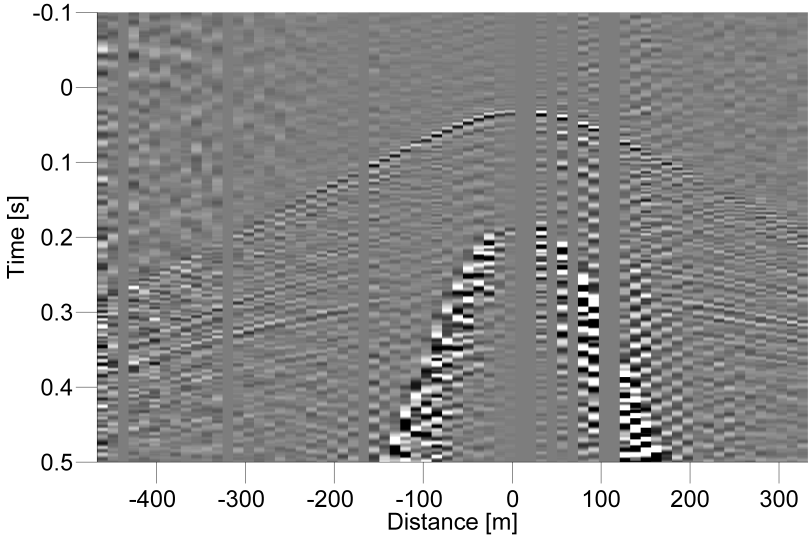

b

Figure 2.13: Seismic records obtained with the vertical geophones at a 50-m depth. (a) Response of the regular sweep and (b) the response of the pseudorandom signal. (Dead traces are blanked.)

To show the ability of the vibrator to send low frequencies, a randomized phase signal with a very steep slope in the amplitude spectrum was designed. This slope makes it possible to have a strong signal at 2 Hz without having the air-spring resonance consume all of the available stroke. A maximal force of approximately 6 kN was used again. The spectra measured at the vibrator, shown in Figure 2.14, show that the reaction mass (Figure 2.14c) follows the designed signal (Figure 2.14a) closely. Because we do not apply feedback on the weighted-sum ground force, the base-plate acceleration (Figure 2.14d) changes the weighted-sum ground force spectra (Figure 2.14b) at the higher frequencies. Figure 2.15 shows the mean ambient noise spectra recorded with the surface geophones and the response curves belonging to these geophones. From this, it is clear that a larger amount of energy of the vibrator is needed for low frequencies to overcome the ambient noise level and lower geophone response. Figure 2.16 shows the seismic record acquired with the low-frequency signal of Figure 2.14. Note that no correction was applied for the geophone response. Different low-pass filters were applied to the data. Figure 2.16a shows the record without applying a low-pass filter. In Figures 2.16b-2.16d, low-pass filters with a cut-off at 4, 6, and 8 Hz were applied. Most ambient noise enters the record from the right as is clearly visible below the surface wave in the 4 Hz version of the record, possibly originating from the road and farms on that side of the line. The surface waves from the LSM vibrator are visible in all versions of the record, but with increasing filter bandwidth, they become more dominant with respect to the ambient noise, as is expected from Figure 2.15.

2.4. DISCUSSION

As with every prototype, one gains much insight going through the process of actually building and testing it. Many choices were made and reconsidered during the design and building phase of the vibrator presented. With the knowledge that we now have, we would make two choices differently. First, we would use an air spring with a larger volume, increasing h_0 in equation 2.11. By doing so, the vibrator would need to get a different safety certification, but the mechanical resonance frequency would be lower and the temperature sensitivity would be smaller. This would allow for easier generation of low frequencies, with less need of a position controller. We would also opt for a different type of amplifier and change the wiring of the system. In the current prototype, six pulse-modulated amplifiers are used to power the LSMs. These amplifiers generate the currents needed by switching on and off a high-voltage source at 20 kHz. This binary high-voltage sequence is then smoothed by passing it through a low-pass filter before it goes to the LSM. These types of amplifiers are very efficient, but the drawback is that they generate EM noise. This EM noise, together with how the vibrator is wired, causes signal distortion that is picked up by the accelerometers. With better amplifiers, the harmonics visible in Figure 2.11 can be reduced significantly. This is supported by data from a smaller LSM vibrator recently built (see Drijkoningen and Noorlandt, 2014). That vibrator does not have an air spring because the movement is perpendicular to the gravity force. It only contains two LSMs to drive the reaction mass and uses linear amplifiers to drive them. The harmonics observed with this vibrator, as shown in Figure 2.17, are extremely small: The recorded pilot signal is free of harmonics, and the harmonics visible in the weighted-sum ground force signal are 30 dB below the fundamental sig-

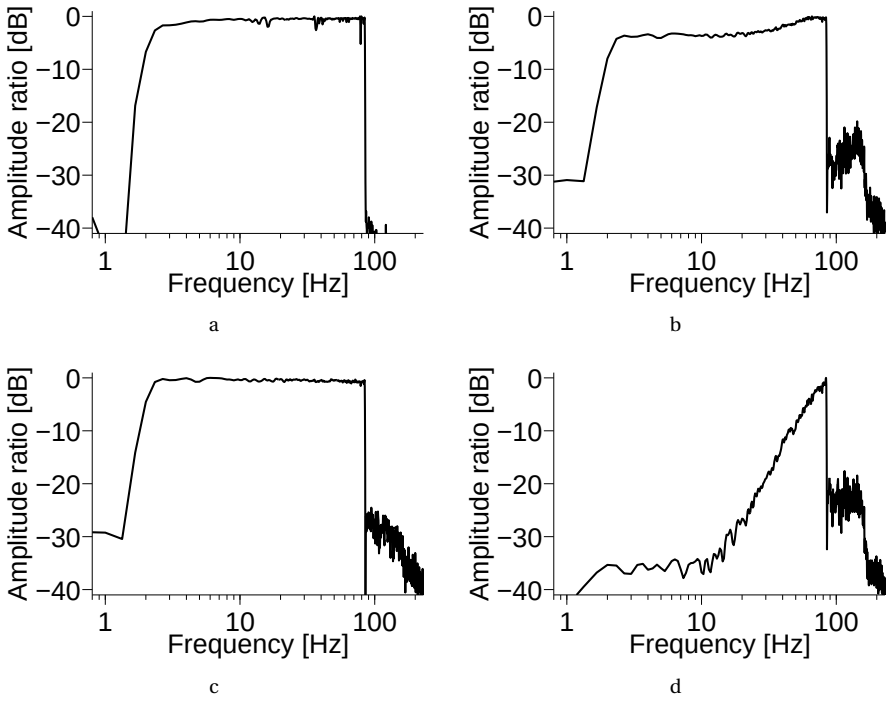

Figure 2.14: Pseudorandom signal with a very sharp low cut in the frequency domain. (a) Pilot signal, (b) weighted-sum ground force, (c) reaction-mass acceleration (after time averaging the three sensors), and (d) base-plate acceleration. The seismic record belonging to this signal is shown in Figure 2.16.

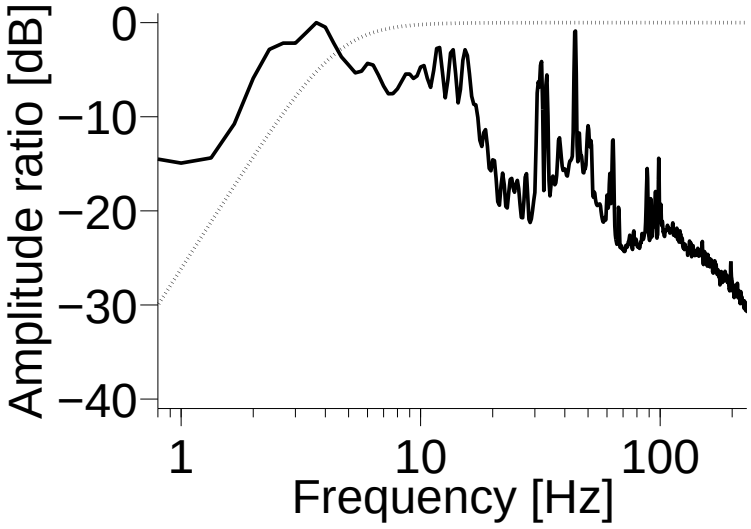

Figure 2.15: Spectra of the background noise (solid line) and the 4.5-Hz geophone response (dashed line).

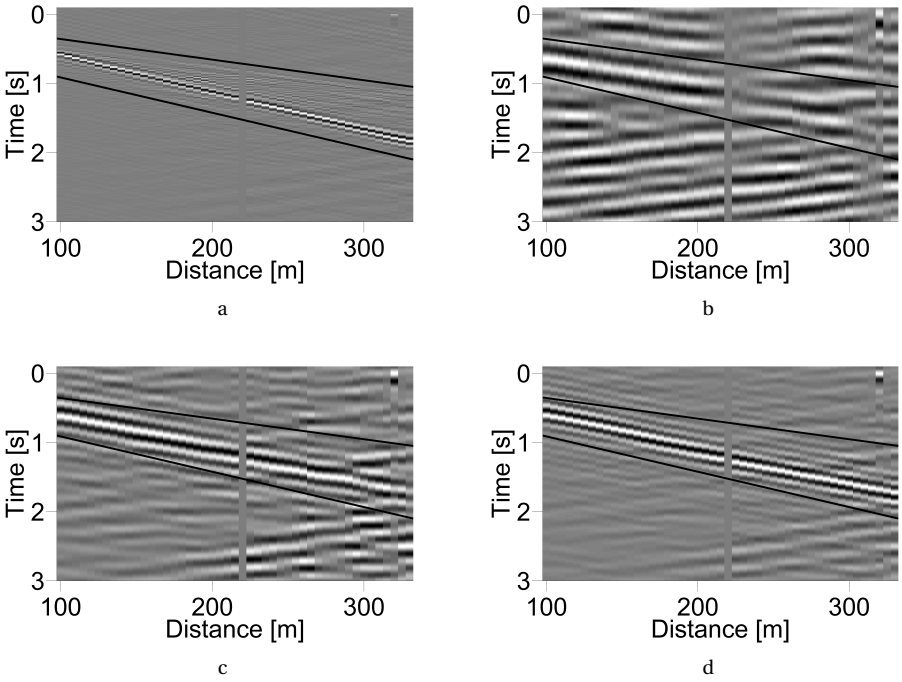

Figure 2.16: Seismic waves as recorded by the surface geophones using the signal shown in Figure 2.14. (a) Unfiltered, (b) low pass up to 4 Hz, (c) low pass up to 6 Hz, and (d) low pass up to 8 Hz. Surface waves coming from the vibrator are marked with a black line above and below their arrival. (Dead traces are blanked.)

nal. These harmonics completely come from the base plate because the reaction mass is free of harmonics up to -80 dB. The low-frequency distortion originates from the support springs and has an amplitude of -45 dB. This shows that LSM-driven vibrators can indeed reproduce a designed wavelet, including the low frequencies, faithfully.

The main purpose of our prototype LSM vibrator is to show the feasibility of an LSM-driven vibrator. The current vibrator can be used for shallow monitoring studies (Arts *et al.*, 2013). For deeper targets (deeper than 1 km or so) and larger offsets, the current force is not large enough. To upscale, more or stronger LSMs would be needed. They are readily available, but the circular design might not be well suited to position a large number of LSMs. The radius of the vibrator has to increase, which makes it more sensitive for rocking due to the longer leaf springs and the increased moments of the engines. A rectangular design could be more suitable in that case. Depending on the frequency range desired, the stroke and reaction mass should be changed as well. If the source should be used for exploration depths of a few kilometers, with a lot of source positions, the portability should be enhanced as well. The prototype vibrator can be lifted as soon the base plate is manually locked to the reaction mass. This locking should be made automatically, or one should change the base plate such that it can be lifted directly to reduce time needed to reposition the source. Of course, having a dedicated vibrator truck, as typical exploration vibrators have, would allow operation in the field to speed up even more.

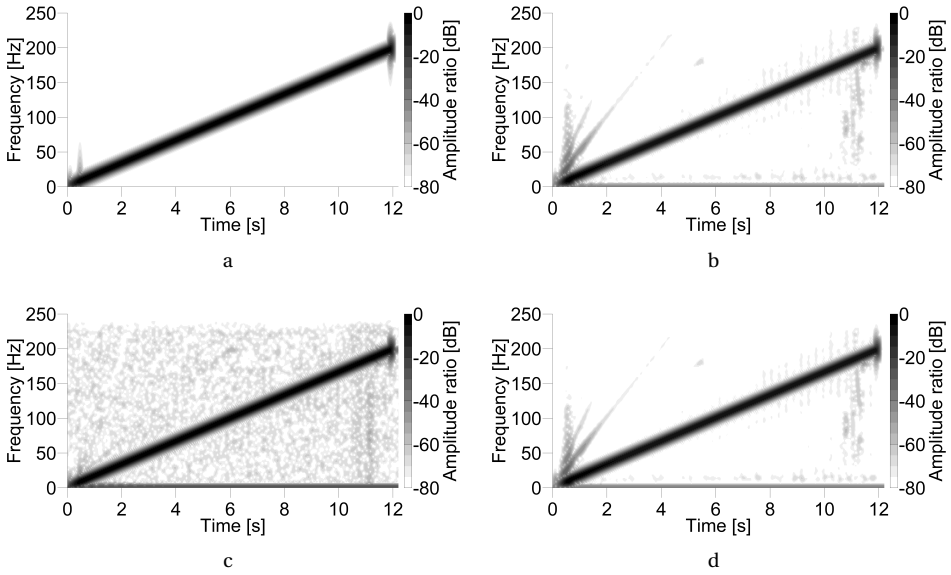

Figure 2.17: Time-frequency plot of the (a) pilot signal, (b) weighted-sum ground force, (c) reaction-mass acceleration, and (d) base-plate acceleration obtained with a small LSM vibrator (Drijkoningen and Noorlandt, 2014). Note that the color scale extends to -80 dB in contrast to the -60 dB scale used in Figure 2.11.

2.5. CONCLUSION

LSMs can be used to drive a seismic vibrator. We successfully designed and built a prototype LSM vibrator, with which we acquired good seismic data using a wide range of signals. The prototype LSM vibrator easily generates low-frequency signals as well as pseudorandom signals, which makes it a good candidate for simultaneous sweeping. The difference between an LSM and a hydraulic engine was explained, and the steps to be taken to build a production version were discussed.

REFERENCES

R. Arts, X. Zhang, A. Verdel, D. Santonico, J. Meekes, R. Noorlandt, B. Paap, and V. Vandeweijer, *Experiences with a permanently installed seismic monitoring array at the CO_2 storage site at Ketzin (Germany), A status overview,* Energy Procedia **37**, 4015 (2013).

G. Baeten and A. Ziolkowski, *The vibroseis source* (Elsevier, 1990).

A. Castanet and M. Lavergne, *Vibrator controlling system,* US Patent 3,208,550 (1965).

T. Dean, *The use of pseudorandom sweeps for vibroseis surveys,* Geophysical Prospecting **62**, 50 (2014).

G. Drijkoningen, A. Veltman, W. Hendrix, K. Faber, J. Brouwer, and G. Hemstede, *A linear motor as seismic horizontal vibrator,* 68th EAGE Conference and Exhibition, P072 (2006).

G. Drijkoningen and R. Noorlandt, *Pseudorandom signals and EM-type seismic vibrators,* Nederlands Aardwetenschappelijk Congres 12 (2014).

W. Gawronski, *Advanced structural dynamics and active control of structures* (Springer, 2004).

J. Meunier, *Seismic acquisition from yesterday to tomorrow* (Society of Exploration Geophysicists, 2011).

R. Noorlandt, G. Drijkoningen, and R. Schneider, *A seismic vertical vibrator driven by linear motors,* 74th EAGE Conference and Exhibition, P061 (2012).

R. Noorlandt, G. Drijkoningen, J. Dams, and R. Jenneskens, *A seismic vertical vibrator driven by linear synchronous motors,* Geophysics **80**, EN57 (2015).

J. Sallas, *Seismic vibrator control and the downgoing P-wave,* Geophysics **49**, 732 (1984).

J. Sallas, *How do hydraulic vibrators work? A look inside the black box,* Geophysical Prospecting **58**, 3 (2010).

A. Seriff and W. Kim, *The effect of harmonic distortion in the use of vibratory surface sources,* Geophysics **35**, 234 (1970).

R. Unger, *A seismic transmission system for continuous monitoring of the lithosphere: A proposition,* Ph.D. thesis, TU-Delft (2002).

M. van der Veen, J. Brouwer, and K. Helbig, *Weighted sum method for calculating ground force: an evaluation by using a portable vibrator system,* Geophysical prospecting **47**, 251 (1999).

A. Veltman, P. van der Hulst, M. Jonker, and J. van Gurp, *Control of a 2.4 mw linear synchronous motor for launching roller-coasters,* Proceedings of the 17th International Conference on Magnetically Levitated Systems and Linear Drives, PP07301 (2002).

Z. Wei and T. F. Phillips, *On the generation of low frequencies with modern seismic vibrators,* Geophysics **78**, WA91 (2013).

3

EXPERIMENTS ON THE BEHAVIOR OF VIBRATORS

In this chapter we show the influence of the coupling conditions, sweep rate and drive level on the behavior of a vibrator and the spectra it generates. Just after the prototype LSM vibrator, described in the previous chapter, was built, several field tests near Schoonebeek were performed. These tests, among others, consisted of placing different mats between the vibrator and the ground, performing the same sweep at different drive levels and sweep over the same frequency range with different sweep rates. These experiments showed that coupling mats and drive level change the shape of the vibrator's spectral amplitude, while the sweep rate scales the spectrum uniformly. The change with drive level was investigated in more detail in another experiment using a hydraulic driven exploration vibrator, able to generate forces up to 266 kN. So a much wider range of drive levels could be studied. From this second dataset we conclude that: the vibrator signal is very repeatable for a given drive level and fixed position; the repeatability of smaller drive levels is reduced when higher drive levels are performed in between; the ground-base plate interaction depends on the drive level in a nonlinear way and not taking these effects into account produces arrival-time and amplitude errors in seismic records.

3.1. INTRODUCTION

Having built the prototype LSM vibrator, described in the previous chapter, one of the first questions was how it would perform in the field. Therefore a series of field tests near Schoonebeek were performed. At the time of the tests a seismic monitoring system was just installed with a large number of buried geophones and hydrophones (Hornman and Forgues, 2013). NAM and Shell kindly allowed us to perform our tests on that location and to use the data recorded. Two of the tests performed will be discussed in this chapter. In the first test presented, (Section 3.2) four different mats were placed between the

Parts of this chapter were presented at the EAGE 2012 Noorlandt *et al.* (2012) and EAGE 2013 Noorlandt *et al.* (2013).

vibrator and the road, showing that coupling significantly affects the vibrator's signal. In a second test (Section 3.3), the effects of changing the power of the signal by changing the drive level, as well as by changing the sweep rate are investigated. What will be shown is that sweep rate controls strength of the amplitude spectra uniformly, while the drive level also changes the shape of the spectra.

The observation that the drive level affects the behavior of the vibrator in a nonlinear way, was further investigated when the three companies; ION, INOVA and Shell, created the opportunity to carry out field experiments with a regular-sized hydraulic-driven exploration vibrator. The experiments were carried out at a test site near Devine, Texas (The University of Texas) and consisted of repeating multiple series of sweeps with different drive levels at two different locations. The advantages of these experiments were that a larger force range could be investigated (up to about 266 kN, compared to the 7 kN of the LSM vibrator), a deep borehole equipped with geophones was available such that the far-field wavelet could be measured and that the location and coupling conditions were different from the experiments performed with the LSM vibrator. The results of the drive-level experiments with the hydraulic-driven vibrator will be discussed in Section 3.4.

3.2. INFLUENCING GROUND-VIBRATOR COUPLING BY MATS

During data acquisition, the base plate of the LSM vibrator needed to be protected from the tarmac it was placed on. Because the plate is made out of aluminum, it was expected that the unevenness of the tarmac would cause very high point stresses on the base plate that would leave their marks. Therefore a thin mat was placed between the vibrator and the ground. Initially no large influence on the behavior of the vibrator was expected, but to be sure four different materials were tried. The materials used were bubble Sof-Tred, polyurethane foam, open cell neoprene and solid rubber. A photo of each mat is presented in Figure 3.1.

Placed on the different mats the vibrator performed the same 30-s linear sweep from 2 to 200Hz at 2000 kN without any feedback loop active. As Figure 3.2 clearly shows our initial expectation was wrong and the mats affect the behavior of the vibrator significantly. Because the sweep was identical for the test with each mat, the curves in Figure 3.2a overlap. For the particular sweep used the overshoot at both the low and high frequency end is about 10%. The weighted-sum ground force spectra (Figure 3.2b) are clearly affected by the choice of mat. The solid-rubber mat produces the flattest spectrum compared to the others, and also produces the smallest amplitudes at frequencies between 60 and 160 Hz. At about 120 Hz the force produced on this mat is only 40% of the one produced on the polyurethane-foam mat. The reaction-mass force spectra (Figure 3.2c) make clear that the mass is not the cause of this change of ground force. The spectra are very similar to the pilot spectra. Note that at the time of these tests no optimization, as described in Chapter 2, of the motor gains or sweep was performed. Therefore the spectra contain more variation in amplitude than the examples shown in Chapter 2. The amplitude increases slightly towards the low end of the spectrum due to the vibrator's air-spring resonance. The step in the amplitude just below 50 Hz is caused by a mode of the reaction-mass and is not affected by the mat used. The variation in amplitude around 130 Hz is caused by the leaf springs in reaction to the base-plate move-

a

b

c

d

Figure 3.1: Different mats used to protect the base plate. (a) bubble Sof-Tred, (b) polyurethane foam, (c) open cell neoprene and (d) solid rubber.

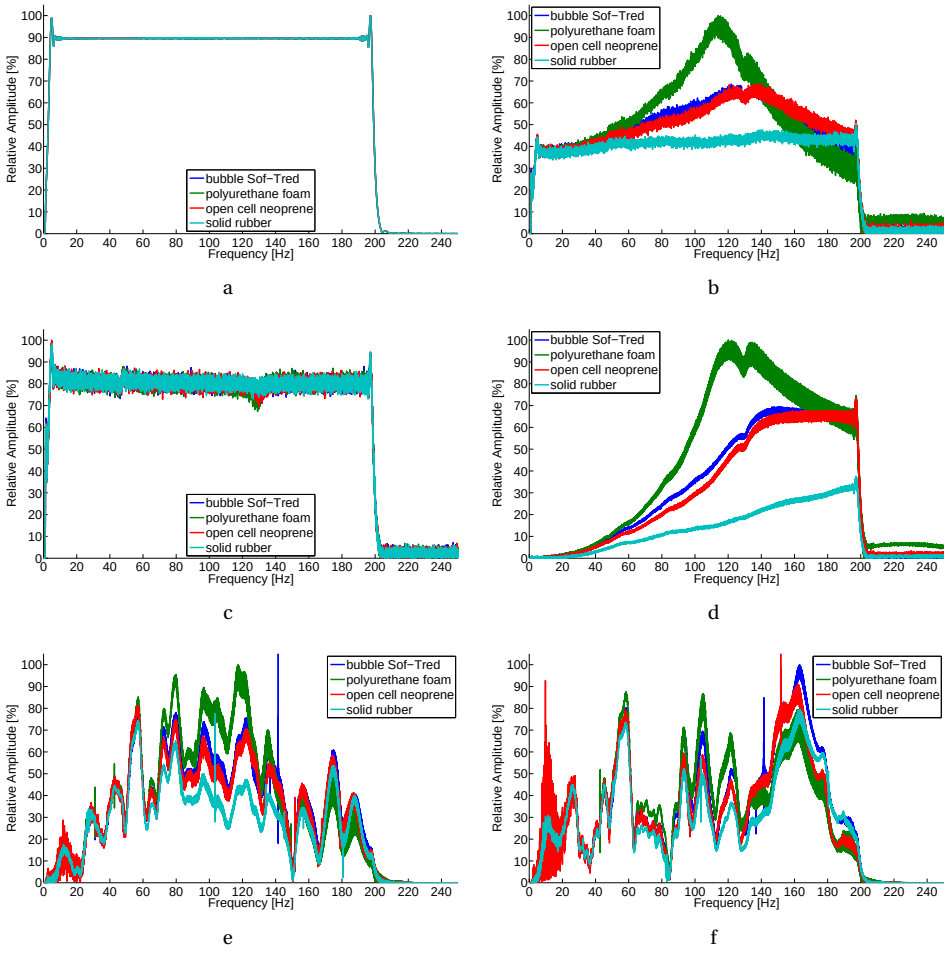

Figure 3.2: Spectra measured for different mats placed between base plate and tarmac. (a) The pilot signal, (b) weighted-sum ground force, (c) reaction-mass force, (d) base-plate force, (e) buried hydrophone and (f) geophone at 9 m below the source. The spikes in (e) and (f) are caused by other mono-frequent sources active during our experiments.

ment. This is the only part of the reaction-mass spectrum that depends on the mat used. As expected the biggest difference in spectra is visible for the base-plate force as shown in Figure 3.2d. It is clear that the solid-rubber mat reduces the base-plate acceleration, while the polyurethane-foam mat seems to enhance it, compared to the other two mats. The amplitude variation at 130 Hz becomes more noticeable for the larger amplitudes. Also the generation of harmonics, as visible by the "thickness" of the curves and the amplitudes above 200 Hz, becomes stronger with amplitude, especially for the foam mat.

Recordings were not only made on the vibrator itself but also in the ground underneath the vibrator, at approximately 9-m depth with a hydrophone and a geophone. It is interesting now to compare the source spectrum estimated at the vibrator (Figure 3.2b) with what was registered by the hydrophone and geophone at depth (Figures 3.2e and f respectively). The spectra registered with the ground sensors are much more erratic than those registered at the vibrator. One explanation for this is the fact that the ground sensors are within the near-field and record a superposition of different waves with different paths. The two ground sensor types also have a different sensitivity, which explains why the geophone spectra are different from the hydrophone spectra. Comparing Figures 3.2e and f, it is clear that the hydrophone is less sensitive outside a frequency band from approximately 30 to 140 Hz. Still the influence of the mats is reflected in the spectra measured in the ground; the order of the colors and their relative amplitudes are comparable with those shown in Figure 3.2b.

To indicate the impact of these mats on the seismic signal in the time domain, Figure 3.3 presents the signals recorded at the vibrator after correlation with the pilot. As expected from the spectral results, the correlation of the pilot (Figure 3.3 a) and reaction-mass force (Figure 3.3 c) hardly changes with the mat used. However, the base-plate (Figure 3.3 d) and the weighted-sum ground force (Figure 3.3 b) do change. Again this confirms that the the mats mainly influence the base plate behavior, which than impacts the total force the vibrator exerts on the ground. Figure 3.3 b indicates that the seismic far-field wavelet depends on the mat used.

Which mat was used also affected the harmonic distortion of the vibrator. Spectrograms of the weighted-sum ground force for the different mats are shown in Figure 3.4. For the open-cell materials (Figure 3.4 b and c) the second harmonic is more pronounced, up to -25 dB relative to the fundamental signal, compared to the closed-cell/solid mats (Figure 3.4 a and d), were it reaches -35dB at most. The coupling influences the different harmonics independently, visible in the results using the polyurethane-foam mat (b). The second harmonic is relatively strong (about -25dB), but the third harmonic (about -35dB) is relatively weak.

3.3. INCREASING POWER

Often, one wants to put as much power into the ground as possible, in order to maximize the signal-to-noise ratio. There are two ways to do that with a seismic vibrator: increase the force or increase the duration of the sweep. In the experiments at Schoonebeek with the LSM vibrator, both were done and the results are presented here.

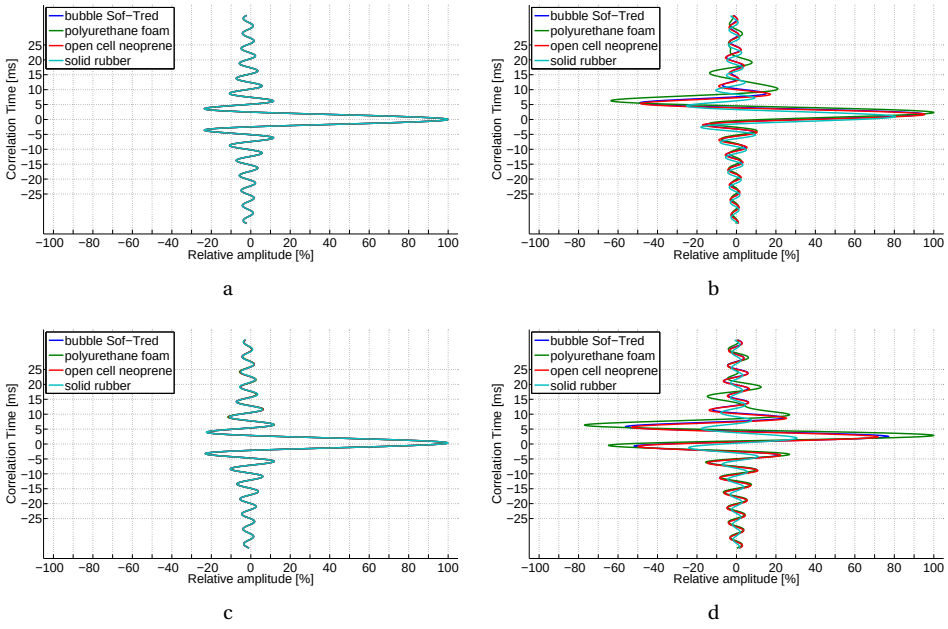

Figure 3.3: Correlation of the pilot signal (a), weighted-sum ground force (b), reaction mass force (c) and base-plate force (d) with the pilot signal for the different coupling conditions.

3.3.1. WITH DRIVE LEVEL

In the first power-increase test, the drive level of the vibrator was varied. Figure 3.5 presents the spectra obtained when linear sweeping from 20 to 200 Hz in 20 s at drive levels ranging from 0.5 kN to 6 kN, while the vibrator was placed on the bubble Sof-Tred mat. In a perfect linear world all spectra measured should simply scale with the driving force. In our case this is only true for the pilot signal (Figure 3.5a). The weighted-sum ground force spectra display the same features as before. The bump around 50 Hz is present as well as the amplitude reduction around 130 Hz. However, because the sweep starts at 20 Hz the air spring does not influence the spectra measured. It can also be observed that the features near 50 and 130 Hz become more prominent with drive level, this is especially visible in the reaction-mass force and base-plate force spectra (Figure 3.5 c and d). One effect visible in the data that has not been discussed yet, is the observation that the frequency at which the maximum ground force occurs shifts with drive level. At 0.5 kN the maximum is located at around 130 Hz, while at 6 kN this occurs already at about 110 Hz. It is clear that this is dictated by the behavior of the base plate. Comparing Figure 3.5b with 3.2b, it seems that increasing the drive level makes the bubble Sof-Tred mat behave more like the polyurethane-foam mat. It is also interesting to see that the lower half of the spectrum scales differently with drive level than the upper half. Compare for example the results at 60 Hz with those at 160 Hz. At 60 Hz the curves are much further apart than at 160 Hz. This is also reflected in the hydrophone and geophone spectra (Figure 3.5 e and f).

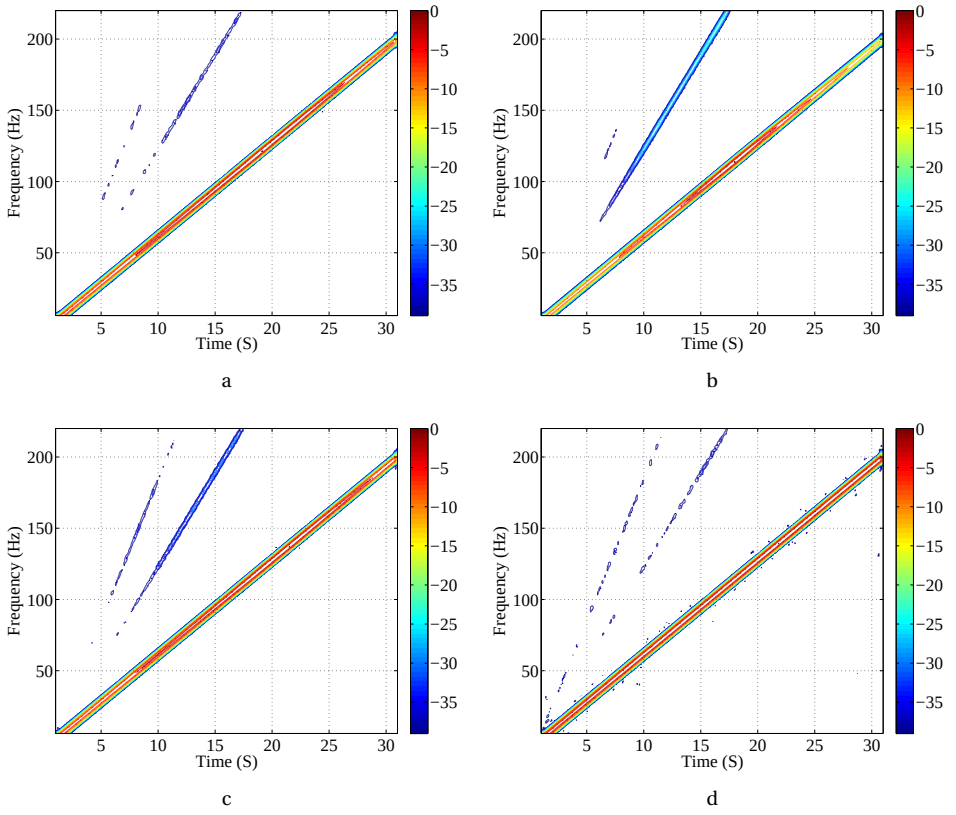

Figure 3.4: Time-frequency contour plots of the weighted-sum ground force for different materials placed between the vibrator and the ground. (a) bubble Sof-Tred, (B) polyurethane foam, (C) open cell neoprene and (D) solid rubber. Amplitude scale is given in dB relative to the maximum amplitude in each individual plot.

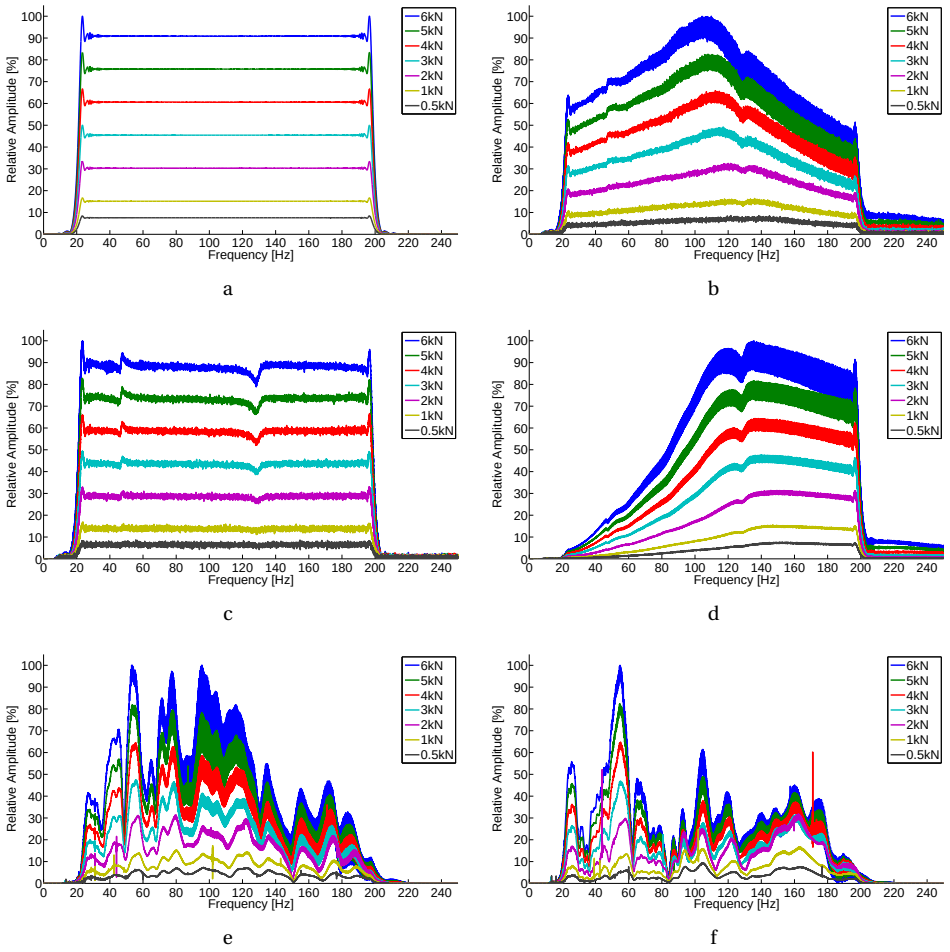

Figure 3.5: Spectra measured for various driving forces. (a) The pilot signal, (b) weighted-sum ground force, (c) reaction mass force, (d) base-plate force, buried hydrophone (e) and geophone (f) at 9 m below the source. The spikes in e and f are caused by other mono-frequent sources active during our experiments.

3.3.2. WITH SWEEP DURATION

Another way to affect the amplitude after correlation, is by varying the sweep rate. Keeping the bandwidth of a sweep constant, the duration of the sweep will determine its amplitude after correlation. In that case the spectral amplitude scales approximately with the square root of the duration of the sweep (equation A6 of Rietsch, 1977). In the second power-increase test, the vibrator was again placed on the bubble Sof-Tred mat. The drive level was fixed at 2000 kN and the duration of the 2-to-200 Hz sweep was varied from 20 up to 160 s. In Figure 3.6 the obtained spectra are shown. Because the sweep starts at lower frequency than in the previous power-increase test, the uplift at the low end of the spectrum is more pronounced. More striking however, is the observation that the spectra do not change shape with changing sweep duration. If the amplitude would be corrected for duration, the spectra would overlap perfectly. Although not explicitly shown here, this can be easily verified, because a four times longer sweep will double the spectral amplitude. The results of the 80 (or 160) s sweep should therefore be twice that of the 20 (or 40) s sweep. Comparing the two power-increase methods it seems that increasing the duration of the sweep (Figure 3.6 e and f) is more beneficial for the higher frequencies than increasing the drive level (Figure 3.5 e and f).

3.4. DRIVE-LEVEL AND REPEATABILITY EXPERIMENT

The impact of drive level on the vibrator signals were studied in more detail when ION, INOVA and Shell created the opportunity to carry out field experiments with a regular-sized hydraulic-drive exploration vibrator. The experiments differed in a number of ways from the LSM vibrator drive-level test described above: The probed force range was much larger; The sequence of sweeps not only allowed to asses the drive-level dependency, but also the repeatability of the vibrator; A deep borehole was available such that the far-field wavelet could be measured; The tests took place in another setting, on a different soil, than the tests with the LSM vibrator; The vibrator controller used a feedback loop on the ground force.

3.4.1. FIELD LAYOUT AND EXPERIMENT SETUP

At the test site a linear array of 24 geophones, with a spacing of 25 m, were placed at the surface. Twelve geophones were placed in the borehole at depths from 2450 to 3000 feet (approximately 747 to 914 m) with an interval of 50 feet (15.24 m). Two vibrator locations were used. At the first location the vibrator was placed at about 180 m from the borehole and 28 m from the first geophone. The second location was only 20 m apart from the first and was about 195 m away from the borehole and 45 m away from the first geophone. At the first location four extra geophones were placed more closely to the vibrator with an interval of 2 m. An overview of the setup is given in Figure 3.7a, the vibrator used is shown in Figure 3.7b.

On both locations the same drive-level experiment was performed, repeating a 8-to-80-Hz 12-s sweep at ten different drive levels. The drive levels were set to 5, 10, 20, 30, 40, 50, 60, 70, 80 and 90% sequentially. For each drive level the sweep was repeated ten times. After finishing the first set of 5-to-90% drive levels, the whole sequence was repeated, so per location a total of 200 sweeps were performed without moving the vi-

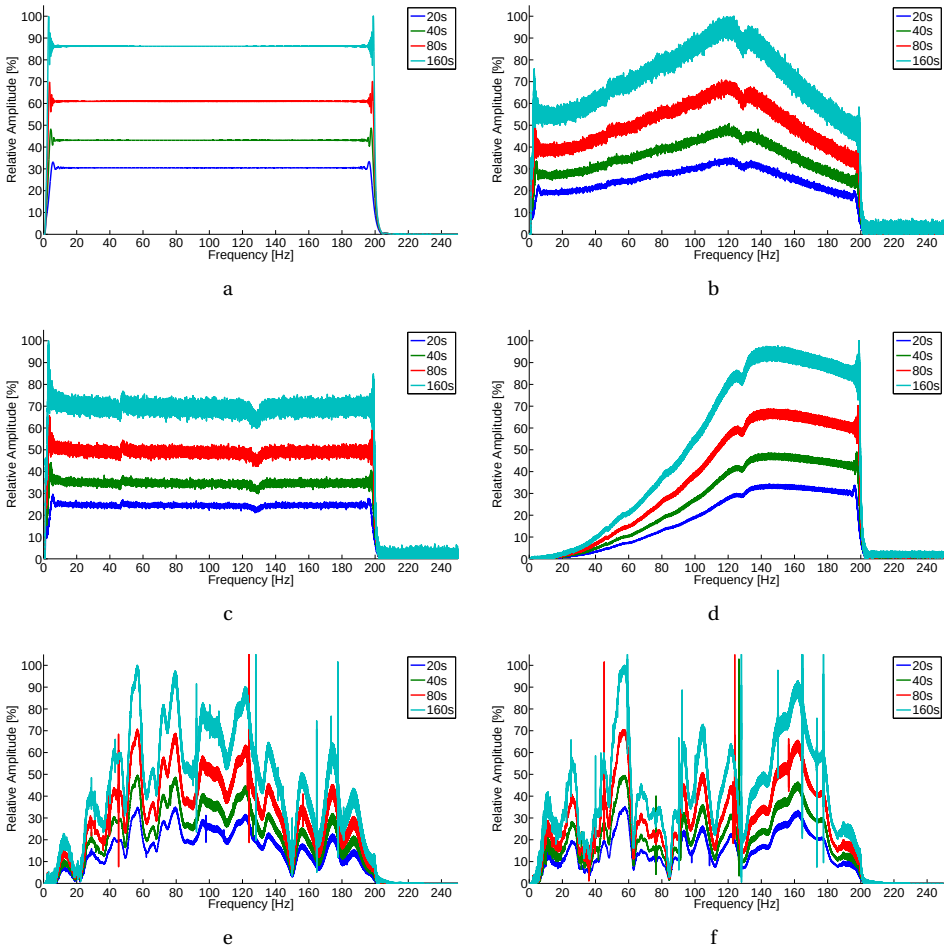

Figure 3.6: Spectra measured for different sweep lengths. (a) The pilot signal, (b) weighted-sum ground force, (c) reaction mass force, (d) base-plate force, buried hydrophone (e) and geophone (f) at 9 m below the source. The spikes in e and f are caused by other mono-frequent sources active during our experiments.

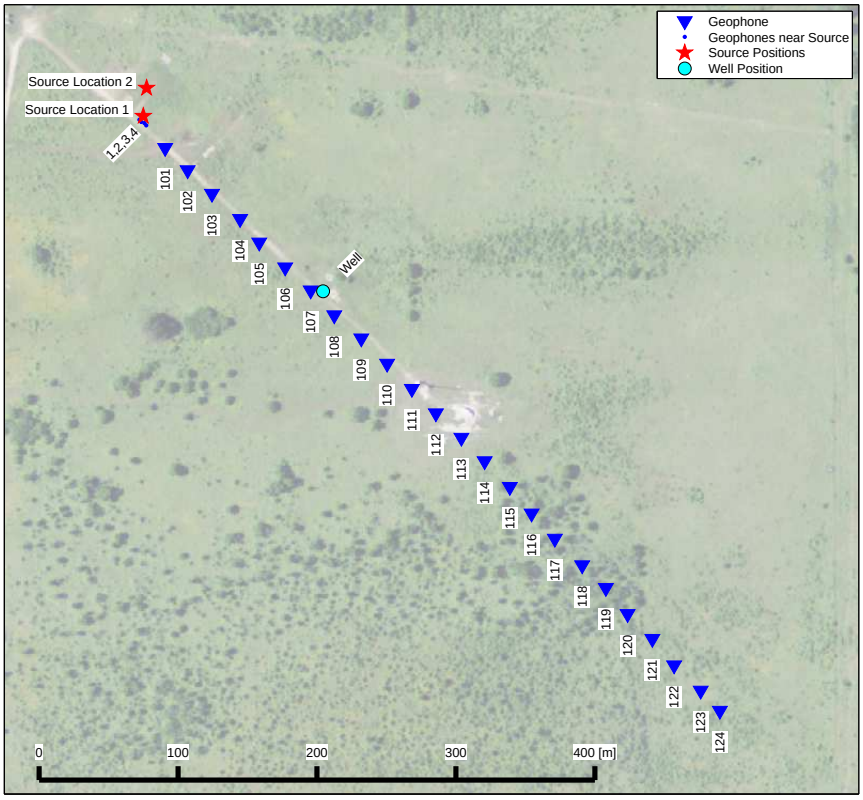

a

b

Figure 3.7: Field layout (a). Geophones are indicated in blue, the vibrator positions are red, and the borehole is colored magenta. The borehole contained twelve geophones (BH01 - BH12) at depths of 750 - 915 m. (b) INOVA's modified 266kN vibrator used for the experiments.

brator or lifting its base plate. Figure 3.8 gives an overview of the drive levels and vibrator location over time.

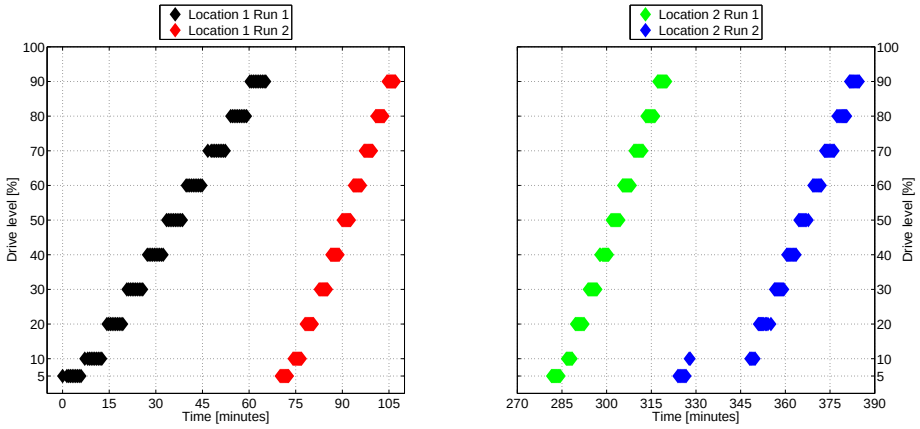

Figure 3.8: Drive levels and locations over time.

3.4.2. EXPERIMENT RESULTS

Figure 3.9 shows the amplitude spectra of the reaction-mass acceleration, the base-plate acceleration and the weighted-sum ground force derived from both measurements. Apart from the lowest drive levels in the first location and the highest drive levels at the second location, most spectra at the same drive level and of the same sequence overlap very well. Each drive level was repeated ten times, but their difference is not visible on the scale of Figure 3.9. It is also clear that the feedback loop on the weighted-sum ground force worked well for both locations and all drive levels. The amplitude spectra of the force are flat, especially above 20 Hz, and are very similar, although not shown here, to the amplitude spectra of the sweeps used. Interestingly the relative contributions of the reaction-mass and base-plate accelerations differ significantly with drive level. At the first location the acceleration spectra contain a swell that shifts from about 50–55 Hz at 5% drive level to about 30–35Hz at a drive level of 90%. It also becomes more pronounced with drive level. At the second location a similar structure is visible, but less pronounced and at slightly higher frequencies. From these plots it is also clear that in the second sequence (indicated by the dashed lines in Figure 3.9) the relative contributions of the reaction-mass and base-plate accelerations to the force signal is different from the first sequence, especially for the lower drive levels. In the first location the base-plate acceleration is relatively weaker than in the second sequence, while at the second location its contribution is stronger in the second sequence.

The seismic data from the first location are shown in Figure 3.10 and 3.11. They make clear that the vibrator's drive level has a larger influence on the seismic records than what might be expected from the flat spectra of the weighted-sum ground forces shown in Figure 3.9a. Figure 3.10 shows the seismic records obtained at four different drive levels (10, 20, 40 and 80%) after correlation and stacking. Relative amplitudes of events change

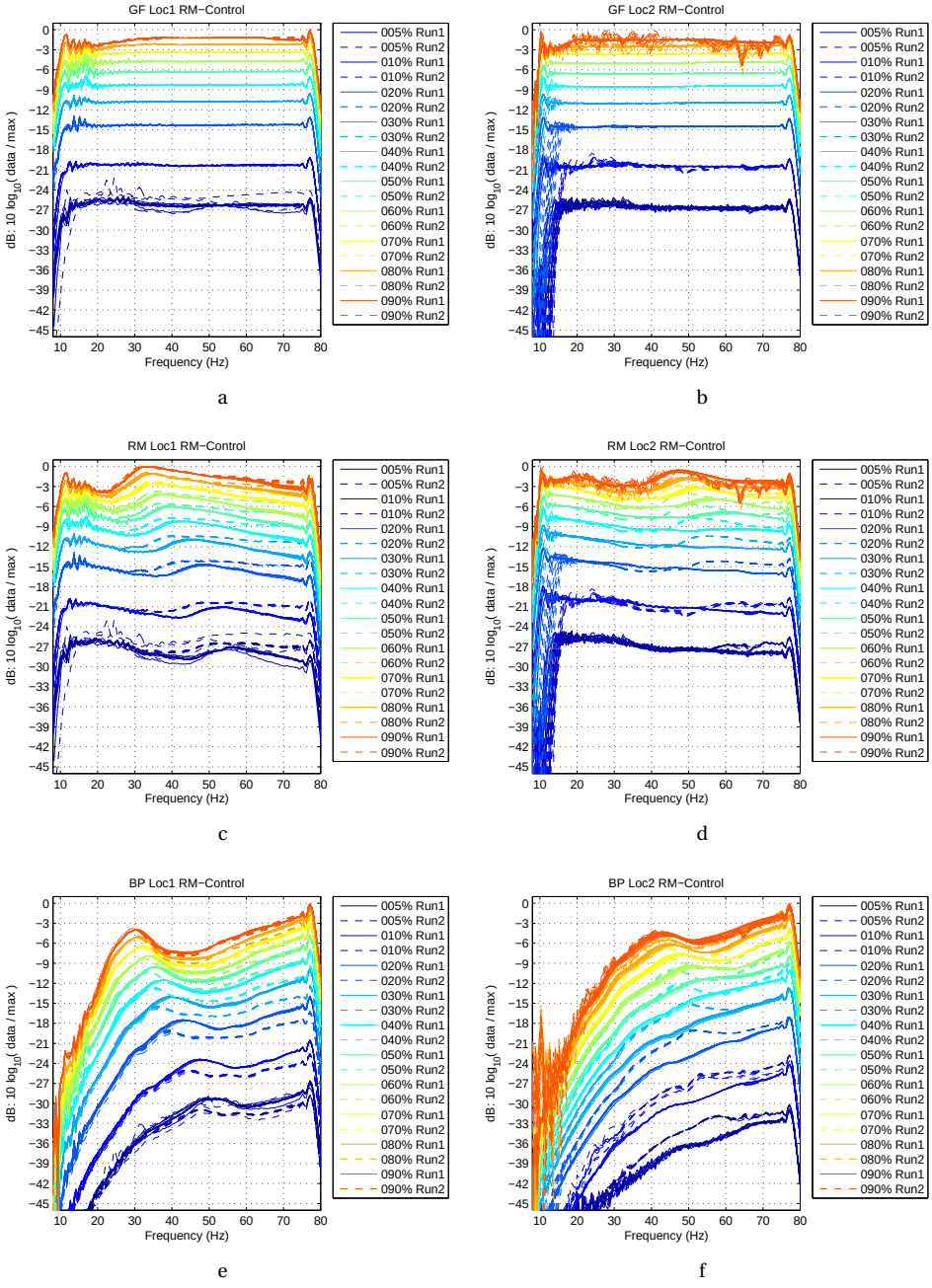

Figure 3.9: Spectra of different vibrator signals (weighted-sum ground force (a & b), reaction-mass acceleration (c & d) and (e & f) base-plate acceleration) for different drive levels. Left: first location. Right: second location. First sequence represented with solid lines, second with dashed lines. Drive level is indicated with different colors.

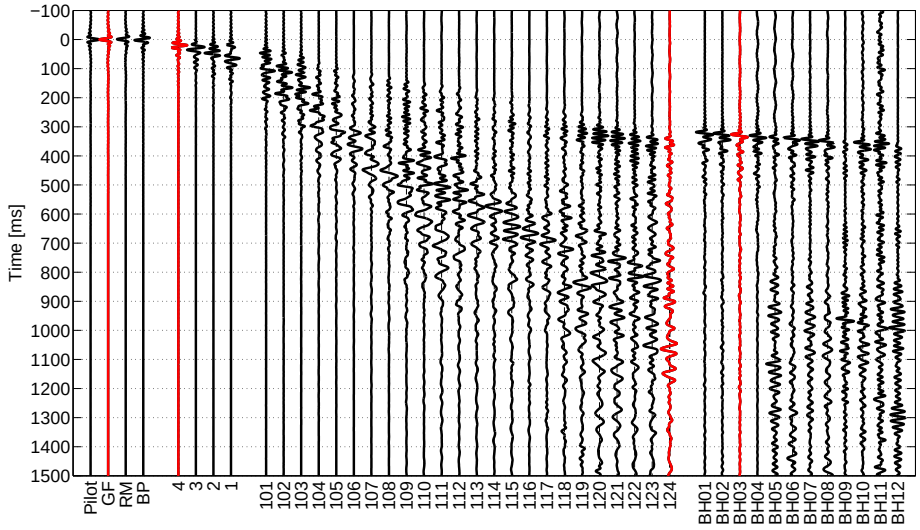

a

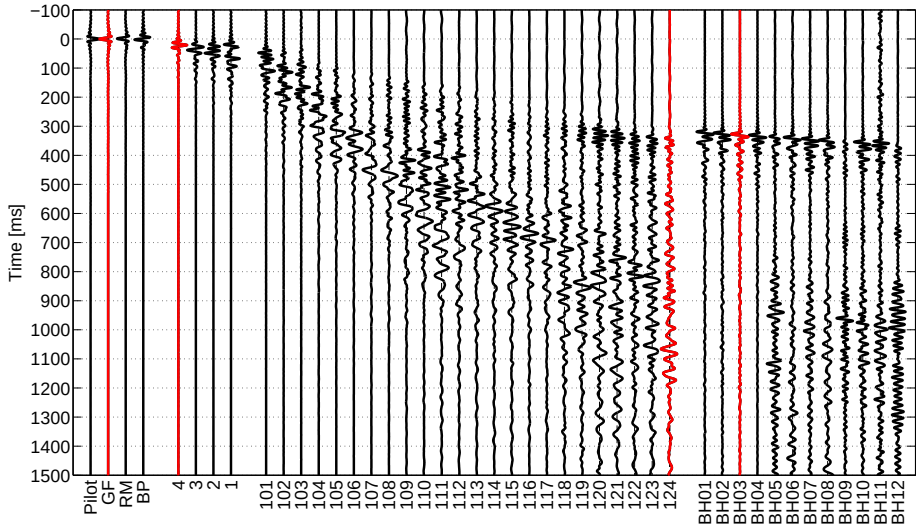

b

Figure 3.10: Seismic records acquired after correlating the acquired records with the pilot signal for different drive levels. Stack of the ten records at 10%(a) and 20%(b) drive level. Per record: 4 vibrator signals, 4 geophones close to the vibrator (2 m apart), 24-geophones spread (25 m apart) and 12 borehole geophones (15.24 m apart). Traces are individually scaled by their maximum amplitude. Red-colored traces are also plotted in common receiver gather for all drive levels in Figure 3.11.

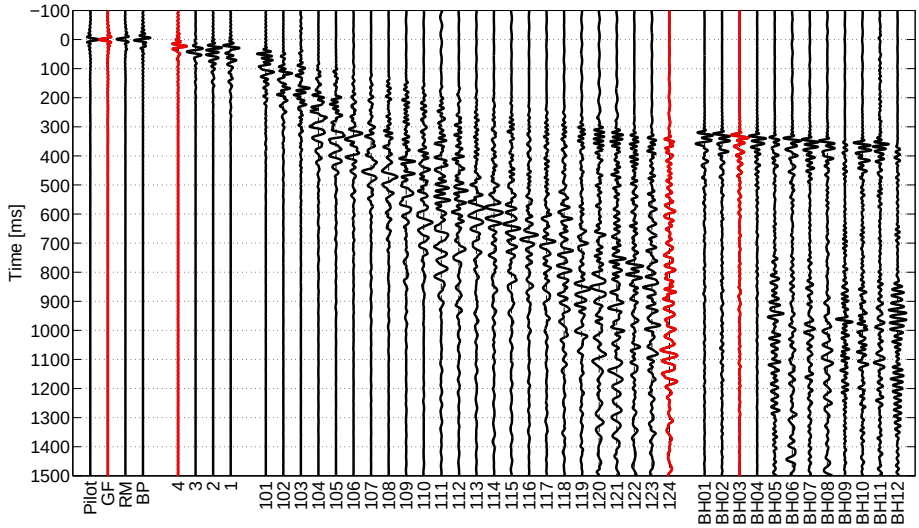

c

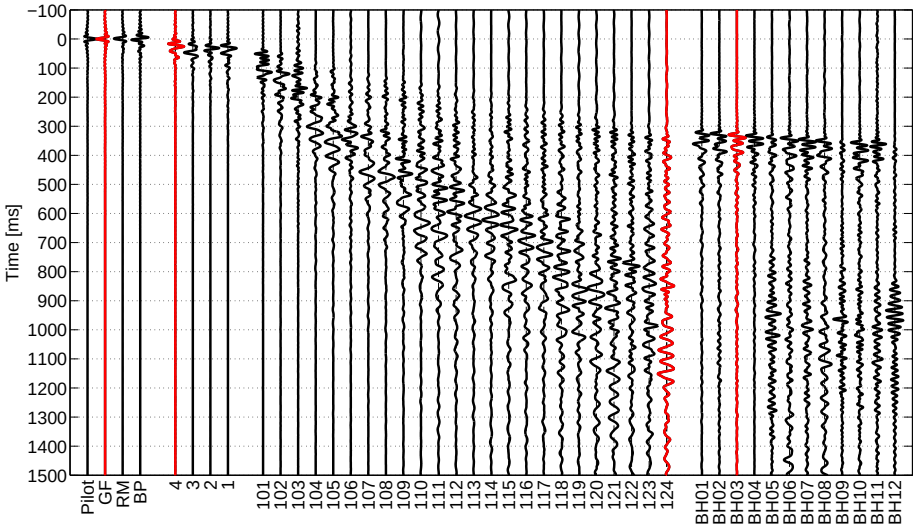

d

Figure 3.10: Seismic records acquired after correlating the acquired records with the pilot signal for different drive levels. Stack of the ten records at 40%(c) and 80%(d) drive level. Per record: 4 vibrator signals, 4 geophones close to the vibrator (2 m apart), 24-geophones spread (25 m apart) and 12 borehole geophones (15.24 m apart). Traces are individually scaled by their maximum amplitude. Red-colored traces are also plotted in common receiver gather for all drive levels in Figure 3.11.

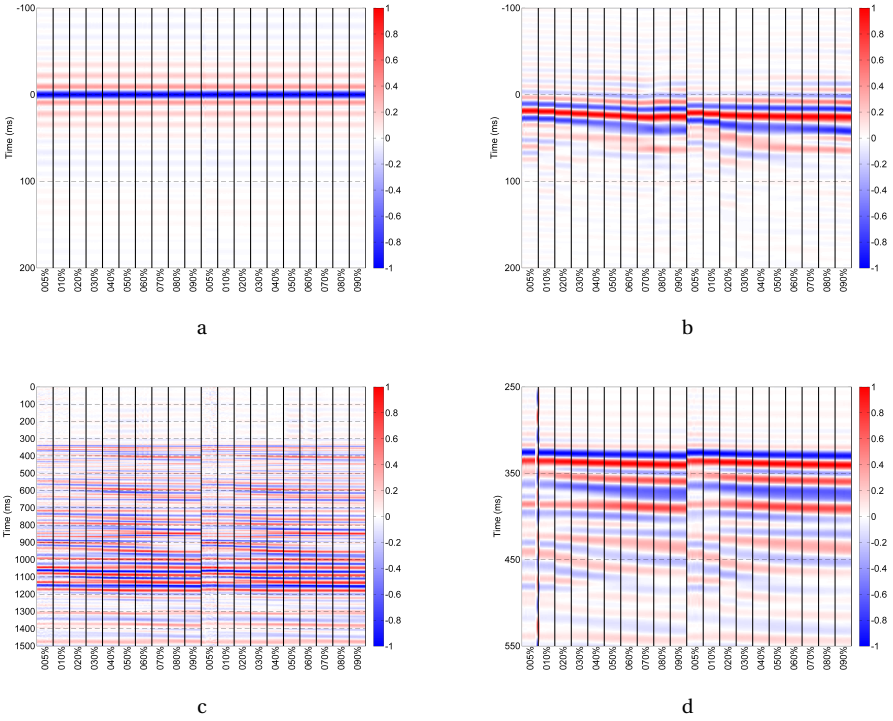

Figure 3.11: Common receiver gathers for four different signals after correlation with the pilot signal. (a) Weighted-sum ground force (“GF”), (b) surface geophone at about 4 m from the vibrator (“4”), (c) surface geophone geophone at 600 m (“124”) and (d) borehole geophone at an offset of 180 m and depth of 777m (“BH03”). Each plot shows 100 traces in groups of ten different drive levels. Color indicates normalized signal amplitude. Note that the length of the time window of plot c is different from the other plots.

with drive level; compare, for example, the first arrivals on far-offset surface geophones at about 300 ms, with later events, including the surface waves, around 900 ms for the different drive levels. Figure 3.11 presents four different receiver gathers for both drive-level sequences performed at the first location, 200 shots in total in panels of 10 shots at equal drive level. Again each recording was correlated with the sweep. In general the signals are very similar within the same drive-level panel. The weighted-sum ground force as measured at the vibrator (Figure 3.11a) hardly changes with drive level. The data from the geophone close by the vibrator (Figure 3.11b) shows shifts of a couple of ms, but also amplitude and bandwidth variations. Similar changes can be observed for the far offset surface geophone and bore-hole geophone (Figure 3.11c and d respectively). Not all "events" seem to be affected equally strong, some arrivals present at low drive level vanish with larger drive level and vice versa, while others are present at all drive levels.

At the second location, the vibrator was placed on the bare soil. In the field it could be observed that each time the vibrator got to the higher frequencies of the sweep dust clouds from underneath the plate were formed. The fact that this occurred at the higher frequencies makes sense, because the vibrator's base plate experienced most acceleration in that case (see Figure 3.9f). A photo of one of the dust clouds is shown in Figure 3.12a. The amount of dust did not decrease with the number of sweeps. Just next to the plate small heaps were formed of material transported from underneath the base-plate, see the photo in Figure 3.12b. This photo also clearly shows that there was an air gap between the soil and the edge of the base plate. After the experiment was finished and the base plate was lifted, the imprint the base-plate left behind in the soil was not uniform. Therefore it can be concluded that the base plate did not generate a uniform pressure field on the ground during the experiments. These observations, similar to the observations at the mat experiments, suggest that the contact between the vibrator and the ground plays a crucial role in transforming the vibrator's driving force to a seismic wave.

a b

Figure 3.12: Photos taken at the second location. Showing (a) dust clouds at the high end of the sweep and (b) small heaps next to plate and air gaps between the plate and ground.

3.5. CONCLUSION

From the measurements and their analysis as shown in this chapter several conclusions can be drawn. Placing a material between the vibrator and the ground, thereby affecting the coupling between the vibrator and the ground, can have a significant effect on the behavior of the vibrator and the far-field wavelet it produces. Even if the material is a thin mat.

Controlling the output power of a vibrator can be done via increasing drive level or increasing the sweep duration. The sweep duration affects all frequencies uniformly. However, increasing the drive level also affects the shape of the spectra. Although the vibrator signals (reaction-mass, base-plate accelerations and weighted-sum ground force) can be very repeatable when repeating the same sweep at a fixed drive level, these signals at a certain drive level do change when sweeps with higher drive levels are used in between.

The stability of the weighted-sum signal in the hydraulic vibrator experiments is not reflected in the signals recorded with the geophones. This shows that, for the experiments done, the weighted-sum is not a good estimate of the true source wavelet. The assumption that the base plate exerts a uniform pressure on the ground below was clearly observed not to be valid.

To summarize the observations described here suggest that the material properties and geometry of the material underneath the base plate can influence the behavior of the vibrator significantly, and in a nonlinear way. The effect of the geometry of the contact is studied in detail and presented in the next chapter.

REFERENCES

K. Hornman and E. Forgues, *Permanent reservoir monitoring with onshore surface seismic,* Second EAGE workshop on permanent reservoir monitoring (2013).

R. Noorlandt, G. Drijkoningen, and R. Schneider, *A seismic vertical vibrator driven by linear motors,* 74th EAGE Conference and Exhibition, P061 (2012).

R. Noorlandt, G. Drijkoningen, and C. Faber, *Influence of drive level on the fundamental vibrator signal,* 75th EAGE Conference and Exhibition, Th P11 02 (2013).

E. Rietsch, *Computerized analysis of vibroseis signal similarity,* Geophysical Prospecting **25**, 541 (1977).

The University of Texas, *Devine test site,* http://www.beg.utexas.edu/about/facilities/devine-geophysical-test-site, accessed: 2016-06-13.

4

ON THE MECHANICAL VIBRATOR-EARTH CONTACT GEOMETRY AND ITS DYNAMICS

Rik Noorlandt and Guy Drijkoningen

The geometry of the contact between a vibrator and the earth underneath influences the dynamics of the vibrator. Although a vibrator might appear to be well-coupled with the earth on a macro scale, perfect coupling certainly does not occur on the micro scale. With the aid of contact mechanical modeling and concepts, it can be shown that this lack of contact at the micro scale, or rather the change thereof during a sweep, can have a significant effect on the dynamics of the vibrator-earth system. Modeling of such changing contact predicts that the dynamic behavior varies considerably with the vibrator drive level. The most significant effect predicted by the model is a decrease in the base-plate resonance frequency with an increasing drive level. Extensive drive-level tests carried out in a field experiment confirm this change of resonance behavior with drive level.

4.1. INTRODUCTION

Seismic vibrators are typically used to send out sweep signals. Distributing frequency content over time reduces the amount of instantaneous power that a vibrator has to deliver, but these lengthy signals need to be compressed during processing. To do this, one needs to know the source signal, which is most commonly measured at the vibrator.

This chapter has been published as a journal paper in Geophysics, 81(3), P37–P45 (Noorlandt and Drijkoningen, 2016). Note that minor changes have been introduced to make the text consistent with the other chapters of this thesis.

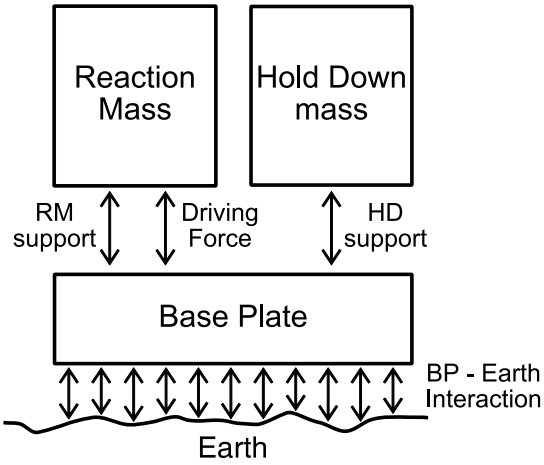

Figure 4.1: Model of main components of a seismic-exploration vibrator. The driving engine is placed between the reaction mass and base plate (driving force). Parallel to this there might be a support structure to hold the reaction mass (RM support). To prevent the base plate (BP) from decoupling from the earth a hold-down system might be present (HD support). The translation of the forces between the elements of the vibrator to a seismic wave occurs at the contact between the base plate and the earth (BP-earth interaction).

Measuring the source signal, however, is not a trivial task, because the source consists of multiple elements that dynamically interact with each other. A model of the main components of a vibrator is shown in Figure 4.1. The most common method to determine the source wavelet is the weighted-sum-ground-force method (Castanet and Lavergne, 1965). This method relies on two basic assumptions: First, it is assumed that the total force a vibrator exerts on the ground can be measured, and second, it is assumed that this force is a measure of the seismic wavelet in the far-field.

The force the vibrator exerts on the ground is determined by summing the measured accelerations of the reaction mass and base plate, after being multiplied with their respective mass. In this way, the net forces on the reaction mass and base plate are added together. From Figure 4.1, it is clear that the forces between the plate and reaction (RM support and driving force) are removed from this sum. The forces left in the sum are the support of the hold-down mass and the total of the interaction between the base plate and the earth (HD support and BP-earth interaction). Typically, the hold down mass is ignored because its support is designed to pass its weight without affecting the dynamics of the base plate at frequencies above approximately 5 Hz. Therefore, the weighted sum of the reaction-mass and base-plate accelerations equals the total force on the ground (with opposite sign). Although this method is now most common, there was some debate before it was accepted, see papers by Lerwill (1981), Sallas and Weber (1982), Lerwill (1982) and Sallas (1984).

The assumption that the seismic wavelet measured in the far-field is, up to a derivative, proportional to the total force the vibrator exerts on the ground, can be taken from the work of Miller and Pursey (1954, 1955). Miller and Pursey (1954), similar to the earlier work of Reissner (1936), formulate the behavior of an isotropic elastic half-space when

a uniform pressure field of circular shape is acting on it. They find that, in such a case, the particle displacement is proportional to the pressure. If the pressure beneath the base plate is uniform, it simply equals the force divided by the plate area, and therefore, the seismic wavelet in the far-field should be proportional to the weighted-sum ground force.

However, in practice, there is a difference between the weighted-sum-ground-force signal and the wavelet observed in the far-field. Many papers are devoted to the mismatch among the actual force (typically measured with load cells), the weighted-sum-ground-force method, and the seismic far-field wavelet; see, for example, Baeten and Strijbos (1988), van der Veen *et al.* (1999), Wei (2008), Wei (2009), Shan *et al.* (2009), Saragiotis *et al.* (2010), Wei *et al.* (2010), Sallas (2010), and Poletto *et al.* (2011). Any difference between the seismic far-field wavelet and the source wavelet measured at, and used to control, the source will cause a decrease of source repeatability and seismic resolution. Martin and Jack (1990), Aritman (2001), and Meunier (2011) provide some examples.

The mismatch is a direct consequence of the assumptions made not being valid. The vibrator components are typically assumed to be rigid, whereas in practice they are not. Baeten and Ziolkowski (1990) propose a model to account for the flexibility of the base plate. In their model, the contribution of the base-plate acceleration to the weighted-sum ground force is adjusted and decreases with frequency. Their model shows that flexure of the base plate is mainly of importance at high frequencies. Lebedev and Beresnev (2005) come to the same conclusion and also show that although the flexure is not influencing the waves radiating from the source much, it does affect the measurement of the base-plate acceleration. In their examples, different positions of the acceleration sensor on the base plate cause travel time mismatches of up to approximately 0.6 ms.

In addition to the base-plate flexure, the fact that the vibrator is placed on a rough surface (as indicated in Figure 4.1), also causes the assumption of a uniform pressure distribution beneath the base plate to be violated. Although this will mainly affect the propagation at higher frequencies only, where wavelengths becomes more nearly equal to the size of the base plate (Lebedev and Beresnev, 2005), it can have a major influence on the dynamics of the vibrator, as we will show in this chapter.

The contact between the vibrator and the earth as a cause of signal distortion has been mentioned in the past. Lebedev and Beresnev (2004) and Lebedev *et al.* (2006) propose a model in which the contact acts as a nonlinear spring. In their model, the "contact spring" is weaker in tension (base plate moving away from the contact) than in compression (base plate moving toward the contact). In this chapter, this contact behavior is studied in more detail. First, we show some results of quasistatic modeling. The importance of the shape of a contact is made clear by an analytical example. The outcome of numerical modeling of a rough contact and its sensitivity to several parameters are presented. Then, we describe a dynamic model that can not only reproduce the quasistatic results of the rough contact but also is capable of predicting the behavior of the contact when a sweep force is applied to the base plate. The predictions of the dynamic model are then compared with some field measurements. The field measurements were carried out to investigate the nonlinear, drive-level-dependent behavior of the vibroseis setup. We conclude this chapter with a discussion of this work, its implications for field surveys and conclusions that may be drawn.

4.2. CONTACT MECHANICS

Normally, a seismic vibrator is not fixed to the ground, and its contact is simply established by its weight. The driving engine is then used to generate a time-varying pressure that is added to the static pressure caused by gravity. The total pressure can increase and decrease, but care is taken to make sure that some pressure is left to keep the vibrator, at least at macroscale, in contact with the ground. Normally, the (static) gravity component is ignored because it is not recorded by the geophones. However, this can only be done if the vibrator-earth system behaves linearly, which is most probably not the case as indicated by the harmonics observed in the field. The displacement of the ground might not be linearly related to the driving force due to the intrinsic material properties or the geometry of the setup or both. Although material-induced nonlinearity changes from material to material, geometry-induced nonlinearity can in principle occur with every material beneath the vibrator, such as soil, rock, asphalt, concrete, ice, etc. The main goal of this chapter is to describe the effect such a contact geometry might have.

Although the vibrator plate is relatively flat, the ground underneath is not. Therefore, at the microscale, the plate will not be in contact with the ground over its complete or nominal area, as shown in Figure 4.1. In general, the true contact area, places where ground and base-plate molecules interact, is only a fraction of the nominal contact area. Measurements presented by Dean *et al.* (2015) show that 3% of the contact area can carry as much as 20% of the total load. The distribution of the plate-earth contacts is a function of the applied force and therefore will change under dynamic loading.

The study of the pressure and contact distribution is part of the field of contact mechanics; for a good introduction, see the book of Popov (2010). Hertz (1882) published one of the first papers describing the behavior of two elastic materials in contact. He shows that if two curved elastic half-spaces are pressed together, the displacement and contact area are related in a nonlinear way to the force applied.

4.2.1. SIMPLE CONTACT GEOMETRY

The exact force-displacement relation strongly depends on the shape and material of the bodies brought in contact. To illustrate the effect of shape, Figure 4.2 shows the cross section of differently curved bodies and their force-displacement relations when pressed on a flat half-space of the same material. The shape of these modeled bodies has a vertical axis of symmetry and a height h proportional to the distance to this symmetry axis r raised to a certain power n:

$$h(r) = \alpha^{(1-n)} r^n, \tag{4.1}$$

where α is a normalization constant. In our example, the value of α was set to 250 mm, equal to maximum value of r. The base of these shapes becomes flatter with increasing power. The behavior of such axisymmetric contacts has, for example, been described by Heß (2012) and Popov (2013). The force-displacement relation for power law profiles shown in Figure 4.2a is given by equation 21 of Popov (2013) and is proportional to the applied force to a power $\frac{n}{n+1}$ as plotted in Figure 4.2b. The flatness of the base is clearly reflected in these force-displacement curves. It is clear that the smallest displacement for a given force is produced by two flat surfaces brought into contact. The flatter the contact, i.e., the higher the power used, the better it approaches the linear behavior of

two flat bodies brought into contact. For contacts with this geometry, the contact acts as a spring that becomes stiffer (weaker) with increasing (decreasing) force.

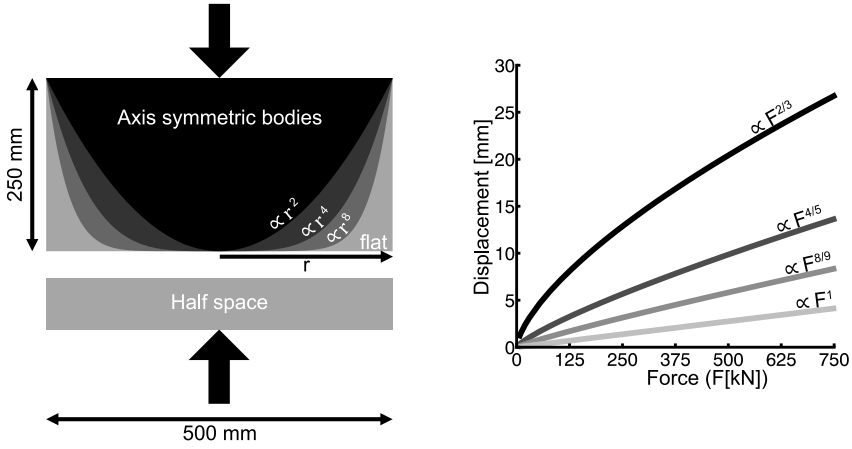

Figure 4.2: The 3D axis symmetric bodies. (a) Different gray scales and (b) their force-displacement relation when pressed onto a half-space of the same material. Black arrows indicate direction of the force and displacement. Values for parameters: Shear modulus: 200 MPa; Poisson's ratio of 0.45.

4.2.2. ROUGH SURFACE CONTACT

Although the axisymmetric contact example shows an important property of contact mechanics, it is not well-suited to describe real-life situations for at least two reasons. First, the geometries are assumed to be perfect, and second, there is only a single contact acting. If two real materials are pressed together there typically will be several locations were the two materials are in contact. The number of locations and the shape of these contacts change with the applied load. The calculation of solutions to this problem is not straightforward because "the displacement at any point of the surface depends on the entire pressure distribution inside the contact area (Heß, 2012)" and, in general, numerical schemes solve this iteratively. Typically, a certain total displacement is assumed, and the associated deformation and pressure distributions are calculated. The total of the pressure distribution is then compared with the applied load and the total displacement is adjusted until they match. To investigate the behavior of the vibrator-ground contact, we made use of a program based on Vollebregt (2014), but similar results can be obtained with the code made available by Sainsot and Lubrecht (2011). Both programs are able to quasistatically model the deformation of arbitrary, but discretized, surfaces brought into contact under different loading. In principle, the smallest details of the ground microtopography should be taken into account, but, following the argument of Persson (2001), there typically exists a natural macroscopic limit to the smallest details needed to accurately model the contact behavior.

To obtain an idea of the typical force-displacement curves belonging to the vibrator-

ground contact, a sensitivity study was carried out, using varying profile roughness (lateral and vertical) and soil materials. The base plate was modeled as a flat solid steel plate with a constant shear modulus of 80 GPa and a Poisson's ratio of 0.3. The grid that was used to perform the calculation was 1 × 1.8 m, similar to the size of the base plate of the vibrator used in the field which is described later, and was sampled every 2.2 mm, resulting in a grid of approximately 370,000 height samples. Three different levels of profile coarseness were created with a pseudorandom number generator. The coarsest grid was created by populating 100 samples uniformly over the 370,000 grid points and interpolating in between. For the finer grids 900, respectively and 8100 samples, respectively, were used as starting point. The grids were filtered to remove wavelengths below 10 mm, as to prevent numerical artifacts in the modeling. Finally, these three grids were cumulatively summed and normalized. Figure 4.3 shows an example of the three grids produced in this way.

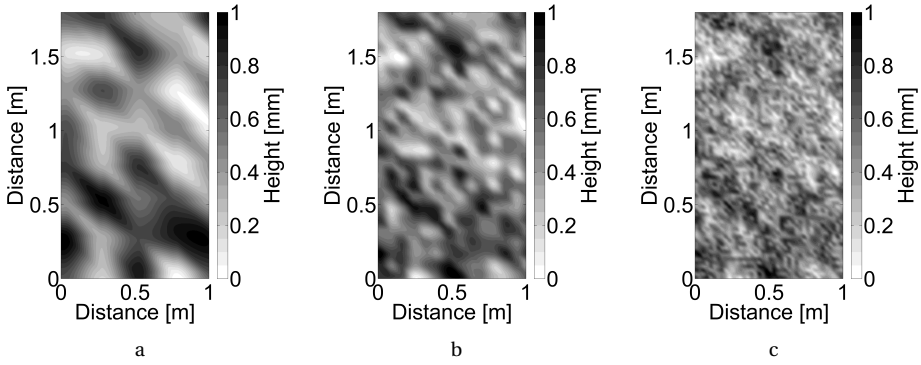

Figure 4.3: Profiles as used to model the force-displacement relations. Increasing lateral details from (a-c).

Figure 4.4a shows the force-displacement relation when the steel base plate is pushed onto the different profiles presented in Figure 4.3, assuming a ground shear modulus of 100 MPa, a Poisson's ratio of 0.45, and a maximal profile height of 1 mm. For comparison, the result obtained with a flat profile has been plotted as well. The force range was chosen roughly the same as that of a typical vibrator with a static hold-down force of approximately 300 kN and a driving force of approximately ± 275 kN. The results of the rough contact profiles differ significantly from that of the flat contact, but are mutually hardly distinguishable. Using the profile in Figure 4.3c, the height, shear modulus, and Poisson's ratio were varied to study their impact on the force-displacement curves. These results are shown in Figure 4.4b–d, respectively.

From the curves in Figure 4.4, it is clear that the force-displacement relation shows a different behavior at small and large loads. At small loads, the curve is nonlinear and similar to the force-displacements shown in Figure 4.2; the contact becomes stiffer with force. At larger loads, the curves shown in Figure 4.4 deviate from those in Figure 4.2 by showing almost linear behavior. The reason for this dual behavior is simple. At small loads, only a limited number of contacts are actively carrying the load. With an increasing load, the area of contact expands rapidly, until, at high loads, this expansion rate

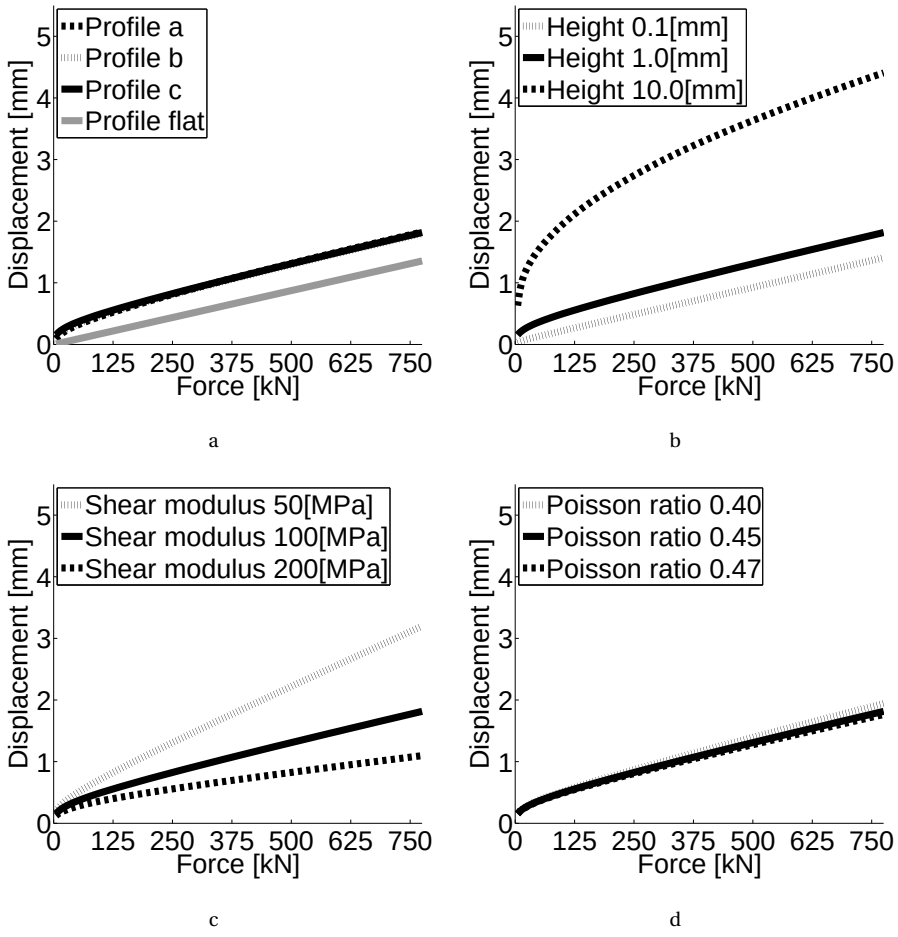

Figure 4.4: Force-displacements curves for (a) the different profiles of Figure 4.3 (also including flat soil surface response), (b) different maximum profile heights, (c) different shear moduli, and (d) Poisson's ratios. The solid black curve is repeated in all plots and represents a reference: profile c with a maximum height of 1 mm, a shear modulus of 100 MPa, and a Poisson's ratio of 0.45.

decreases and the contact starts to behave more and more as one single flat contact, leading to a more linear behavior. This is also the reason why profile height and strength play a dominant role because they control how easily the profile becomes “flat” under loading. The different profiles and Poisson’s ratios did not affect the force-displacement relation significantly. Because the modeling relies on the pseudorandom number generator, the calculation was repeated for 20 different starting seeds. These calculations produced very similar force-displacement relations.

It is important to note that the loads in Figure 4.4 represent total load, i.e., the sum of the static and dynamic forces of the vibrator. It shows that in those parts of a sweep in which the dynamic force on the base-plate points in the downward direction, i.e., increasing the total load, the contact behaves more linear. However, if the dynamic force drives the base plate upwards, the contact becomes less linear. At high drive levels, the total load can decrease significantly during parts of the sweep, and although the vibrator stays in contact with the ground, the relative resistance it experiences from the ground is greatly reduced. In that sense, base-plate decoupling should be considered as a gradual process, instead of a binary one. Also note that, comparing these results with the contact models of Lebedev *et al.* (2006), the rest position and load of the vibrator does not act as special situation from which behavior is different in a compression or tension state. In the examples given in Figure 4.4, a transition between behaviors occurs at forces that only depended on the geometry and parameters of the contact itself.

The curves shown in Figure 4.4 are only valid for elastic interaction, such that the profiles recover their original shapes, when they are not in contact anymore. The ground-vibrator interaction, however, causes permanent deformation, mainly to the ground, as well. When the base plate is lowered and the hold-down system is activated, the pressure on the individual contact points can easily exceed the elastic limit. The soil will deform until both surface profiles are more alike and the pressure is shared by a larger contact area. During a sweep, the pressure on the ground dynamically reaches (much) larger values, and as long as the contact area is not large enough to sustain the local pressure elastically, permanent deformation will occur. It is expected that the role of permanent deformation will decrease after several sweeps, such that the elastic behavior, with a force-displacement relation similar to that of Figure 4.4, but with a fixed permanent displacement offset, becomes dominant. Although the role of permanent deformation is expected to decrease with the number of sweeps, it will not always be the case. Meunier (2011, p. 112, Figure 20) provides an example, in which even after 60 sweeps the difference between the 59th and 60th record, amplified by a factor of 20, resembles the 59th record. This clearly indicates that conditions between the 59th and 60th varied and most probably were caused by permanent deformation of the road on which the vibrator was placed.

4.2.3. CONTACT DYNAMICS; SINGLE NONLINEAR SPRING

Knowing the force-displacement relation of a quasistatic contact, it is instructive to investigate the dynamic effect such a relation would have on the base plate. Because our main interest is the effect of the contact, we ignored the dynamic behavior of the reaction mass and hold-down system, but did take into account their weight on the top of the base plate. The contact spring (beneath the base plate) was chosen to behave such as the

reference contact (solid black curve of Figure 4.4). This setup has some similarities with a Duffing oscillator (Walker, 1995). Analytic solutions for such systems can only be found under some very restrictive conditions, mainly due to the fact that the solutions strongly depend on the driving amplitude and damping. Therefore, we chose to model the time behavior numerically, using a standard ordinary differential equation (ODE) solver. The driving force was a simple 12-s 8-to-80 Hz linear sweep, with 250 ms cosine tapers on both ends, the same was used for the field measurements described later. Some damping was needed to prevent the base plate from decoupling. The amount of damping was set such that at 100% drive level, the dynamic forces on the base plate just did not exceed the static ones.

Figure 4.5 shows a small time window of the modeled acceleration of the base plate for different drive levels. At low drive levels, the signal stays sinusoidal, but at high drive levels, the acceleration amplitude becomes asymmetric and more sawtooth shaped. It is clear that even for a linear elastic earth, the contact between the vibrator and soil can cause a nonlinear distortion on the base-plate acceleration and therefore will affect the weighted-sum-ground-force signal.

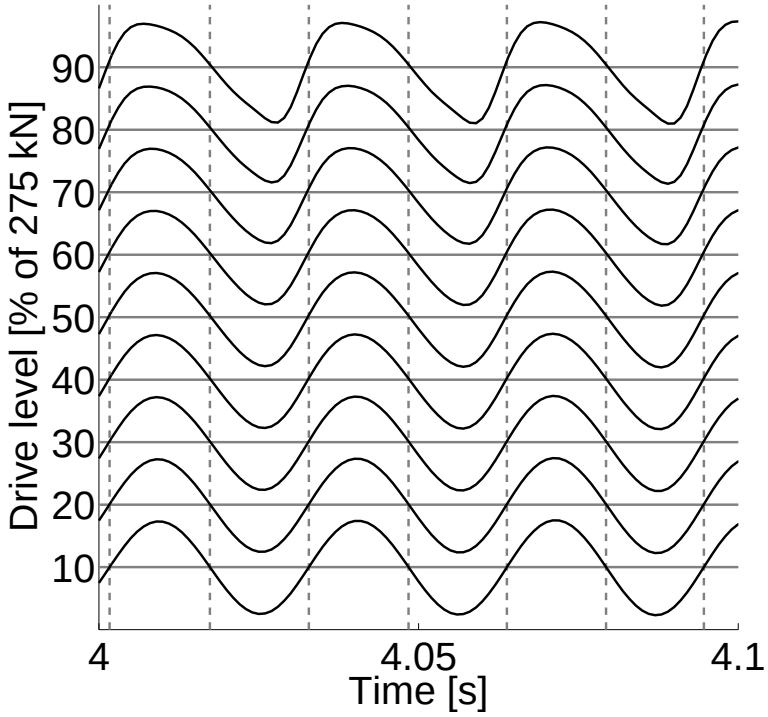

Figure 4.5: Small time window of the modeled base-plate acceleration when driven by a 12-s linear sweep from 8 to 80 Hz and placed on a contact spring with a force-displacement shown by the solid black line in Figure 4.4. Amplitudes were normalized for drive level.

4.2.4. CONTACT DYNAMICS; WINKLER FOUNDATION

Up to now, we have used the quasistatic approach to determine the contact behavior. Although this gives useful insights, a crucial property of the contact dynamics might have been ignored. Consider the potential vibrator-ground contact area to be divided in three groups: part of the area will stay in contact at all times, part of that area will never get in direct contact, and in some area the contact will be made and lost repeatedly during the sweep. The behavior of this last group is not well-represented in the examples above nor in the model proposed by Lebedev and Beresnev (2004) and might give a twist to the quasistatic results presented before, because this group might behave dynamically on their own while not in contact with the vibrator.

To solve the rough contact problem dynamically in a full 3D setup is difficult and there is hardly any literature available on this topic. For these kinds of problems, the difficult 3D problem is typically replaced by a phenomenological model that is much simpler, but captures the essence of the problem. Instead of the contact, a set of linear springs with different heights, also called a Winkler foundation, is modeled. Rules for converting the full problem to such a model can be found in the work done by Heß (2012) and Popov (2013). Lebedev and Beresnev (2004), based on the work of Rudenko and Vu (1994), propose to use a Winkler foundation model (Figure 1 in their paper) to describe the vibrator-earth contact. To analyze the dynamic behavior of the contact, we use a similar model, see Figure 4.6, with the difference that the contact springs (top springs in Figure 4.6) are not allowed to extend beyond a certain threshold value (different for each spring) and are connected to some "ground" mass. Each individual ground mass is allowed to move freely but has a restoring force with respect to its displacement from a certain reference plane. In this model, the ground can move independently from the base plate, making the dynamic behavior most likely different from its static behavior.

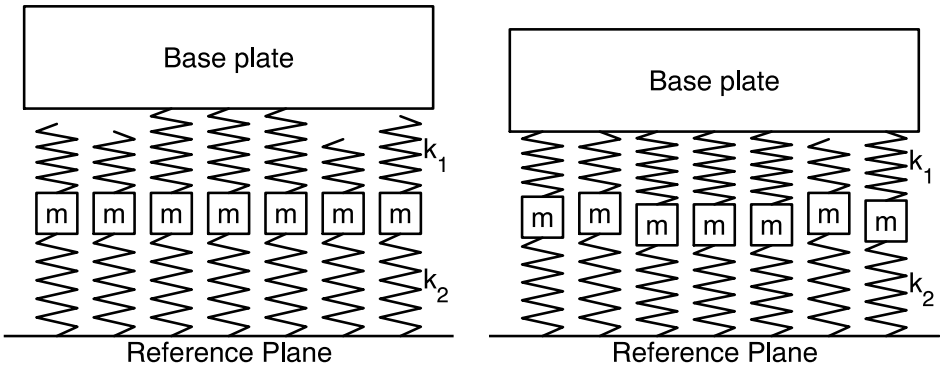

Figure 4.6: Multispring contact model. (a) Base plate just before it exerts a force on the ground, only a few springs are in contact. (b) After applying the static load of the weight of the base plate, reaction and hold down mass, more springs are in contact and some masses are displaced.

Instead of trying to convert our rough profiles shown in Figure 4.3 to an equivalent

Winkler foundation directly, we chose to use the quasistatic results (Figure 4.4), modeled with the program from Vollebregt (2014), and fit these with the multispring model of Figure 4.6. The force-displacement curves obtained with rough surfaces, presented in Figure 4.4, indicate that the contact becomes stiffer with increasing load. For the multispring model, this translates to more springs being in contact with the base plate at higher loads. Two steps were made to determine the appropriate spring height distribution, and hence the number of springs in contact at a certain displacement, to fit the reference force-displacement relation of Figure 4.4. First, the spring constants were fixed to a fraction of the smallest stiffness found in the force-displacement curve. Second, the number of springs needed to compensate the load was calculated at every displacement along the curve. For the reference curve in Figure 4.4, approximately 50 springs were needed. As a last step, the masses between the springs were chosen such that their sum equaled the mass of the base plate.

With these parameters, the behavior of the base plate was then determined numerically when loaded with a static force of approximately 320 kN and driven by a linear sweep at many different drive levels ranging from 10% to 90% of 275 kN. Some damping was added to the masses to keep the base plate in contact to at least a single mass-spring unit.

It is interesting to study the resulting transfers from the driving force, the linear sweep, to the base-plate displacement for different drive levels. Figure 4.7 shows the amplitude and phase response of the system when driven by a 12-s linear 8-to-80-Hz sweep. For this contact model, the base plate has a resonance frequency of approximately 60 Hz at the 10% drive level, which interestingly drops down to approximately 44 Hz at the 90% drive level. If the system is described as a single harmonic oscillator, the resonance frequency would be proportional to the square root of the effective stiffness. A frequency drop of approximately 75% thus translates to a reduction of the effective stiffness by almost a half. The amplitude and the width of the frequency peak increases slightly from low drive level to higher. Some striped patterns below the resonance frequency and especially at large force levels, indicating harmonic distortion, are also visible.

4.3. FIELD OBSERVATIONS

In 2012, a data set was obtained specifically focused on determining the amplitude-dependent behavior of vibrator-soil interaction. Part of the data shown here were presented before by Noorlandt *et al.* (2013). The experiment took place near Devine, Texas. The vibrator used was a modified 266 kN (60,000 lbf) vibrator from INOVA, mounted on an AHV-IV vehicle. The modifications mainly dealt with reducing the harmonic distortion. The experiment basically consisted of repeating the same linear 12-s 8-to-80-Hz sweep, with different drive levels. Ten different drive levels from 5% to 90% were used, and each drive level was repeated 10 times. After finishing the last sweep at a drive level of 90%, the whole sequence was repeated. In total, 200 sweeps were performed without moving the vibrator or lifting the base plate. The entire experiment was repeated at a second location only 20 m from the first, but with different top soil conditions. At the first location, the base plate was placed on grass-covered soil, at the second location on bare soil. The vibrator controller was set to follow the amplitude of weighted-sum ground force and the phase of the reaction mass. This was done such that the vibrator

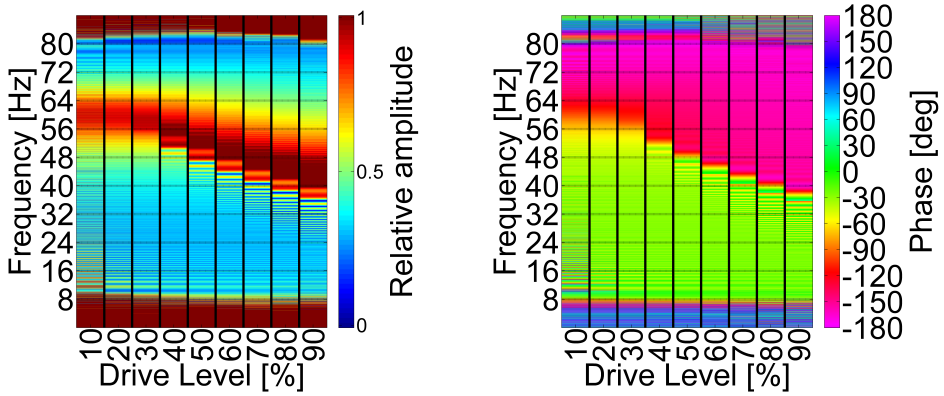

Figure 4.7: Transfer of driving force to base-plate displacement for the multispring contact model (Figure 4.6). (a) Amplitude and (b) phase spectra for different drive levels.

stayed within safe limits, without incorporating too much phase information from the base plate.

The idea behind this procedure is to get information on the influence of the drive level, permanent deformation, and repeatability of the source. Permanent deformation is thought to be dependent mainly on the soil characteristics directly beneath the base plate, the maximum amount of force applied, and the number of sweeps. By keeping the vibrator on the same location during the experiment, it is expected that the compaction of the soil reduces with number of sweeps performed. It is thus expected that the last sweeps of each set of 10 are more comparable than the first, and that after completing the first sequence, the lower drive-level sweeps of the second sequence are more repeatable than those of the first sequence.

Figure 4.8 shows the measured accelerations and weighted-sum-ground-force amplitude spectra for the first location. In that figure, each force strip consists of 10 consecutive sweeps. The figure displays a total of 200 sweeps. The amplitudes have been divided by drive-level percentages to make them comparable. Several observations can be made. First of all, it is clear that the controller does a good job, especially above approximately 24 Hz; the weighted-sum-ground-force signal has a flat amplitude spectrum, whereas the individual acceleration signals have not. The 10 sweeps done at each drive level produce very comparable amplitude spectra and the repeatability in both sequences seems to be equal. The most striking, however, is that the base-plate acceleration signals show a resonance, whose frequency decreases with the drive level. In the second sequence, the amplitude of the base-plate resonance is a little bit smaller at the lower drive levels.

To study this behavior in more detail, a correction has to be made for the fact that the driving signal was adjusted dynamically by the controller and thus has no flat spectra, as is clearly shown in Figure 4.8a. To remove the effect of the controller, the dynamic transfer from the total driving force acting on the base plate to its displacement was cal-

culated. Ignoring the hold-down system again, the total driving force equals the reaction mass times its (negative) acceleration (Figure 4.1). The base-plate displacement can be found by twice integrating its acceleration, which was done in the frequency domain. Having determined both signals, the transfer function is obtained by dividing the displacement signal by the force signal.

Figure 4.9 shows the transfer functions obtained for the first location, whereas Figure 4.10 shows the transfers for the second location nearby. The responses at these locations differ a bit, but the main features coincide. In both cases, a resonance is present that becomes stronger with the drive level. Also the frequency at which this amplification occurs decreases with the drive level; although, this is clearer in the first location and sequence than in the second location. Comparing the first sequence with the second sequence, it is notable that the behavior at the low drive levels is less comparable between sequences than those of the high drive levels. This is probably caused by the permanent deformation of the ground beneath the vibrator due to the high force levels in the first sequence. Furthermore, at the second location, where the vibrator was placed on bare soil, dust clouds from underneath the base plate were observed at high frequencies. The amount of dust did not noticeably decrease, even for the very last sweep, indicating that the contact was relatively poor and still reshaping even after approximately 200 sweeps.

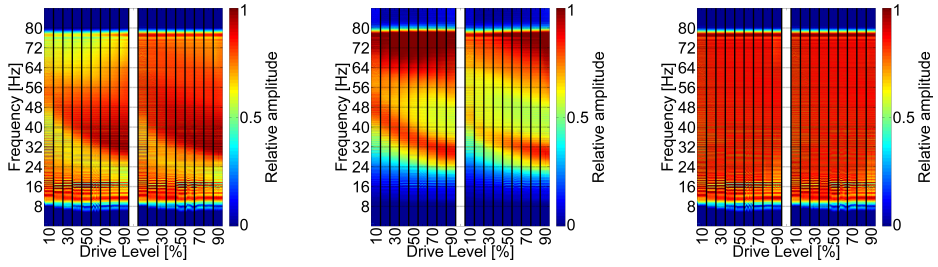

Figure 4.8: Measured amplitude spectra for two sequences of increasing drive levels at the first location (grass-covered soil). (a) Reaction-mass, (b) base-plate acceleration, and (c) the weighted-sum combination of both. Amplitudes divided by drive-level percentages.

Besides the dynamic aspects of the vibrator, the wavelet that the vibrator produces at different drive levels is, from a seismic perspective, even more interesting. Figure 4.11 shows for the first location the measured weighted-sum ground force and geophone response at 850 m depth after correlation with the pilot signal. The ground-force signal is almost completely the same for all drive levels and the two different sequences. It is also symmetric in time, indicating that the pilot and weighted-sum ground force are very alike. However, the signal measured in the borehole is not as stable and changes with drive level. The first arrival shifts a couple of ms to later times when comparing the 5% and the 90% case, for both sequences. The recordings of both sequences are very similar, indicating that the difference in spectra between these sequences (Figures 4.8 and 4.9) only have minor effect. Similar time shifts with drive-level variation were observed by Martin and Jack (1990). Therefore, it should be stressed that the weighted-

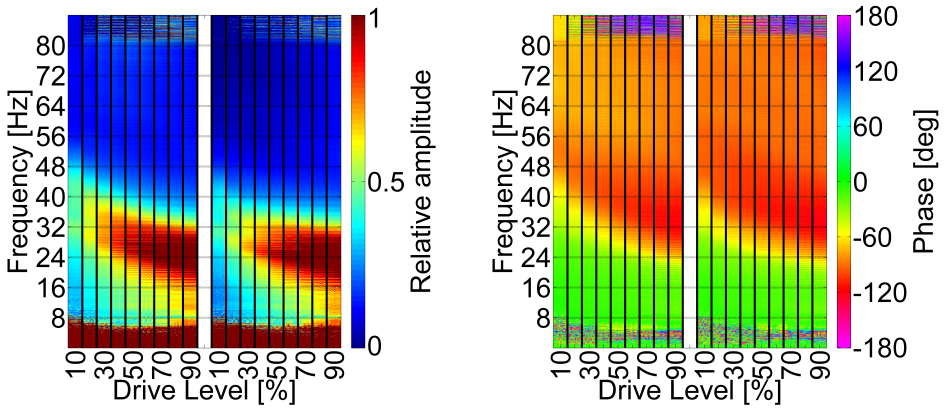

a b

Figure 4.9: Transfer of total driving force to base-plate displacement for field data at the first location (grass-covered soil). (a) Amplitude and (b) phase spectra for two sequences of increasing drive levels.

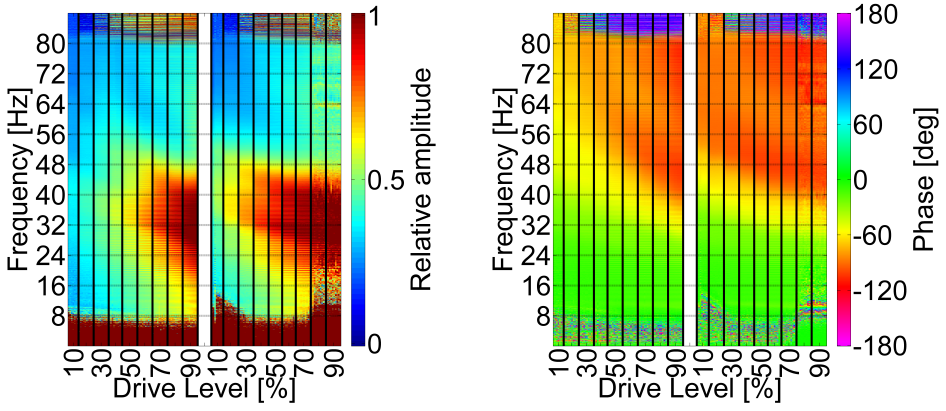

a b

Figure 4.10: Transfer of total driving force to base-plate displacement for field data at the second location (bare soil, 20 m away from the first location). (a) Amplitude and (b) phase spectra for two sequences of increasing drive levels.

sum-ground-force signal is only an estimate of the vibrator signature, and depending on soil conditions and drive level, might be less applicable. Similar observations were presented by Meunier (2011, p. 109, Figure 16).

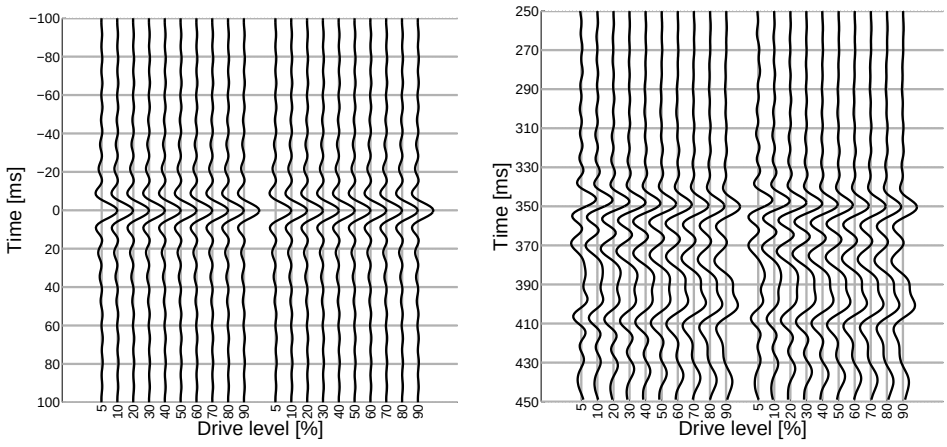

Figure 4.11: Weighted-sum ground-force signal (a) and (b) vertical-component borehole-geophone signal correlated by the normed pilot signal for different drive levels. For each drive level, the eighth sweep was plotted. Amplitudes were divided by drive-level percentages and normed by overall maximum per plot.

4.4. DISCUSSION

There are quite some similarities between the measured transfer signals shown in Figures 4.9 and 4.10 and the modeled transfers of the Winkler foundation model shown in Figure 4.7. In both cases, a resonance frequency is present whose frequency decreases with amplitude. Such shift of frequency cannot be predicted by a fully linear model in which source amplitude does not play a role in the dynamic behavior. It is therefore tempting to interpret the frequency shifts observed in the field as a contact-mechanical effect; however, the vibrator-earth contact might not be the only effect observed.

Reust (1993) argues that, because most soils are sublinear (force weakening), a decrease of resonance frequency with increasing drive level could be expected (see his Figure 5). In a field experiment comparable to ours, Johnson *et al.* (2009) find very similar decreases of resonance frequency with drive level. They attribute this frequency decrease to "modulus softening as a function of drive amplitude" and show that this happens at the source and between the (nearby) receivers (see their figures 7 and 8). Their argument to calculate the receiver-receiver ratios is to "reduce any contamination from potential nonlinear coupling of the vibrator plate to the ground." Because the resonance behavior in their source-to-receiver ratios is different from their receiver-to-receiver ratios, we conclude that contact mechanics played a role in their measurements.

It would be nice to be able to distinguish material and contact induced nonlinearity, but for this, further investigation of this topic is needed. Below, we discuss several

shortcomings and improvements possible to the modeling, experiment, and processing.

Several simplifications were made in the modeling. All of the results in this work are based on the assumption that the materials in contact can be described as linear elastic continua, which might not be appropriate for the materials a seismic vibrator encounters in the field, such as rock, soil, asphalt, concrete, etc. From the often observed permanent deformation of the material below the base plate, it is clear that this material does not behave purely elastically or, as the work of Johnson *et al.* (2009) indicates, linear. In our approach to use the quasistatic results in the multispring model (Figure 4.6), the horizontal interaction within the contact was ignored completely. This should be taken into account because a vertical stress will convert to vertical and horizontal displacements and thus will lead to a different deformation of the contact area than the one predicted by the current model.

On the experiment side, the main shortcoming is that only two vibrator parameters are measured, such as the accelerations of the base plate and reaction mass. Converting these two macroscopic parameters to many microscopic parameters is inherently non-unique. Load cells or more accelerometers will not solve this problem because first of all they provide macroscopic information only, and second, in the case of load cells, they alter the contact dramatically. However, insight in the dynamics of the vibrator-ground contact can be obtained with a pressure mapping device, without affecting the contact a lot. Results presented by Dean *et al.* (2015) are promising and show that the pressure underneath the base plate is far from uniform.

Regarding the data processing, one could argue that the concept of a transfer function is only valid in the linear regime and care has to be taken not to over interpret the results for the nonlinear case observed. Some of the responses might be more dependent on timing, and thus on the choice of sweep, than on frequency as suggested by the plot. To be able to determine the time dependency, not only the amplitude of the sweep should be changed, but also its frequency range and sweep rate.

4.4.1. IMPLICATIONS FOR FIELD MEASUREMENTS

Several lessons can be drawn from the conducted studies. From the modeling conducted it is clear that the contact behaves most nonlinear at small total loads (Figure 4.4). To avoid small total loads, the dynamic force on the base plate should be substantially smaller than the static force given by the total weight of the base plate, reaction mass, and hold-down system. Although not directly confirmed by our field data, lower drive levels did produce smaller levels of resonance amplification. Preparation of the contact can help to minimize the contact-mechanical effects. The smaller the height of the air gaps between the base plate and the earth the better (Figure 4.4b). To decrease the influence of permanent deformation insweeping, performing some sweeps before the actual production sweeps, seems to be a good idea, but from the field measurements it is observed that this is probably only effective if the contact preparation sweeps have a (much) larger drive level than the succeeding (production) sweeps. Measuring the pressure distribution underneath the complete base plate with a thin sensor would capture the effect of the base-plate flexure and contact mechanical effects, leading to a better ground force estimation. The work of Dean *et al.* (2015) showed that this is now possible.

4.5. CONCLUSION

We show that the contact between the vibrator and ground can have a significant effect on the behavior of the vibrator. Even if the applied force on the ground stays within its linear elastic limits, the geometry of the vibrator-ground contact can cause the displacement to respond nonlinearly to the applied force. As a consequence, the displacement changes asymmetrically with a force increase or decrease. Extending the quasistatic force-displacement relation to a dynamic study, with the help of a Winkler foundation model, it was shown that a reduction in base-plate resonance frequency with the drive level was to be expected. Field measurements performed with different drive levels show similar behavior, but other causes cannot be excluded and have been discussed. Moreover, the field measurements showed that the measured weighted-sum ground force was stable for different drive levels, but that the shape and timing of the wavelet observed in the borehole was not. Overall, it should be concluded that the drive level, next to the kind of sweep, is an important control variable.

REFERENCES

B. Aritman, *Repeatability study of seismic source signatures,* Geophysics **66**, 1811 (2001).

G. Baeten and F. Strijbos, *Wave field of a vibrator on a layered half-space: Theory and practice,* SEG Technical Program Expanded Abstracts, 92-96 (1988).

G. Baeten and A. Ziolkowski, *The vibroseis source* (Elsevier, 1990).

A. Castanet and M. Lavergne, *Vibrator controlling system,* US Patent 3,208,550 (1965).

T. Dean, P. Vermeer, M. Laycock, J. Tulett, and D. Lane, *The complexity of vibrator baseplate-ground interaction measured with a thin-film pressure pad and a downhole tool,* 77th EAGE Conference and Exhibition, We P6 07 (2015).

H. Hertz, *Ueber die Berührung fester elastischer Körper,* Journal für die reine und angewandte Mathematik , 156 (1882).

M. Heß, *On the reduction method of dimensionality: The exact mapping of axisymmetric contact problems with and without adhesion,* Physical Mesomechanics **15**, 264 (2012).

P. Johnson, P. Bodin, J. Gomberg, F. Pearce, Z. Lawrence, and F. Menq, *Inducing in situ, nonlinear soil response applying an active source,* Journal of Geophysical Research: Solid Earth **114**, B05304 (2009).

A. Lebedev and I. Beresnev, *Nonlinear distortion of signals radiated by vibroseis sources,* Geophysics **69**, 968 (2004).

A. Lebedev and I. Beresnev, *Radiation from flexural vibrations of the baseplate and their effect on the accuracy of traveltime measurements,* Geophysical Prospecting **53**, 543 (2005).

A. Lebedev, I. Beresnev, and P. Vermeer, *Model parameters of the nonlinear stiffness of the vibrator-ground contact determined by inversion of vibrator accelerometer data,* Geophysics **71**, H25 (2006).

W. Lerwill, *The amplitude and phase response of a seismic vibrator,* Geophysical Prospecting **29**, 503 (1981).

W. Lerwill, *Reply to comments by Sallas and Weber on "The amplitude and phase response of a seismic vibrator",* Geophysical Prospecting **30**, 939 (1982).

J. Martin and I. Jack, *The behaviour of a seismic vibrator using different phase control methods and drive levels,* First Break **8**, 404 (1990).

J. Meunier, *Seismic acquisition from yesterday to tomorrow* (Society of Exploration Geophysicists, 2011).

G. Miller and H. Pursey, *The field and radiation impedance of mechanical radiators on the free surface of a semi-infinite isotropic solid,* Proceedings of the Royal Society of London. Series A, Mathematical and Physical Sciences **223**, 521 (1954).

G. Miller and H. Pursey, *On the partition of energy between elastic waves in a semi-infinite solid,* Proceedings of the Royal Society of London. Series A. Mathematical and Physical Sciences **233**, 55 (1955).

R. Noorlandt, G. Drijkoningen, and C. Faber, *Influence of drive level on the fundamental vibrator signal,* 75th EAGE Conference and Exhibition, Th P11 02 (2013).

R. Noorlandt and G. Drijkoningen, *On the mechanical vibrator-earth contact geometry and its dynamics,* Geophysics **81**, P37 (2016).

B. Persson, *Theory of rubber friction and contact mechanics,* The Journal of Chemical Physics **115**, 3840 (2001).

F. Poletto, A. Schleifer, F. Zgauc, and L. Petronio, *Borehole signals obtained using surface seismic sources and ground-force sensors,* SEG Technical Program Expanded Abstracts, 4298 (2011).

V. Popov, *Contact mechanics and friction* (Springer, 2010).

V. Popov, *Method of reduction of dimensionality in contact and friction mechanics: A linkage between micro and macro scales,* Friction **1**, 41 (2013).

E. Reissner, *Stationäre, axialsymmetrische, durch eine schüttelnde Masse erregte Schwingungen eines homogenen elastischen Halbraumes,* Archive of Applied Mechanics **7**, 381 (1936).

D. Reust, *Enhanced servovalve technology for seismic vibrators,* Geophysical Prospecting **41**, 43 (1993).

O. Rudenko and C. Vu, *Nonlinear acoustic properties of a rough surface contact and acousto diagnostics of a roughness height distribution,* Acoustical Physics **40**, 668 (1994).

P. Sainsot and A. Lubrecht, *Efficient solution of the dry contact of rough surfaces: a comparison of fast Fourier transform and multigrid methods,* Proceedings of the Institution of Mechanical Engineers, Part J: Journal of Engineering Tribology **225**, 441 (2011).

J. Sallas and R. Weber, *Comments on "The amplitude and phase response of a seismic vibrator" by W.E. Lerwill,* Geophysical Prospecting **30**, 935 (1982).

J. Sallas, *Seismic vibrator control and the downgoing P-wave,* Geophysics **49**, 732 (1984).

J. Sallas, *How do hydraulic vibrators work? A look inside the black box,* Geophysical Prospecting **58**, 3 (2010).

C. Saragiotis, P. Scholtz, and C. Bagaini, *On the accuracy of the ground force estimated in vibroseis acquisition,* Geophysical Prospecting **58**, 69 (2010).

S. Shan, P. Eick, J. Brewer, X. Zhu, and S. Shaw, *Load cell system test experience: Measuring the vibrator ground force on land seismic acquisition,* SEG Technical Program Expanded Abstracts , 16 (2009).

M. van der Veen, J. Brouwer, and K. Helbig, *Weighted sum method for calculating ground force: an evaluation by using a portable vibrator system,* Geophysical prospecting **47**, 251 (1999).

E. Vollebregt, *A new solver for the elastic normal contact problem using conjugate gradients, deflation, and an FFT-based preconditioner,* Journal of Computational Physics **257**, 333 (2014).

D. Walker, *Harmonic resonance structure and chaotic dynamics in the earth-vibrator system,* Geophysical Prospecting **43**, 487 (1995).

Z. Wei, *Design of a P-wave seismic vibrator with advanced performance,* GeoArabia **13**, 123 (2008).

Z. Wei, *How good is the weighted-sum estimate of the vibrator ground force?* The Leading Edge **28**, 960 (2009).

Z. Wei, M. Hall, and T. Phillips, *Optimizing the weighted-sum signal to represent the actual force output from the vibrator,* 72nd EAGE Conference and Exhibition 2010, P291 (2010).

5

OPTIMIZING VIBRATOR SIGNALS

Linear sweeps are the mostly used signals to drive seismic vibrators. Their constant amplitude over time and flat frequency spectra are desired properties. However, the transfer from the signal used to drive the vibrator to the seismic wave can affect these properties considerably. Design of the phase offset of the sweep can help to reduce the low-frequency energy of a sweep or can be used to assist in separating simultaneous-source records. Furthermore nonlinear behavior of the vibrator, the ground and their contact will distort the sweep and produce harmonics, which, after processing, show up as noise and ghost events in the records. Nonlinear sweeps, with both sweep rate and amplitude carefully designed, can be used to anticipate on these transfer functions and help to remove harmonic noise from the seismic records.

5.1. INTRODUCTION

The goal of an active seismic experiment is to obtain information about the earth, by sending a mechanical wave through it. This wave needs to be generated at the source and captured at a receiver. The source puts constraints on the waves that can be made, while the receiver puts constraints on the waves that can be observed. Crucial is the fact that the receiver should have a way to identify the wave coming from a specific source within all the ambient vibrations received. For impulsive sources, the timing and very high source amplitudes, leading to high instantaneous signal-to-noise ratios, is used to accomplish this. Signals originating from vibrator sources typically have a much smaller amplitude and instantaneous signal-to-noise ratio, but the characteristics of their signal are much better known and can be used to identify them at the receiver end.

The most common signal used to drive a seismic vibrator is the sweep. Sweeps have a number of pleasant properties that make them very effective as vibratory source signal.

1. They are easy to calculate and generate,
2. are continuous in the time and frequency domain,
3. have a low crest factor,
4. have a controllable power spectrum and

5. have good autocorrelation properties.

Although vibrators can be driven with other signals, designing other signals with properties similar to the sweep is very difficult. Improvement of some of the properties of the signal typically reduces the quality of others. Dean (2014) gives an overview on pseudorandom signal designs. All methods he discussed produce signals with either a high crest factor or discontinuities or both. Because the peak amplitude of a vibrator is limited, signals with higher crest factor will have lower root-mean-square amplitude and therefore a lower signal-to-noise ratio.

In this chapter we first review the linear sweep. We will present the role of the taper and phase offset. We then will discuss the difficulty that comes with the commonly generated harmonics. Finally we will present two optimization techniques. The first technique can be used to design sweeps that are more robust against noise of harmonic origin. The second technique presented can be used to determine the sweep rate that produces a signal with a desired power spectrum, given a certain time amplitude.

5.2. LINEAR SWEEPS

Sweep signals can be calculated through (see for example Aldridge, 1992)

$$s(t) = A(t)\sin(\phi(t)), \tag{5.1}$$

where $A(t)$ is a time-varying amplitude term and $\phi(t)$ is a time-varying phase term in radians, not to be confused with the frequency-domain phase spectra. The phase $\phi(t)$ and frequency $f(t)$ of a sweep are related by

$$\phi(t) = \phi_0 + 2\pi \int_0^t f(\tau)\mathrm{d}\tau, \tag{5.2}$$

where the frequency is given in Hertz and ϕ_0 is some constant phase offset in radians. In a linear sweep the frequency changes linearly with time, $f(t) = f_0 + \alpha t$, where f_0 is the starting frequency (sometimes referred to as the carrier frequency) and α is the sweep rate in Hz/s. The phase of the sweep is equal to

$$\phi(t) = \phi_0 + 2\pi(f_0 t + \frac{1}{2}\alpha t^2), \tag{5.3}$$

For $\alpha > 0$ the frequency increases over time and the sweep is called an upsweep. For $\alpha < 0$ the frequency decreases over time and we have a downsweep. For $\alpha = 0$, the signal is just a monotonic sinusoidal with a frequency equal to f_0.

For linear sweeps the amplitude term $A(t)$ is commonly taken constant during the sweep except for a small period of time at the start and end of the sweep, where the amplitude is smoothly going to zero to reduce edge effects.

5.2.1. ROLE OF TAPERS

Part of a design of a sweep is the choice of a taper. The influence of a taper on the power spectrum is best illustrated with an example. Figure 5.1a presents the power spectrum belonging to a linear sweep for three different tapers. Applying a taper helps to reduce the oscillations and amount of overshoot in the frequency domain, but the choice of taper also affects the bandwidth available.

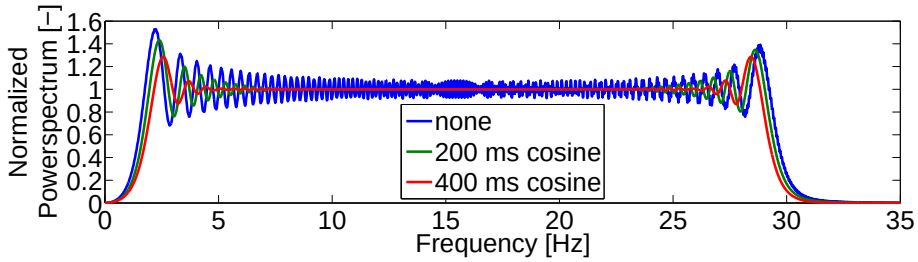

a

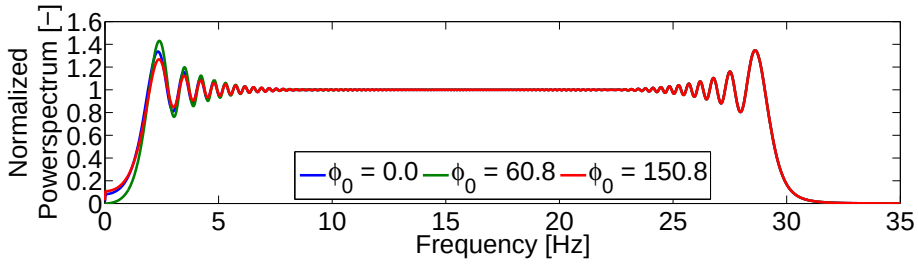

b

Figure 5.1: Impact of the taper (a) and phase offset (b) on the power spectrum of a 15-s linear sweep from 1 to 30 Hz. For the taper plot, the phase offsets were chosen such that the DC component of each sweep was zero. For the phase offset plot, a cosine taper of 200 ms was used.

5.2.2. PHASE OFFSET TO CONTROL LOW FREQUENCIES

The phase offset (ϕ_0 in equation 5.2) has an influence on the lower end of the spectrum as can be seen in Figure 5.1b. For the example given, a phase offset of about 60.8 degrees reduces the DC component of the sweep to zero (green curve), adding an extra 90 degrees increases the DC component to the highest value possible with this sweep (red curve). The blue curve representing a phase offset equal to zero is somewhere in between. Note that the green curve has a small DC component, but a large overshoot, while this is reversed for the red curve.

The phase offset of any kind of sweep can always be chosen such that the DC component equals zero as we will show here. The phase of the sweep, equation 5.2, can be defined as,

$$\phi(t) = \phi_0 + \psi(t), \tag{5.4}$$

where $\psi(t)$ represents the phase change over time due to the, possibly complicated, time-frequency function of the sweep. Instead of calculating the DC component of the sweep directly,

$$X = \int_0^T A(t)\sin(\phi_0 + \psi(t))\mathrm{d}t, \tag{5.5}$$

where T is the duration of the sweep, we integrate the complex version of the sweep,

$$Z = \int_0^T A(t) e^{i(\phi_0 + \psi(t))} \mathrm{d}t = e^{i\phi_0} \int_0^T A(t) e^{i\psi(t)} \mathrm{d}t, \tag{5.6}$$

and use ϕ_0 to rotate the outcome of the integral such that the imaginary part of Z becomes zero. Because X is equal to the imaginary part of Z, this rotation makes sure that the original sweep will have a DC component equal to zero. Although the integral typically has to be evaluated numerically, determining the optimal rotation angle is simple.

The influence of the phase offset on the low frequency of the sweep is generally ignored, but, as indicated by the work of Tellier *et al.* (2014), choosing the phase offset wisely can help to get more output at the low frequencies. At the low frequencies the maximum drive level of a vibrator is restricted due to the finite stroke of the reaction mass and the possible presence of resonances due to (air) springs (see for example Figure 2.8). Therefore the small difference between the curves shown in Figure 5.2b can still have a significant effect on the maximum driving force possible.

5

5.2.3. PHASE OFFSET TO SEPARATE SOURCES

The phase offset of the sweep can also be used to assist in separating source signals in a simultaneous acquisition survey. The basic idea is to make multiple records and give each source an unique phase offset pattern, so that when rotated back during processing, only the desired source signal interferes constructively while all other source signals interfere destructively. A nice description of how this works and overview on the evolution of literature on this topic is given by Meunier (2011). The method itself probably started with changing the sign of the signals used, as described by Silverman (1979) and was later generalized to a multi-phase approach by Landrum (1987). Interestingly the technique might also help to suppress harmonic noise in the data, because the higher harmonics react differently to the phase offset than the fundamental signal, see patents by Rietsch (1977a) and Edington and Khan (1991).

To elucidate the method, an example of the separation of three simultaneously operating sources is given in Figure 5.2. In this example the sources are used to make three records to enable their separation, see Figure 5.2a-c. For each record, the color of the sweep indicates the phase offset used by the sources, blue representing 0 degrees, green representing 120 degrees and red representing 240 degrees. Source A uses the same sweep for all records. Source B uses a sweep with phase offset equal to 0, 120 and 240 degrees. Source C uses phase offsets of 120, 0 and 240 degrees. For illustration purposes source A starts at 1 s, source B at 2 s, and source C at 3 s. Although it is not possible to separate the contribution of each source from the individual records, it is possible by combining the records. This is shown for each source in Figure 5.2d-f. First, the records are correlated with the sweep signal used by the source of interest at the time of recording (taking into account its phase offset, shown in blue, green and red). Second, the obtained correlated records are summed together (shown in black). The correlation rotates the phase offsets of the different contributions of the records, but only the phase offset of the source of interest is rotated to 0 degrees in each record. The phase offsets of the other source contributions vary with the records. The specific phase-offset pattern used in this example makes sure that, after correlation, the phase offset of the other

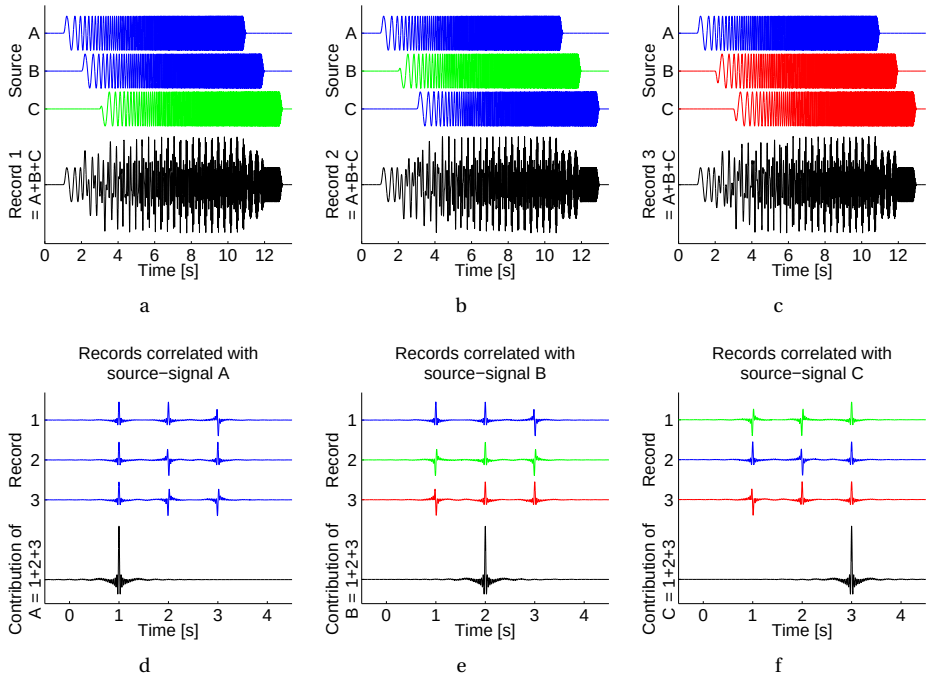

Figure 5.2: Phase offset used in a multi-source setup. (a-c) Contribution of the simultaneously operating sources (A, B and C) to the three recordings. The color of the source signals represent the phase offset used, blue represents 0 degrees, green represents 120 degrees and red represents 240 degrees. (d-f) Procedure to extract the contributions of the three different sources. First, each record is correlated by the sweep used by a specific source (blue, green, red). Second, the results are added together (black).

source contributions is equal to 0, 120 and 240 degrees in one of the records. Therefor by summing the records their contribution vanishes.

Although the example shows that the method works in theory, there are a number of considerations to take into account in practice. First, the method only works if the number of records per location is equal to, or larger than, the number of sources active. If no stacking was needed, i.e. a single sweep per source would suffice, there is no time improvement. Second, the dynamic range of the receivers has to be large enough to be able to record the stronger total signal, but at the same time should be able to capture enough resolution needed for further processing. Third, the method relies on all sources acting completely synchronously in every record. If they do not, the separation will degrade. Similar degradation occurs if the phase offset produced by the vibrators is not accurately enough. Noise and harmonics will further reduce the strength of the method.

5.2.4. SHORTCOMINGS AND HARMONICS

Linear sweeps are very useful, but there are cases where more control is required. The power spectrum of the linear sweep with constant amplitude is flat, which is a good property if it can be retained throughout the process of translating a vibrator drive signal to a traveling seismic wave. However, the transfer function belonging to this translation is typically complex and can alter the spectra significantly. Some frequencies might be boosted due to resonances in the vibrator, ground and their contact, whereas other frequencies might be attenuated strongly. To make a far-field seismic wavelet with a flat amplitude spectrum, the driving sweep should be designed such that it anticipates on the effects of the transfer function. For a linear sweep the only possibility to change the spectrum is by changing its time amplitude and therefore decreasing the average energy output of the vibrator. This might not be desired.

Furthermore, because the vibrator, the ground, and their contact do not act perfectly linear, the source wavelet also gets distorted by harmonics. Harmonics cause the sweep to become self-similar, due to the fact that certain frequencies appear at multiple instances in time. This self-similarity generates ghost events in the seismic record. These ghost events especially present a problem in case the ghost of one event masks the arrival of another event. Especially linear sweeps are not very robust against harmonic noise as we will show below.

The self-similarity of a sweep with a monotonically varying frequency caused by higher harmonics can be elucidated by splitting the frequency range of the sweep into octaves (powers of 2). Starting with the lowest frequency of the sweep f_{min}, we define octave n to have frequencies from $2^{n-1} f_{\text{min}}$ to $2^n f_{\text{min}}$. For the first octave that is (partly) covered by the sweep n equals 1, while for the last octave (partly) covered by the sweep n equals $\lceil \ln\left(\frac{f_{\text{max}}}{f_{\text{min}}}\right) / \ln(2) \rceil$, where f_{max} is the highest frequency in the sweep. Higher harmonics are multiples of the fundamental frequency and because the first harmonic is twice the fundamental, the frequency range of the first harmonic belonging to octave n will by definition overlap with the frequency range of octave $n+1$. Therefore it is obvious that the last octave of a sweep can not cause harmonics that overlap with the frequency range of the sweep. Also, by reversing the reasoning, the frequency range of the first octave of the sweep can not be present in any of the higher harmonics. As a consequence self-similarity due to harmonics does not occur if the sweep spans only one octave or

less. If the sweep spans more than one octave, however, frequencies in the sweep and its harmonics overlap. Typically frequency ranges used to drive vibrators span multiple octaves and therefore self-similarity of the seismic wavelet is difficult to avoid. Note that the amount of overlap between the fundamental and its harmonics is only determined by the bandwidth used and is irrespective of the time-frequency function used to generate the sweep. To illustrate this, Figure 5.3 shows the time-frequency curves of two 15-s 10-to-80 Hz sweeps and their first 9 harmonics. Both sweeps span exactly three octaves, but have different sweep rates. For both sweeps the first 6 harmonics contain frequencies that overlap with the fundamental frequencies of the sweep.

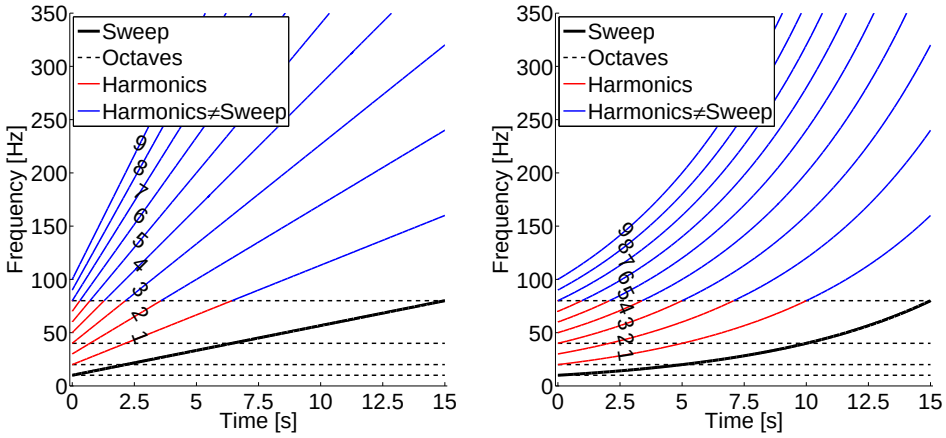

Figure 5.3: Time-frequency curves of two 15-s 10-to-80 Hz sweeps and their first 9 harmonics. (a) Linear sweep and (b) nonlinear sweep. Harmonics are colored red or blue depending if their frequency overlap with the sweep or not.

Figures 5.4a and 5.4b present various correlation and deconvolution results for the linear sweep used in Figure 5.3a. In Figure 5.4a emphasis is put on the main peak, while in Figure 5.4b emphasis is put on the noise by muting the main peak and then applying a gain of 10 to the data. Note the completely different time scales between Figure 5.4a and 5.4b. The cases shown are:

I autocorrelation of the sweep (without harmonics)
II case I deconvolved for the sweep (without harmonics)
III correlation of the sweep including harmonics and the sweep without harmonics
IV autocorrelation of the sweep including harmonics
V case IV deconvolved for the sweep including harmonics
VI as case III but with white noise added
VII as case IV but with white noise added
VIII as case V but with white noise added

The harmonics were modeled with equal amplitude and phase as the sweep. Although this does not completely match with typical observations in the field, it does help to illustrate the problems faced. The white noise added was set to 25% of the peak amplitude

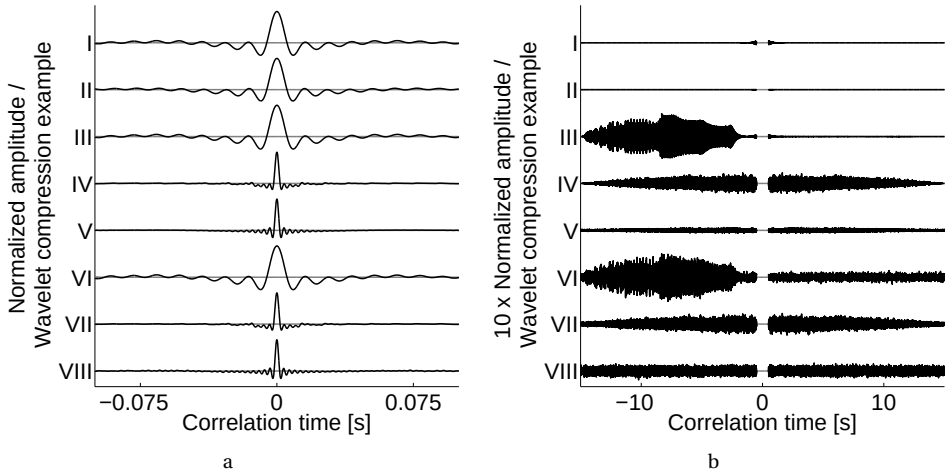

Figure 5.4: Correlation and deconvolution examples at small (a) and large (b) time lags for a 15-s 10-to-80 Hz linear sweep with and without harmonics. In plot b the main peak has been muted ($|t| < 0.5$ s). See text for an explanation of the examples.

in the spectrum of the signal and was only added to one of the signals going into the correlation or deconvolution. Before the wavelet compression step the data were filtered with a low pass filter of 350 Hz.

Case I and II indicate that the linear sweep produces a nice peak (Figure 5.4a) without noise at earlier or later times (Figure 5.4b). Because the linear sweep already has a flat spectrum the deconvolution step (II) does not add much benefits compared to correlation alone (I). The presence of harmonics (case III) does not affect the central peak (compare Figure 5.4a case I and III), but does cause noise at earlier times, so called harmonic correlation noise (compare Figure 5.4b case I and III). If the source wavelet including the harmonics can be estimated and used in the processing, the resolution of the central peak can be enhanced due to the larger total bandwidth of the source wavelet (Figure 5.4a case IV and V), but the price to pay is that the harmonic noise occurs on both sides of the central peak (Figure 5.4b case IV and V). The deconvolution step reduces this harmonic induced noise considerably (compare Figure 5.4b case V with IV) and enhances the central peak a little bit further. In the real world the wavelet produced by the source is not so well known as assumed in case IV and V. To display the effect a mismatch between the true wavelet and wavelet used to compress the data, white noise was added to case VI, VII and VIII. White noise is not the best estimate of the difficulties determining the source wavelet in the field, but does suit the purpose of illustration here. In case VI the recorded "data" contain the noise and are correlated with the "clean" sweep. The output is very similar to case III, but noise is present along the whole time domain (compare Figure 5.4b case VI with III). In cases VII and VIII the recorded "data" are free of noise, but the noise has been added to the wavelet estimate. Comparing case VII with VIII it is clear that correlation is more stable with respect to noise than deconvolution and that the benefits of performing a deconvolution are greatly reduced.

5.3. NONLINEAR SWEEPS: CONTROL ON HARMONIC CORRELATION NOISE

To obtain more control on the power spectrum of a sweep and its robustness against harmonic noise the amplitude and frequency function of the sweep should be optimized. The specific choice of $f(t)$ and $A(t)$ in equation 5.1 control the time behavior of the sweep as well as its frequency content. Qualitatively it is clear that the more time or amplitude is spent on a certain frequency range the more power it will obtain. To quantify this, one needs to solve for the Fourier transform of the sweep,

$$Y(\omega) = \int_{-\infty}^{\infty} A(t) \sin\big(\phi(t)\big) e^{-j\omega t} \mathrm{d}t \tag{5.7}$$

where the phase $\phi(t)$ is defined as in equation 5.2. The power spectrum of the sweep can be found by multiplying equation 5.7 with its conjugate, $P(\omega) = Y(\omega)\overline{Y(\omega)}$. Even for a linear sweep the integral in equation 5.7 can only be solved in terms of Fresnel integrals as shown by Aldridge (1992). A more practical approach is to approximate equation 5.7 with the stationary-phase method. Rietsch (1977b,c) introduced this approximation to the geophysical community and found that the power spectrum $P(\omega)$ of an upsweep can be approximated by

$$P(\omega) \approx \frac{A^2(\tau)}{4f'(\tau)} \tag{5.8}$$

where τ is the stationary point equal to the solution of $\omega = 2\pi f(\tau)$, i.e. where the Fourier transform frequency equals the sweep frequency.

Equation 5.8 can be used to design a sweep that is more robust against the effects of harmonics. Although the generation of harmonics can not really be influenced by the design of the sweep, the timing of the harmonic correlation noise can be modified. For a linear upsweep the harmonic correlation noise appears as dispersed energy arriving before the main event, see Figure 5.4 example III. The time difference between the main event and the harmonic correlation noise is completely determined by the pattern at which the frequencies of the sweep reoccur in its harmonics. For a linear upsweep the time difference of the reoccurrence of frequencies increases over time, causing the harmonic correlation noise to be dispersed. The increase in time difference can be seen in Figure 5.3a as an increase of the horizontal distance between the sweep and its harmonics. The time difference between the sweep and its first harmonic is smallest at the lower end (at 20 Hz the difference is approximately 2.1 s) and increases toward the high end of the sweep (at 80 Hz the difference is approximately 8.6 s). The ghost events due to the first harmonic therefore is to be expected from about 2 to 9 s before the recorded main events. The higher harmonics will produce ghosts that are more dispersed and occur at a larger offset from the main event. Although the horizontal distance in Figure 5.3 give some indication on the expected arrival times of the harmonic correlation noise, one should keep in mind that the finite duration of the sweep will cause the harmonic noise to be present over a larger time window than determined from the time-frequency curves.

To increase the time offset between the main events and their harmonic ghosts for a linear upsweep one should increase the starting frequency of the sweep and decrease

its sweep rate. Increasing the starting frequency is not desired, because it reduces the resolution of the seismic wavelet. Increasing the sweep rate might also not be desired, because it increases the duration of the sweep and reduces the production speed. However, if we allow the sweep to be nonlinear, more options are available. For example if we design a time-frequency function $f(t)$ that obeys $f(t+\Delta) \leq 2f(t)$ we make sure that the time difference between the sweep and its harmonics is at least Δ. Therefore after correlation the ghost will be approximately Δ away from the main event. For sufficiently large Δ the harmonic noise of the last (expected) event will appear well before the first (expected) real event.

One function that obeys $f(t+\Delta) = 2f(t)$ is,

$$f(t) = f_0 2^{\frac{t}{\Delta}}. \tag{5.9}$$

Figure 5.3b actually presents an example of a sweep with such a time-frequency function that covers the same frequency range in the same amount of time as the linear sweep shown in Figure 5.3a. In the example given $f_0 = 10$ and $\Delta = 5$. Comparing this nonlinear sweep with the linear sweep we see that the time difference between the sweeps and their first harmonics is different. The nonlinear sweep has a constant distance (5 s), while the linear sweep starts with smaller distances (approximately 2 s) and ends with larger distances (approximately 9 s). It is thus expected that the nonlinear sweep will have a larger offset between the main event and its harmonic ghosts than the linear sweep.

If the amplitude of a sweep with a time-frequency function as in equation 5.9 is kept constant, the power spectrum will decrease rapidly with frequency. The appropriate time amplitude $A(t)$ belonging to a specified power spectrum $P(\omega)$ can be found by substituting equation 5.9 into 5.8,

$$A(t) = 2\sqrt{P\big(2\pi f(t)\big)\frac{\ln 2}{\Delta} f(t)}. \tag{5.10}$$

For a flat power spectrum, like $P(\omega) = 1$, it is clear that the amplitude needs to increase with frequency to compensate for the increasing sweep rate over time. Two issues make a direct application of a sweep with this amplitude and time-frequency function impractical.

First, a vibrator can only be driven up to a certain maximum amplitude. Therefore the amplitude function has to be fitted into the dynamic range of the vibrator. To be able to produce the strong amplitudes at high frequency, the amplitude at the low frequencies need to be small. This might lead to unacceptable signal-to-noise ratios at the low frequencies.

Second, because the time difference between the occurrence of a certain frequency in the sweep and its first harmonic is constant, the harmonic correlation noise of the first harmonic will be much more focused in time as compared with a sweep with constant sweep rate. Although this happens at a controllable offset from the center peak (at $-\Delta$) this still might not be desired.

To solve these issues we propose to use a hybrid method. At low frequencies use the exponential function and switch to a linear scheme when the sweep rate increases above a certain threshold. An example of this approach is given in Figure 5.5. In this

example a linear 10-s 10-to-100 Hz sweep is optimized. We chose Δ as 3 s, and did not allow the sweep rate to exceed the original sweep rate (9 Hz/s). The optimized sweep uses the time-frequency function of equation 5.9 until the sweep rate is equal to 9 Hz/s (at approximately 6 s) and then continues using the linear time-frequency function, see Figure 5.5a. The original sweep is shown in red and the optimized sweep is shown in blue. The length of the sweep increases to approximately 13 s using this optimization procedure. To make sure the optimized sweep produces the same power spectrum as the linear sweep (as shown in Figure 5.5b) the amplitude of the first part of the sweep is adjusted according to equation 5.10, visible in Figure 5.5c. Figure 5.5d displays the correlation of the sweeps without harmonics with the sweeps including the first 4 harmonics. From this plot it is clear that the optimization procedure indeed is able to move the harmonic noise away from the central peak. Note that although the noise moved away in time, it did become stronger. Therefore this technique should only be applied in case Δ can be made large enough.

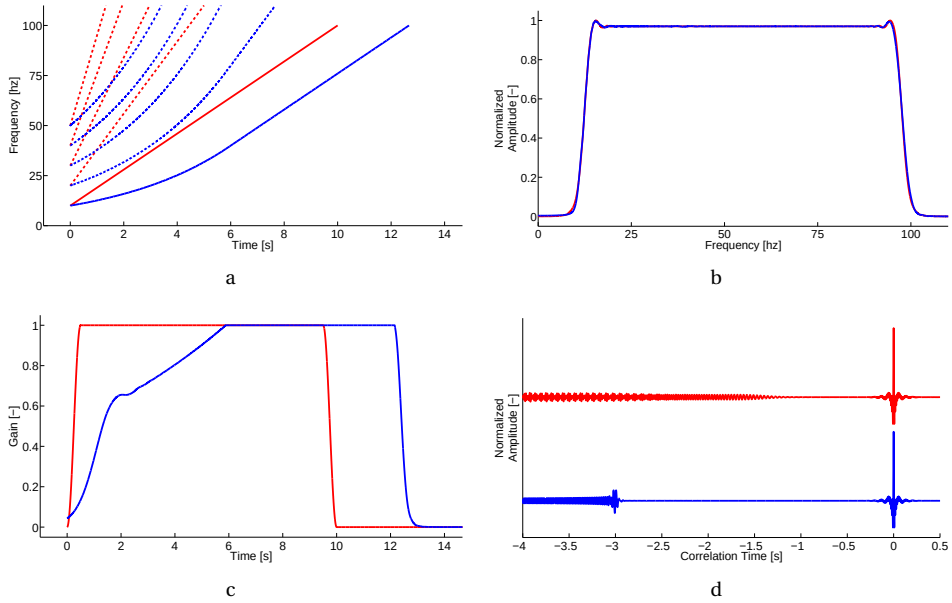

Figure 5.5: Comparison of a linear sweep (red) and nonlinear sweep optimized for less harmonic correlation noise (blue). (a) Time-frequency plot showing the sweeps (solid lines) and their first 4 harmonics (dashed lines). (b) Spectrum belonging to the sweeps (without harmonics). (c) Time amplitude of the sweeps. (d) Sweeps including 4 harmonics after being correlated with the sweeps without harmonics.

5.4. NONLINEAR SWEEPS:
POWER SPECTRUM SHAPING BY SWEEP RATE VARIATION

Another applications of equation 5.8, and the original topic of the paper by Rietsch (1977c), is to determine the frequency-time relation $f(t)$ given a time amplitude $A(t)$

and power spectrum $P(\omega)$. Analytical solutions to equation 5.8 can only be found for very specific, and very limited, amplitude and power spectrum functions. In order to allow for more general functions, numerical solutions are necessary. Rietsch (1977c) proposed to solve equation 5.8 by a finite difference scheme based on Taylor series expansions. He presents two sets of equations. One set can be used for the parts of the sweep where $A(t)$ is constant and the other set is for those parts of the sweep where $A(t)$ changes over time, due to a taper for example.

We like to propose a different method here, which we think is more elegant. Rietsch (1977c) showed (his equation 12 and 13) that equation 5.8 can be rearranged and integrated to get the following equality,

$$\frac{1}{4}\int_0^t A^2(\tau)\mathrm{d}\tau \approx \int_0^t P(2\pi f(\tau))f'(\tau)\mathrm{d}\tau = \int_{f_0}^{f(t)} P(2\pi\nu)\mathrm{d}\nu. \tag{5.11}$$

The difficulty in solving this for $f(t)$ is that the right-most integral should be inverted and applied to the first integral. However, another method is possible to determine $f(t)$. Our method is based on the observations that the first integral is a measure of the energy of the signal in the time domain and the last integral is a measure of its energy in the frequency domain. Both integrals can be solved numerically and extracting the time-frequency curve can be done by simply matching the cumulative energy values from time-domain with those in the frequency-domain.

Before this can be done, however, the energies in both domains should be made compatible. Equation 5.11 approximately holds for a sweep, but it is not likely to hold in case the power spectrum and time-domain amplitude are chosen independently. To make sure that Parseval equation holds, the energy integrals of the chosen functions should be normalized,

$$E(t) = \frac{\frac{1}{4}\int_0^t A^2(\tau)\mathrm{d}\tau}{\frac{1}{4}\int_0^T A^2(\tau)\mathrm{d}\tau} \tag{5.12}$$

$$E(f) = \frac{\int_{f_0}^{f(t)} P(2\pi\nu)\mathrm{d}\nu}{\int_{f_0}^{f_T} P(2\pi\nu)\mathrm{d}\nu} \tag{5.13}$$

where $E(t)$ is the cumulative energy in the time-domain and $E(f)$ is the cumulative energy in the frequency domain. The normalization is possible, because the duration T, the starting frequency f_0 and final frequency f_T of the sweep are known.

The time-frequency curve is found by first constructing the cumulative time-energy integral $E(t)$ and constructing the cumulative frequency-integral $E(f)$. Then for a certain time t, the cumulative energy $E(t)$ is determined, and that value of $E(t)$ is used for $E(f)$ to find the corresponding frequency f. This latter can involve interpolation. This is repeated for many different values of t to construct the full time-frequency curve. If the time steps are chosen small enough the time-frequency curve can be reconstructed with enough resolution for practical purposes.

Figure 5.6 presents an example that illustrates the method. In Figure 5.6a the prescribed amplitude curve is shown. Figure 5.6b shows the specified power spectrum. Note that the absolute values of the curves in Figure 5.6a and 5.6b are not of importance

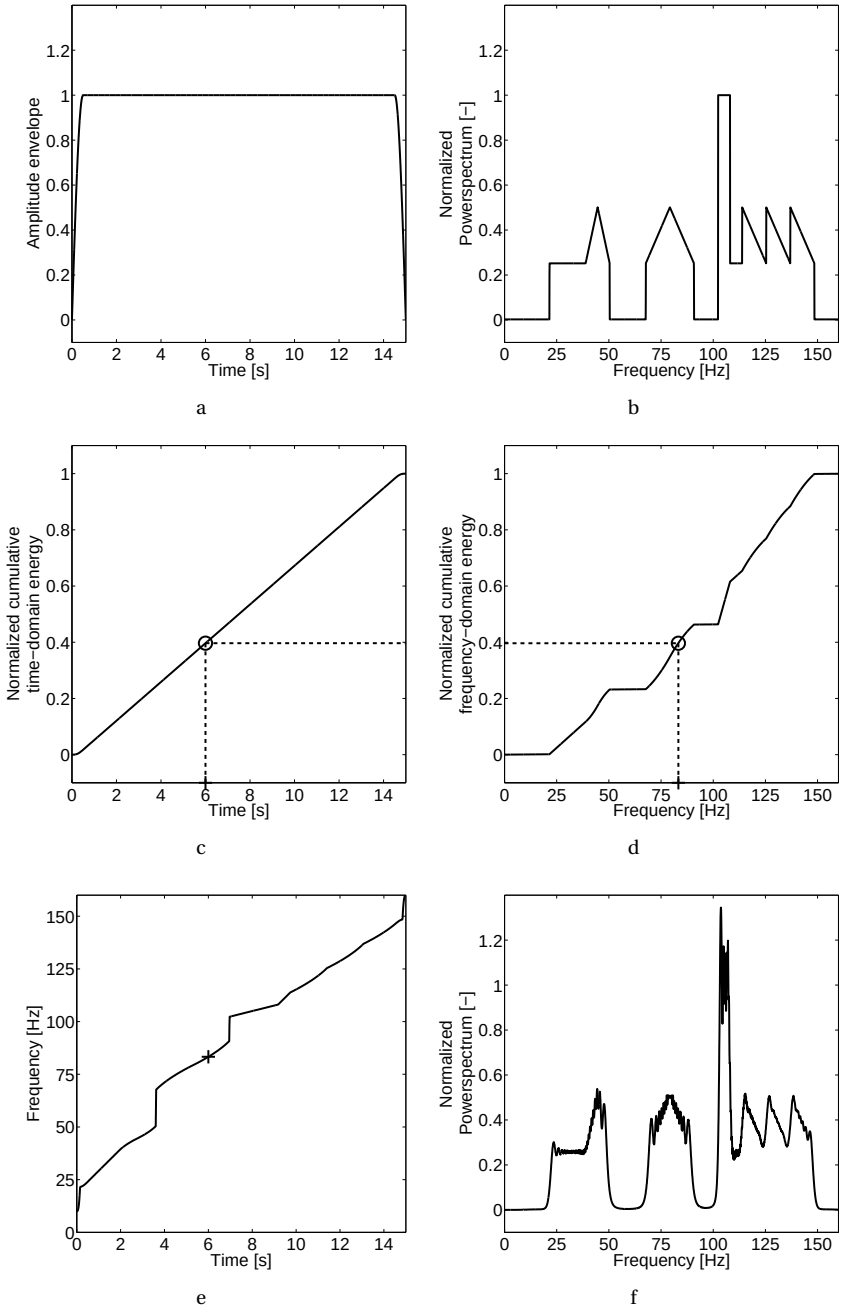

Figure 5.6: Design of a nonlinear sweep with prescribed time amplitude and power spectrum. (a) Prescribed time amplitude, (b) specified power spectrum (design), (c) normalized cumulative energy of the time amplitude, (d) normalized cumulative energy of the frequency spectra, (e) time-frequency relation calculated and (f) realized power spectrum.

for the method due to the normalization step. In Figure 5.6c and 5.6d, $E(t)$ and $E(f)$ are plotted respectively. The method of determining a single point on the time-frequency curve is illustrated. First, the energy belonging to a certain time instance (6 s in this case, indicated with a cross in Figure 5.6c) is determined (0.4 in this case, indicated with a circle). Second, the crossing of the energy found in the time domain with the energy curve in the frequency domain is determined (circle in Figure 5.6d), because they need to be the same according to equation 5.11, and the frequency at which this happens is recorded (approximately 83 Hz indicated with a cross). Repeating this for enough different time values the whole time-frequency curve can be determined, as shown in Figure 5.6e. A sweep with a time-amplitude as shown in Figure 5.6a and time-frequency curve as shown in 5.6e produces a power spectrum that closely resembles the shape of specified power spectrum, compare Figure 5.6f and 5.6b. The difference between the spectra are due to the finite length of the sweep and the approximation involved.

Although the skyline spectrum used for the example in Figure 5.6 has little practical use, it does illustrate how well the method is able to produce a signal with a spectrum that has rapid transitions between high and low values. The strength of the method, for practical purposes, is contained in the fact that it can be used to optimize the time-amplitude and power spectrum of a sweep independently.

If the time amplitude of the sweep is kept fixed, it is possible to increase or decrease the energy of the sweep at certain frequencies by varying the sweep rate. This can be used to flatten the spectrum of the output signal, by designing the input signal such that it compensates for the transfer function of the system. For seismic vibrators the input signal is the driving sweep and depending on the knowledge of the system the transfer function can be modeled or measured, and might include the dynamics of; the vibrator, the vibrator-ground coupling, and the propagation path towards the receivers. The output signal that is optimized can thus be the force on the base plate, the force on the ground or the seismic wavelet recorded at the receivers.

Another use of the method is to increase the energies of those frequencies at which the vibrator is unable to operate at high amplitude, either due to environmental constraints or due to its natural limitations. Typically this kind of amplitude constraint is more dependent on frequency than on time and it is beneficial to replace $A(t)$ in equation 5.8 by $A(f)$. Bagaini (2006); Bagaini *et al.* (2008) showed that the equation then can be used to design a sweep that compensates for the amplitude drop at the low end of the spectrum caused by the finite stroke of the vibrator. The amplitude drop is simply balanced by spending relatively more time at these low frequencies (typically below 5 to 10 Hz), similarly as in the nonlinear sweep shown in Figure 5.5.

5.5. CONCLUSION

In this chapter we have discussed a number of aspects of sweeps. Starting with the linear sweep the role of tapers and phase offsets was made clear. It was shown that the phase offset, irrespective of the choice of taper or sweep, can always be used to remove the DC component from a sweep signal. Some of the challenges to deal with, like the generation of harmonics were explained in detail and we have shown that although the linear sweep has several desirable properties, changing the frequencies in a nonlinear way can be beneficial. Using the stationary-phase approximation of the Fourier transform of the

sweep we presented two different optimizations. In the first optimization, the sweep rate was adjusted in such a way that the arrival time of the harmonic correlation noise could be controlled. This enables the design of sweeps that are more robust to the effects of harmonics. In the second optimization we presented a new method to determine the time-frequency relation when the time-amplitude and power spectrum are given. This method can be used to design sweeps that have a predefined power spectrum without having to reduce the driving amplitude. This method can be useful if one wished to correct for amplitude effects due to the transfer from the driving force of the vibrator to the seismic wavelet it produces in the ground.

REFERENCES

D. Aldridge, *Mathematics of linear sweeps,* Canadian Journal of Exploration Geophysics **28**, 62 (1992).

C. Bagaini, *Enhancing the low-frequency content of vibroseis data,* SEG Technical Program Expanded Abstracts , 75 (2006).

C. Bagaini, T. Dean, J. Quigley, and G. Tite, *Systems and methods for enhancing low-frequency content in vibroseis acquisition,* US Patent 7,327,633 (2008).

T. Dean, *The use of pseudorandom sweeps for vibroseis surveys,* Geophysical Prospecting **62**, 50 (2014).

B. Edington and T. Khan, *Method of source coding and harmonic cancellation for vibrational geophysical survey sources,* US Patent 4,982,374 (1991).

R. Landrum, *Simultaneous performance of multiple seismic vibratory surveys,* US Patent 4,715,020 (1987).

J. Meunier, *Seismic acquisition from yesterday to tomorrow* (Society of Exploration Geophysicists, 2011).

E. Rietsch, *Method of seismic exploration,* US Patent 4,042,910 (1977a).

E. Rietsch, *Computerized analysis of vibroseis signal similarity,* Geophysical Prospecting **25**, 541 (1977b).

E. Rietsch, *Vibroseis signals with prescribed power spectrum,* Geophysical Prospecting **25**, 614 (1977c).

D. Silverman, *Method of three dimensional seismic prospecting,* US Patent 4,159,463 (1979).

N. Tellier, G. Ollivrin, and D. Boucard, *Optimizing the generation and QC of low-dwell sweeps,* 76th EAGE Conference and Exhibition, Tu ELI2 16 (2014).

6

GENERAL DISCUSSION AND OUTLOOK

6.1. GENERAL DISCUSSION

The goal of a seismic source is to generate a seismic wave that samples the earth in an optimal way. For vibratory sources, optimal implies that the waves transmitted by the vibrator carry a unique signature that can be recorded and identified at the receiver side, and can be used to resolve the seismic transferal properties of the earth between the source and the receiver with the best possible temporal resolution. The vibrator thus has to faithfully reproduce the designed signature. However, a perfect vibrator cannot be built and the transmission of the vibrator-force signature to the seismic signature in the ground cannot be completely controlled either. As a consequence there is a need to measure the actual, seismic, output signature of the vibrator. The weighted-sum ground-force method that is routinely applied can only estimate the correct seismic signature to some extent. Therefore the used signal to drive the vibrator should be robust against the most common distortions due to the imperfections of the vibrator and the measurement of the actual seismic signature produced. These aspects have recurred in different ways in the previous chapters.

Improvement of the accuracy of seismic vibrators might be achieved by using a different driving engine. In Chapter 2 we have shown that it is possible to build a vibrator driven by linear synchronous motors (LSMs). The potential benefits of such an engine compared to the more commonly used hydraulic or voice-coil engines have been explained. These benefits are all directly related to the improvement of the resolution due to the accurate generation of a designed signal and the increase of the frequency band at the lower end of the spectrum. However, as should be clear from Chapter 2 as well, the driving engine is not the only component determining the quality of the vibrator. In the development of the prototype LSM vibrator a significant amount of work has been put in tuning the vibrator components and finding solutions for resonance frequencies and eigenmodes belonging to the vibrator as a whole. Measuring the acceleration of the

reaction mass and base plate without too much interference from the large AC currents needed to drive the LSMs was a specifically hard problem to solve.

Because the faithful generation of a seismic wave with a predefined signature is so difficult and all the seismic data are correlated with the source signature, measuring the actual signature of the wave emitted by the source is of great importance. Literature indicates (see Chapter 4 and references therein) that the de-facto standard of the weighted-sum-ground-force approximation does not always predict the emitted signature properly. This can also be observed in some of our experiments described in Chapter 3. The coupling with, and the properties of, the ground beneath the vibrator has a significant impact on the behavior of the vibrator and the wavelet it emits. In the experiment where the weighted-sum ground force was controlled (Section 3.4), drive-level dependency of the wavelet recorded in a borehole was observed, while this dependency was not reflected in the ground-force estimate. The amplitude at which the vibrator operates clearly has an important imprint on the signature it produces.

One of the implicit assumptions of the weighted-sum approach is that the vibrator can be modeled as an 1D system that is in perfect contact with the ground. This assumption neglects that the true contact will vary over the base-plate area. In Chapter 4 we showed that a rough vibrator-ground contact influences the behavior of the base plate in a nonlinear way. The model predicted a decrease of base-plate resonance frequency with drive level, similar to that observed in the field experiments (Chapter 3). Although the modeling was limited, it does indicate that the 2D/3D effects cannot be ignored if one aims to improve resolution of the method.

Although the driving engine of a vibrator might be improved (Chapter 2), factors such as the vibrator-ground contact (Chapter 4) will always alter the seismic signature produced to some unknown extent (Chapter 3). Therefore besides optimizing the vibrator and the method of determining the source signal, one should also make the intended source signature robust against the expected distortions. In Chapter 5 we described a number of methods to facilitate a robust design of a sweep. We showed that with a proper design of a sweep, the harmonic correlation noise can be moved to arrival times where it is less harmful to the record. We also presented a new method to determine the time-frequency distribution when the time-amplitude and power spectrum are given. With this method it is possible to adjust the output power spectrum of the vibrator without having to reduce the time amplitude, possibly compensating for the transfer function of the vibrator.

The chapters of this thesis should at least have clarified that the vibroseis method is complicated. Some parts of the setup are more or less static and can be controlled, such as the design of the vibrator and the signature it should produce. Other parts of the setup are more dynamic, spatially and temporally, such as ground properties and vibrator-ground contact. If one aims to improve the vibroseis method per se, all these aspects should be considered together as they are inextricably intertwined.

6.2. OUTLOOK

As with every research, answering one question nearly automatically generates a next one. Here we would like to present a list of topics that are worth investigating further.

- We have successfully proven the concept of an LSM-driven vibrator. However, a question remains if the technique can be scaled up for deep, i.e. a few kilometers, exploration purposes. In principle we do not see many difficulties, because only the number of LSMs needs to be increased. Of course the mechanical structure of the vibrator should be fit for this larger number of LSMs and the power supply should be carefully designed.
- LSMs are also well suited to drive a shear-wave vibrator. Due to their flat shape, it is possible to design a shear-wave vibrator whose driving force is applied very close to the base plate. This will help reduce resonances and nonlinearities commonly seen for example with voice-coil driven vibrators, in which there is a considerable vertical distance between the point at which the force is applied and the base of the plate. A small (700kN) prototype has been developed, but again the question of scalability is unanswered.
- To investigate the role of geometric nonlinearity due to the vibrator-ground contact, it would be interesting to repeat the drive level test with a shear-wave vibrator. Because the vertical load on the ground does not significantly change with drive level for a shear-wave vibrator, it is expected that the effects caused by a changing contact geometry with a vertical vibrator would be absent in case a shear-wave vibrator is used. Therefore comparing the outcome of a vertical and horizontal drive-level test, would help to understand the role of contact between the vibrator and the ground.
- Another experiment that would help to gain insight in the effects caused by the vibrator-ground contact is to measure the contact area and pressure over the whole base plate during the excitation. Literature shows that a number of attempts were made in this direction, but until now no data was obtained over the entire base plate or without affecting the dynamics too much.
- Next to the geometric-induced nonlinearity, the intrinsic nonlinear properties of the ground should be studied as well. The permanent deformation beneath the base plate visible in the field, is definitely a manifestation of nonlinear ground behavior. The question is whether its dynamic effects diminish after a number of sweeps and whether it is somehow possible to take these effects into account.
- We showed that robust sweeps can be designed such that recorded seismic data is less affected by harmonic correlation noise and the transfer from the vibrator to the ground. However, the approach used depends on the assumption that amplitude and time can be interchanged, i.e. a signal with short duration and high amplitude will produce the same spectral strength as a signal with smaller amplitude and longer duration. Although this is true in the noise-free case, ambient noise will impose a limit to how small the amplitude can be and still be detected. The signals designed with the methods described should therefore be tested in the field to find out to what extent the methods can be applied.

CURRICULUM VITÆ

Richard Pim NOORLANDT

PERSONAL INFORMATION

Date of birth	21 September 1983
Place of birth	Rhenen, The Netherlands

EDUCATION

2005–2007	Master Earth Science Utrecht University
2003–2005	Bachelor Earth science Utrecht University
2002–2007	Bachelor Physics Utrecht University
1996–2002	Atheneum (high school) Christelijk Lyceum Veenendaal

EMPLOYMENT

2008–Present	Geophysicist Deltares
2007–2008	Geophysicist TNO

PUBLICATIONS RELATED TO THIS RESEARCH

R. Noorlandt and G. Drijkoningen, *On the mechanical vibrator-earth contact geometry and its dynamics*, Geophysics 81, P37 (2016), DOI: 10.1190/geo2015-0271.1.

R. Noorlandt, G. Drijkoningen, J. Dams, and R. Jenneskens, *A seismic vertical vibrator driven by linear synchronous motors*, Geophysics 80, EN57 (2015), DOI: 10.1190/geo2014-0295.1. This paper has received the award for *Best Paper in Geophysics 2015*.

G. Drijkoningen and R. Noorlandt, *Pseudorandom signals and EM-type seismic vibrators*, Nederlands Aardwetenschappelijk Congres 12 (2014).

R. Noorlandt, G. Drijkoningen, and C. Faber, *Influence of drive level on the fundamental vibrator signal*, 75th EAGE Conference and Exhibition, Th P11 02 (2013), DOI: 10.3997/2214-4609.20130302.

R. Arts, X. Zhang, A. Verdel, D. Santonico, J. Meekes, R. Noorlandt, B. Paap, and V. Vandeweijer, *Experiences with a permanently installed seismic monitoring array at the CO_2 storage site at Ketzin (Germany), A status overview*, Energy Procedia 37, 4015 (2013), DOI: 10.1016/j.egypro.2013.06.301.

R. Noorlandt, G. Drijkoningen, and R. Schneider, *A seismic vertical vibrator driven by linear motors*, 74th EAGE Conference and Exhibition, P061 (2012), DOI: 10.3997/2214-4609.20148468.

R. Noorlandt and G. Drijkoningen, *A seismic source based on linear motors*, Nederlands Aardwetenschappelijk Congres 11 (2012)